BULGARIAN CHEMICAL COMMUNICATIONS

2023 Volume 55 / Special Issue C

Journal of the Chemical Institutes
of the Bulgarian Academy of Sciences
and of the Union of Chemists in Bulgaria

EUROPEAN UNION
EUROPEAN REGIONAL
DEVELOPMENT FUND

OPERATIONAL PROGRAMME
SCIENCE AND EDUCATION
FOR SMART GROWTH

Project № BG05M2OP001-1.002-0005, Personalized Innovative Medicine (PERIMED)

Term of implementation: 30 March 2018 – 31 December 2023
Starting funding: 23 472 019.71 leva (11 982 673 Euro)

Leading organization:

Medical University, (MU Plovdiv). Plovdiv, Bulgaria, https://mu-plovdiv.bg

Partners:

University of Plovdiv "Paisii Hilendarski", (PU) Plovdiv, Bulgaria, www.uni-plovdiv.bg_

Institute of Mineralogy and Crystallography "Acad. Ivan Kostov", Bulgarian Academy of Sciences (IMC-BAS), Sofia, Bulgaria, http://www.imc.bas.bg

Associated partners:

University Multi-profile Hospital for Active Treatment /UMHAT/ "SAINT GEORGE"

NEOPHARM BULGARIA Ltd., Sofia, Bulgaria, http://neopharm.bg/

University of Manchester, UK

Instituto De Agroquimica y Tecnologia de Alimentos as a part of the State Agency, Madrid, Spain

This Special issue of the Bulgarian Chemical Communications contains selected papers, reported as oral or poster presentations at the final Conferences organized by the partners of the Center of Competence in Personalized Innovative Medicine.

The Center of Competence in Personalized Innovative Medicine (PERIMED) stands as a pivotal entity in the transforming of biomedical research into viable therapies, significantly improving the quality of life for patients and the general population. Ini-

tially, it brings together a consortium of three partners: the Medical University of Plovdiv, Plovdiv University "Paisii Hilendarski", and the Institute of Mineralogy and Crystallography at the Bulgarian Academy of Sciences. This collaborative effort lays the grounds for advancements in personalized medicine.

With an eye towards future developments, PERIMED is ready for strategic expansion in its next phase, PERIMED II. This expansion includes broadening the consortium to include four partners by incorporating an NGO. This new addition is tasked with a critical role in bridging the gap between PERIMED research and business. It will offer initiatives in managing interactions between research entities and businesses, overseeing the development and guidance of spin-off and startup companies, and facilitating the transfer of intellectual properties. This evolution marks a significant step in enhancing the consortium capacity to translate scientific achievements into commercial opportunities, fostering a more direct impact on both the healthcare industry and society at large.

The Center of Competence PERIMED is dedicated to fostering collaborative research and innovation among scientists from the Medical University of Plovdiv, Plovdiv University "Paisii Hilendarski", and the Institute of Mineralogy and Crystallography at the Bulgarian Academy of Sciences. Its goal is to augment the market relevance of their research and development endeavors, thereby facilitating business partnerships. The project bridges strategic commitment to innovation, collaboration, and the practical application of research findings, ensuring the project's sustained influence on personalized medicine and its accessibility to the market.

The establishment of PERIMED as a nationally significant scientific infrastructure complex, integrated into European networks in personalized medicine and focused on three primary areas:

- *Molecular and biological methodologies for application in personalized medicine and implementation of a personalized approach in the treatment of critically ill patients;*
- *Innovative drug delivery systems for targeted therapy and personalized medicine;*
- *Bioengineering technologies and biosensors.*

The strategy to achieve the project's objectives was built on three pillars:

- *Providing state-of-the-art equipment;*
- *Developing advanced health-related technologies; and*
- *Building academic resources with significant potential and scientific capacity.*

The successful implementation and advancement of the PERIMED project is fully achievable, as all participants recognize the profound responsibility they bear towards human health. The project's execution is expected to offer substantial benefits to society, categorized into health-related, educational, and economic aspects:

Health related:

- Enhanced quality of diagnostic and therapeutic practices based on contemporary scientific principles;
- Adoption of personalized treatment approaches for cancer patients and critically ill individuals;
- Tailored use of medical products to fit patient-specific needs;
- Increased effectiveness and safety of therapeutic methods;
- Improved living conditions, leading to more patients being cured and saved.

Educational:

- Acquisition of new knowledge vital for scientific and entrepreneurial ventures;
- Development in various pharmaceutical science and biotechnology domains – including nanotechnology, alternative drug administration routes, targeted therapy, intensive medicine, immobilized biocatalysts, natural bioactive substances, biopolymers, new materials, and biosensors;
- Enhancement of capacity for innovative scientific research;
- Conducting research to European standards;
- Encouraging young scientists to pursue their careers in Bulgaria.

Economic:

- Business growth through the application of innovative scientific findings and the commercialization of technological innovations;
- Reduced treatment costs for socially significant diseases;
- Creation of a new model for research-business interaction, fostering mutual benefits;
- Job creation;
- Enhanced collaboration among professionals in medicine, genetics, pharmacy, bioinformatics, medical statistics, and pharmacoeconomics;

- Improved management of oncology and intensive care units;
- Establishment of new spin-off and startup companies with the potential for business and profit.

From March 30, 2018, to December 31, 2023, the PERIMED consortium utilized the funding of 23,472,019.71 leva, dedicating at least 75% to infrastructure and the remainder to maintenance, specializations, and dissemination, among other necessities. The consortium faced significant administrative burdens at the project's onset due to evolving implementation rules set by the Executive Agency "Programme Education" and the impact of the COVID-19 pandemic, which basically halted research activities and reduced the Medical University of Plovdiv's administrative capacity (March 2020 to March 2022). To achieve its objectives, PERIMED worked on the execution of twelve work packages (WP), ranging from the creation and validation of gene panels for cancer diagnosis to the development of drug delivery systems and biosensors, showcasing a comprehensive approach to advancing personalized medicine.

WP 1. Creation and validation of a panel of genes for monitoring of tumor heterogeneity, molecular resistance, tumor load and minimum residual disease in patients with verified breast cancer;
WP 2: Creation and validation of a panel of genes for precise molecular-genetic diagnosis in patients with chronic myeloid leukemia (CML) and monitoring of minimal residual disease;
WP 3. Molecular biomarkers for medical application;
WP 4. Application and development of the method of flow cytometric monitoring of the minimal residual disease in children with acute lymphoblastic leukemia;
WP 5. Creation and introduction of comprehensive personalized approach in critically ill patients;
WP 6. Molecular biomarkers of the microbiota of the gastrointestinal tract;
WP 7. Immuno-biomarkers for tumor and autoimmune diseases;
WP 8. Drug-delivery systems for targeted effect of medications and personalized medicine;
WP 9: physicochemical characterization of innovative medical forms;
WP10. Biocatalysts and natural bioactive substances;
WP 11. Biopolymers and new materials;
WP 12. Biosensors.

This main part of the investment led to the establishment of modern research laboratories by the consortium partners, each specialized in crucial areas of personalized medicine. This infrastructure was instrumental in advancing research and development efforts. The laboratories and acquired state-of-the-art equipment supported the implementation of twelve work packages:

Medical University – Plovdiv, PERIMED laboratories:

1. Drug delivery systems for targeted effect of drugs and personalized medicine,
2. Molecular genetic markers for medical use.

Plovdiv University "Paisii Hilendarski", PERIMED laboratories:

3. Molecular biomarkers of the microbiota;
4. Immunobiomarkers;
5. Biocatalysis and biologically active substances;
6. Biopolymers and new materials;
7. Biosensors.

Institute of Mineralogy and Crystallography, BAS, PERIMED laboratory:

8. Laboratory for physico-chemical control of innovative medicinal forms (pharmaceutical ingredients)

The laboratory of "Drug delivery systems for targeted effect of drugs and personalized medicine", has been equipped with a nano-spray dryer, microencapsulation equipment, and highly specialized equipment for structural-morphological characterization of drug delivery systems and for studying biological samples. Namely, a state-of the-art FEI 200 cryo transmission electron microscope (cryoTEM) for working at low temperatures and a scanning electron microscope (Figure 1). The laboratory also has four flow cell apparatus necessary for the biopharmaceutical and pharmacokinetic characterization of the developed drug carriers, to ensure accuracy, repeatability, and a high degree of correlation between *in vitro/in vivo* studies. There is also suitable equipment for cell culturing, allowing for tests on drug toxicity and biocompatibility and achieving targeted drug release in experimental animals.

The laboratory of "Molecular genetic markers for medical use" supports WPs 1, 2 and 3. It is fo-

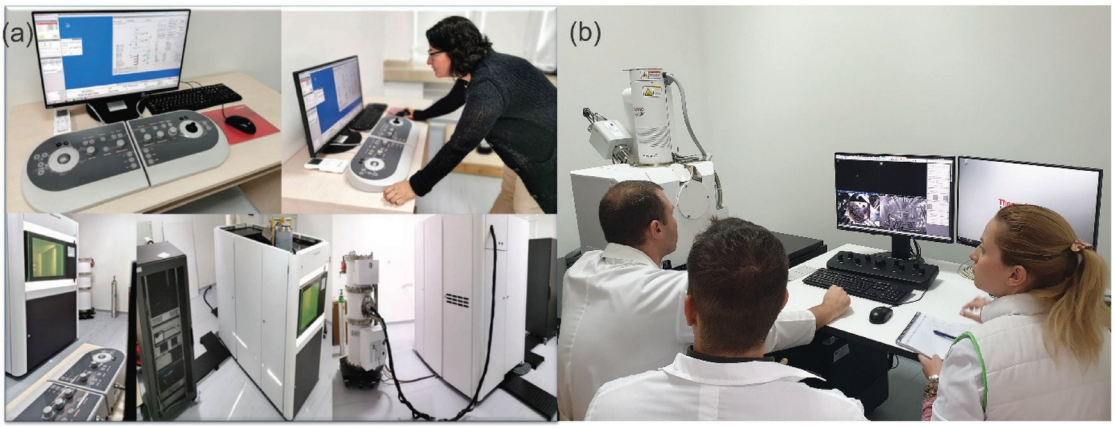

Figure 1. Installed (a) FEI 200 cryo-transmission electron microscope (cryoTEM) and (b) scanning electron microscope at the laboratory of Drug delivery systems for targeted effect of drugs and personalized medicine – MU Plovdiv.

cused on establishing and use of new molecular biomarkers for medical use and diagnosis of breast cancer (WP 1) and chronic myeloid leukemia (CML) and minimal residual disease (WP 2), while WP 3 combines the results of 1 and 2 and thus improves the prognosis of treatment of the diseases studied and monitored. The major acquired infrastructure includes a next generation sequencer and a digital droplet PCR (Figure 2). In brief, a protocol has been developed to detect variants of a specific (DPYD) gene – the cause of severe side effects in the treatment of cancer patients, the development and validation of a panel of genes for accurate molecular diagnosis in patients with CML is being tested and tests for detection of target mutations associated with resistance to antitumor treatment by digital droplet PCR are being developed.

The application and development of the method of flow cytometric monitoring of the minimum residual disease (MRD) in children with acute lymphoblastic leukemia (ALL) required the acquisition of a Cell Sorter based on 4 laser multiparameter flow cytometry (Figure 3). As result of WP4 were created and validated:

Figure 2. Major infrastructure and equipment at the laboratory "Molecular genetic markers for medical use" (a) next generation sequencer and (b) digital droplet PCR system.

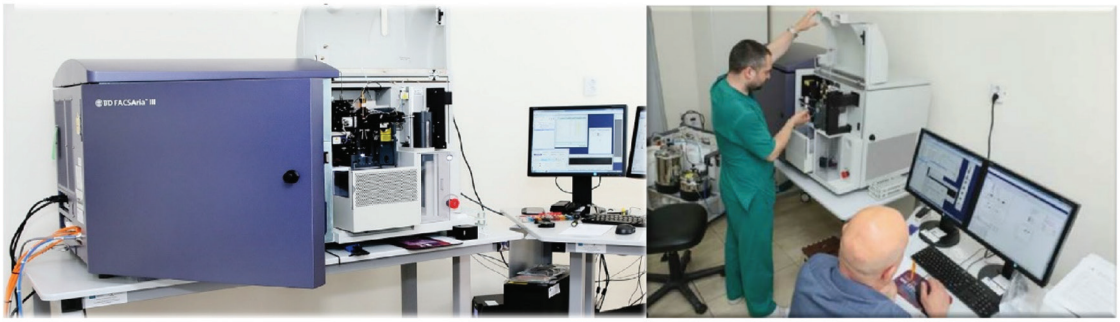

Figure 3. Cell Sorter based on 4 laser multiparameter flow cytometry.

1. A modern methodology for the study of MRD in children with hematological and oncological diseases;

2. An innovative science-based algorithm for research and assessment of the minimum residual disease in children with ALL;

3. Standardized panels for the study of MRB implemented as an objective criterion for monitoring the effect of the treatment.

Work package 5 was focused on the development of a Critically ill patient monitoring system (Web based Portal for telemonitoring):

- through the simultaneous tracking and analysis of multiple patient's vital parameters;
- detection and objectification of their relationships (Algorithm for personalized assessment and follow-up).

Work packages 6 and 8 worked together on Nano- and microcarriers of drugs with different polymers for targeted release in the gastrointestinal tract (spray drying, ionotropic gelling):

- Optimal condition analyzes for the highest yield of carriers, high productivity, reproducibility of the results without loss of material;
- Protecting the drug from the aggressive stomach environment – the drug reaching the target unchanged.

Similarly, Work packages 8 and 9 worked on the development of new inorganic drug carriers for antitumor therapy:

- Four types of silicate micro- or nano-carriers were developed by WP 9 (Figure 4b);
- The processes of activation and loading of the silicate nanocarriers with paclitaxel and other drugs, used in antitumor therapy were optimized (WP 9);
- The release of paclitaxel has been studied by the liquid chromatographic method with mass detection WP 8.

In addition WP 8 developed models of casein nanoparticles (Figure 4a) with daunorubicin as promising drug carriers to achieve highly effective and safe antitumor therapy. Another study explored the use of casein micelles as nanocarriers for benzydamine delivery, demonstrating the formulation of nanoparticles for controlled and targeted drug release. This aligns with PERIMED's goal to develop innovative drug delivery systems, showcasing the potential of naturally occurring materials in improving therapeutic outcomes (https://www.mdpi.com/2073-4360/13/24/4357).

The next five laboratories are located in the Centre of technologies of the Paisii Hilendarski University of Plovdiv – an infrastructure, building, that has been a subject to construction work, funded by the PERIMED project (Figure 5). The laboratories supported the research of five WPs:

- WP 6. Molecular biomarkers of the microbiota of the gastrointestinal tract (Figure 6);
- WP 7. Immuno-biomarkers for tumor and autoimmune diseases;
- WP 10. Biocatalysts and natural bioactive substances (Figure 7);

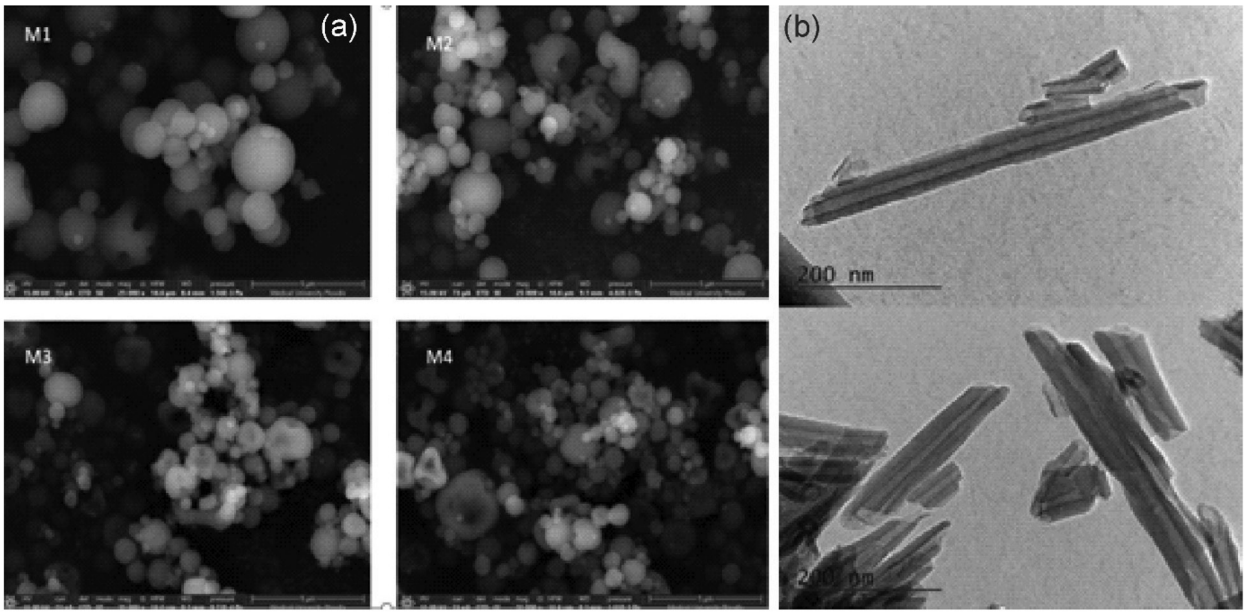

Figure 4. SEM visualization of the polymer nanoparticles (a) and (b)TEM visualization of the silicate nanocarriers.

Figure 5. The Centre of technologies at the Paisii Hilendarski University of Plovdiv.

Figure 6. Laboratory of Molecular biomarkers of the microbiota of the gastrointestinal tract.

Figure 7. Laboratory of Biocatalysts and natural bioactive substances.

- WP 11. Biopolymers and new materials (Figure 8);
- WP 12 Biosensors (Figure 9).

As a result of the work, the development of a biosensor for detecting dopamine and L-epinephrine confirms PERIMED's work on bioengineering technologies. This biosensor, based on laccase-catalyzed assays and immobilized on a gold-modified electrode, represents an innovative approach to neurotransmitter measurement, with potential applications in both clinical diagnostics and research (https://www.mdpi.com/2079-6374/12/9/719).

Figure 8. Laboratory of Biopolymers and new materials.

Figure 9. Laboratory of Biosensors.

The "Laboratory for physico-chemical control of innovative medicinal forms" (pharmaceutical ingredients) is located at the Institute of Mineralogy and Crystallography, BAS. The Infrastructure premises of the laboratory were subject to complete renovation according to the requirements of the equipment. The Laboratory supports the research work of WPs 8 to 12, while the main effort is concentrated on the physico-chemical characterization and control of existing an innovative medicinal forms, active pharmaceutical ingredients and excipients. The main laboratory equipment includes a diffractometer (Empyrean, Figure 10), DSC (TA-250, Figure 11), surface area and porosity analyzer (BETsurface, micro- and meso-pore size and porosity) (3FLEX, Figure 13), Isothermal titration calorimetry – ICT TA-Affinity (Figure 12), UV-Vis Carry 4000 and planetary ball mill Pulverisette 7 premium Fritsch. Additional infrastructure allowing synthesis, antibacterial, elemental analysis etc., to the support of the research is also available. New and existing pharmaceutical entities (active pharmaceutical ingredient-APIs) are required to possess physicochemical characteristics that result in adequate reproducibility. The most common problem is the low solubility of the pharmaceutical entities that is very often overcome by the engineering of metastable phases. Physicochemical characterization focuses on the determination of thermal stability, polymorphism, dissolution or hydration, and the presence of undesirable contaminants in pharmaceutical products. The package is focused on providing data and investigation of solid form (polymorphs) by XRD, thermal stability by DSC, loading of active substances and their interaction with excipients (auxiliary substances) by surface area, strong interaction by ITC.

In pharmaceutical research, the focus of WP 9 was on developing drug delivery systems using synthetic zeolites. This involved synthesizing zeolite phases, loading drugs onto them, and studying drug release. Different surface modifications and methods were explored. Dexamethasone was initially tested, and later Taxol and Cyclophosphamide were added for analysis. UV-Vis studies were conducted, leading to several outcomes:

- A methodology for loading paclitaxel onto HNT1 was established, including specific activation and pH-dependent release;
- Another porous material for protected drug release in heart conditions is being investigated.

The applied research was focused on the polymorphism that is a significant problem for pharma-

Figure 10. Diffractometer Empyrean. Applications: qualitative phase/polymorphs and quantitative analysis (wt%), Cu (1.5406 Å) and Co (1.7902 Å) sources; modes: reflection, transmission, microdiffraction (spot of 50 µm), measurements at different temperatures and different gas environments, low temperature (to –200 °C), high-temperature (to +600 °C), controlled atmosphere, SAXS/USAX, thin layers (up to 500 nm), microdiffraction, xyz stage etc.

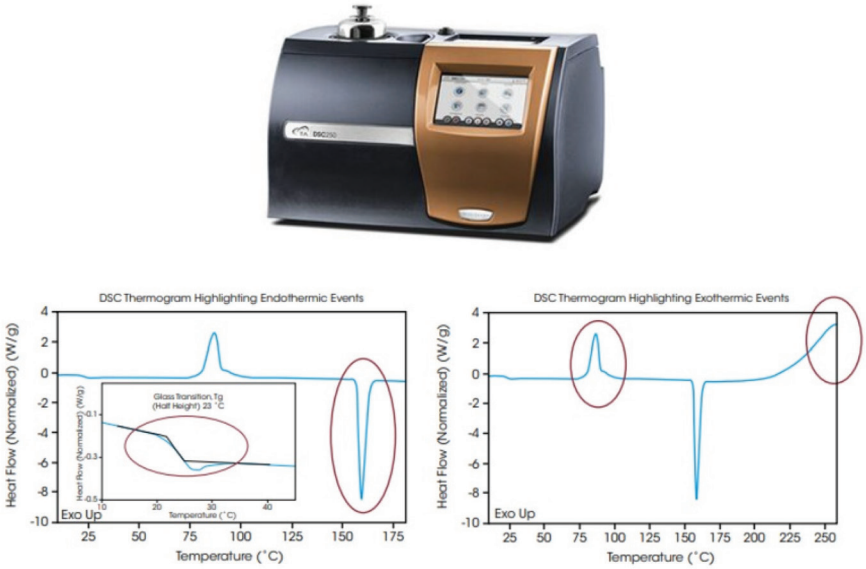

Figure 11. DSC250 TA Instruments: melting points, phase transitions, solvent evaporation, dehydration and rehydration, analysis of purity ASTM. Small amount of sample 0.1 mg, ambient, nitrogen, argon conditions. –120 to 450 °C, suitable for Protein/DNA denaturation, folding analyses.

ceutical industry. A consolidated analytical technique based on Powder X-ray Diffraction has been developed, being the definitive test for the identification of polymorphs and crystal phases. However, its application for quantitative analysis is hindered by matrix effects: the presence of excipients requires a complete knowledge of samples' composition. Thus, univariate calibration methods require the matrix effect to be studied and adjusted but still suffer from the co-presence of different phases in the sample. Multivariate analysis is the only way to bypass problems. In particular, the

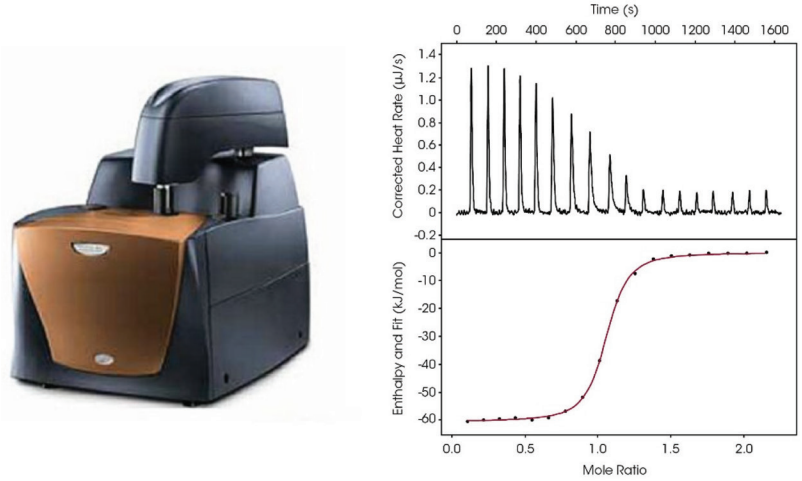

Figure 12. Affinity ITC, TA Instruments – detects interaction between protein/DNA/antibody and drug (ligand), works with solutions, cell volume (190 µl), syringe volume (250 µl), temperature range (2–80 °C), measured heat range (0.04–5000 µJ).

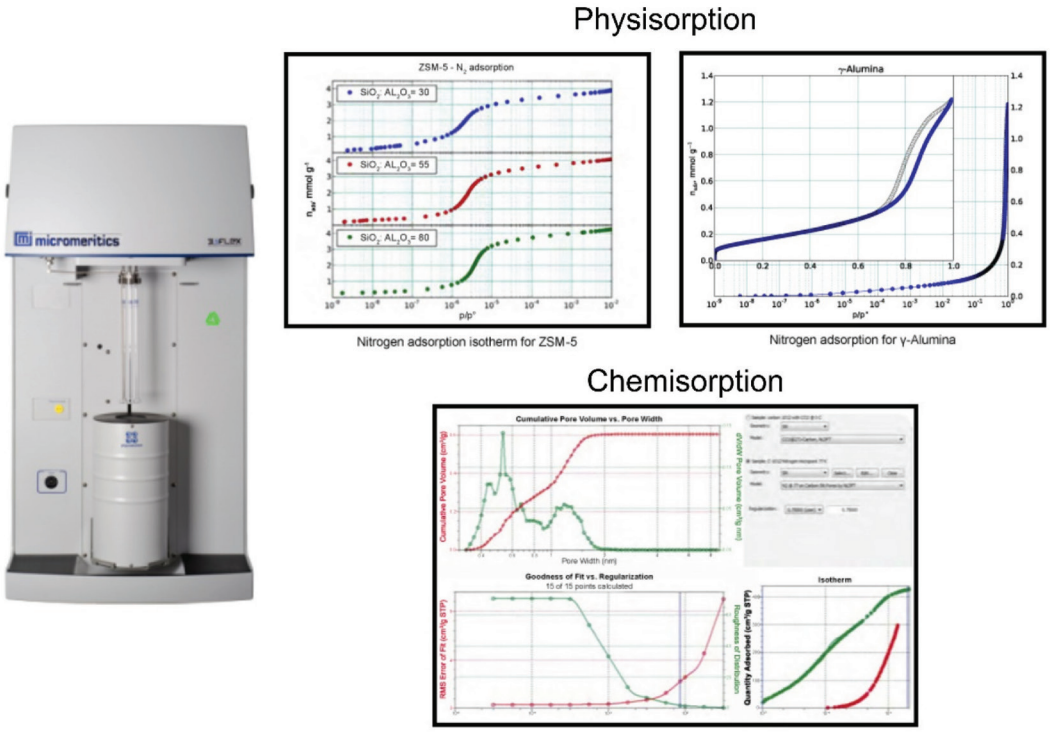

Figure 13. Surface area analyzer – BET, 3Flex Micromeritics: nanopowders surface area, detects the loading of drugs on nanocarriers, determines suface are, pores sizes.

multivariate standard addition method (SAM) is promising. Combing PXRD with complimentary DSC/TGA etc. will provide a cross-check for definite polymorph analysis.

The main outcomes of PERIMED project were presented at the conferences organized by the three partners "Personalized Innovative Medicine" (PERIMED) 4-th and 5-th MU-Plovdiv, 5-th and 6-th December 2023 Plovdiv, Bulgaria, IMC–BAS.

Through its dedicated work packages, PERIMED has carried out pioneering research in personalized medicine. Notable scientific achievements include

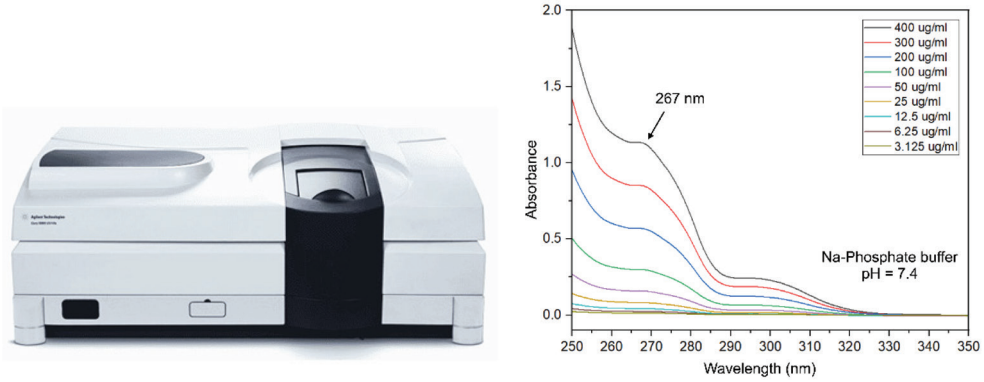

Figure 14. UV-VIS Cary 4000 , range 175–900 nm; works with solid and liquid sample solid volume ~1 cm^3, liquid sample volume from 0.2 to 3.5 ml; the system is optimal for analyzing solid samples or liquid biological samples with minimal sample preparation. Monitoring drug release, degradation, sedimentation, comparing solutions *vs* solid state in APIs.

Figure 15. Extract of the Conference program.

the creation and validation of gene panels for cancer diagnosis and monitoring, the development of novel drug delivery systems for targeted therapy, and the advancement of bioengineering technologies. These efforts have led to improved diagnostic and therapeutic practices, tailoring treatments to individual patient needs.

PERIMED has successfully established eight modern research laboratories across its consortium partners, equipped with cutting-edge technology. These laboratories specialize in various critical areas, including drug delivery systems, molecular genetic markers, molecular biomarkers, immunobiomarkers, biocatalysis, biopolymers, new materials, and biosensors. This infrastructure and the studies, funded and facilitated by the PERIMED project, reflect the comprehensive effort to advance personalized medicine through cutting-edge research in pharmacogenetics, drug delivery systems, immunology, and biosensor technology. Each effort contributes to the overarching goal of enhancing patient care by tailoring medical treatments to individual genetic profiles and physiological needs, paving the way for more precise and effective therapies.

PERIMED's work has directly benefited society across health-related, educational, and economic dimensions. It has contributed to enhanced quality of life through improved diagnostic and therapeutic methodologies, personalized treatment approaches, and increased effectiveness and safety of medical treatments. Additionally, PERIMED has played a pivotal role in education by providing new knowledge, encouraging young scientists, and enhancing research capacity.

The project has stimulated economic growth by promoting business development through innovative scientific findings. It has created new jobs, reduced diagnostics and treatment costs for significant diseases, and with the strategic inclusion of NGO in PERIMED II has expanded the consortium, enhancing its capability to bridge research and business. The founding of new spin-off and startup companies has also contributed to the economic landscape.

Throughout the 2018–2023 period, PERIMED's achievements have not only advanced the field of personalized medicine but also set a foundation for future innovations and collaborations. The consortium's dedication to transforming biomedical research into practical therapies has positioned it as a leader in personalized medicine, with a lasting impact on patient care, scientific research, and economic development.

Prof. Boris Shivachev,
Member of the Scientific board of PERIMED
Organizing committee of the final Conference "Personalized Innovative Medicine" (PERIMED), December 2023, Plovdiv, Bulgaria

Bulgarian Chemical Communications, Volume 55, Special Issue C (pp. 17–24) 2023 *DOI: 10.34049/bcc.55.C.0001*

Approaches for detection of minimal residual disease in childhood B-cell precursor acute lymphoblastic leukemia by FlowJo and Infinicyt softwares

A. Baldzhieva[1,2,3], H. Burnusuzov[2,3,4], H. Andreeva[2,5], T. Kalfova[1,2], S. Petrov[1,2], D. Dudova[1], K. Vaseva[1], T. Dimcheva[6], H. Taskov[2], M. Murdjeva[1,2,3]

[1] *Department of Medical Microbiology and Immunology – "Prof. Dr. Elissay Yanev", Faculty of Pharmacy, Medical University of Plovdiv, Bulgaria*
[2] *Research Institute, Medical University of Plovdiv, Bulgaria*
[3] *Laboratory of Clinical Immunology – St. George University Hospital, Plovdiv, Bulgaria*
[4] *Department of Pediatrics and Medical Genetics, Faculty of Medicine, Medical University of Plovdiv, Bulgaria*
[5] *Department of Immunology and Molecular Genetics; Laboratory Medicine Division, Diagnostic Clinic, University Hospital of North Norway, Tromsø, Norway*
[6] *Department of Medical Informatics, Biostatistics and E-Learning, Faculty of Public Health, Medical University of Plovdiv, Bulgaria*

Received: November 2023; Revised: December 2023

Acute lymphoblastic leukemia (ALL) involves the aggressive proliferation of lymphoblasts in the bone marrow (BM), peripheral blood or extramedullary sites. "Minimal, or Measurable Residual Disease" (MRD) is a crucial prognostic factor, helping categorize the risk of relapse and guide treatment decisions. Both multiparameter flow cytometry (FC) and molecular (PCR) approaches can detect cancer cells at very low levels, beyond the capability of traditional microscopy. This study focuses on exploring a new potential within FC analysis as a primary diagnostic tool for ALL to examine the distribution of pathological cells in MRD samples stained by standardized 8-color labelling method by multidimensional softwares FlowJo® and Infinicyt® compared to conventional FC. The study included 50 patients diagnosed with B-cell precursor ALL (BCP-ALL). They were retrospectively processed and analyzed by conventional (DIVA) and multidimensional (FlowJo and Infinicyt) softwares. All of them were systematically assessed for the level of residual tumor cells in bone marrow on days with proven prognostic significance: day 15, day 33, day 78 and other time points, according to a Berlin-Frankfurt-Munster (BFM) ALL treatment protocol. There was no significant difference ($p>0.05$) between conventional (DIVA) and multidimensional (Infinicyt and FlowJo) softwares in terms of determining the percentages of residual blast cells, but FlowJo has the advantages of a semi-automated analysis tool. Data analysis based on multidimensional approach by FlowJo® and Infinicyt® softwares is able to corroborate the results of the conventional FC analysis. Additionally, it can simplify the analysis and can be used as a complementing tool for cases that require more detailed examination.

Keywords: MRD, BCP-ALL, Infinicyt, FlowJo.

INTRODUCTION

Acute lymphoblastic leukemia (ALL) is the most common malignancy in children, with peaks between 2 and 5 years of age. ALL is characterized by the rapid growth of lymphoblasts in the bone marrow (BM), peripheral blood, or extramedullary locations. "Minimal, or Measurable Residual Disease" (MRD) represents a population of leukemic cells found in the bone marrow, or less frequently in the peripheral blood. These cells exhibit resistance to chemotherapy and radiation therapy, increasing the risk of relapse. They can either be residual blasts present prior to therapy or transformed secondary blasts [1,2]. Identification of MRD represents significant prognostic factor that guides therapeutic decisions, especially in pediatric cases where achieving a balance between anti-leukemic effectiveness and long-term toxicity is crucial [3–9]. During the treatment of pediatric patients with B-cell precursor ALL (BCP-ALL), the assessment of MRD involves

* To whom all correspondence should be sent:
E-mail: Alexandra.Baldzhieva@mu-plovdiv.bg

periodic monitoring of bone marrow or peripheral blood samples at various intervals. Specifically, evaluations occur at the time of diagnosis, on the 8th, 15th, and 33rd days after beginning of therapy (following BFM-type protocols), before the commencement of consolidation, before reinduction, at the conclusion of intensive therapy, and during maintenance therapy based on clinical indications [10]. Currently, prognostic significance is attributed to residual cell levels ranging from 1×10^{-4} to 1×10^{-5} cells [11]. The current emphasis is on detecting MRD at the earliest possible stage using highly sensitive, specific, and reproducible methods. As a result, there is a concerted effort in developing multiparameter flow cytometry (FC) [8–11]. Both multiparameter flow cytometry (FC) and molecular techniques such as polymerase chain reaction (PCR) can identify cancer cells at exceptionally low levels, surpassing the capabilities of conventional microscopy [11–13] (Table 1).

This study aims to investigate a new potential of FC analysis as a primary diagnostic tool for ALL [14, 15].

Although less sensitive, FC has some advantages over genetic methods, namely: applicable in more than 90% of cases, highly informative with reduced expenses and quicker processing. Yet, there are several disadvantages such as: sample processing should occur within 24 hours following collection; regeneration of bone marrow post-induction could potentially result in false-positive results; interpretation becomes challenging in cases of hypocellularity, and ongoing training is necessary [11, 12, 16, 17].

The aim of this study was to investigate the distribution of pathological cells in MRD samples stained by a standardized 8-colour methodology using FlowJo and Infinicyt multidimensional software compared to conventional FC, and to investigate whether these software tools offer additional advantages in the diagnosis and follow-up of children with ALL.

MATERIALS AND METHODS

Materials

The study included 50 children with leukemia associated immune phenotypes (BCP-ALL) diagnosed and treated in the pediatric oncohematology center in University Hospital ‘‘St. George’’ in Plovdiv, Bulgaria. The research received approval from the institutional ethics committee, and individual written informed consents were obtained from the patients’ guardians. Flow cytometry procedures were conducted at the immunological research center of Plovdiv Medical University. They were systematically assessed for the level of blasts in BM on days of proven prognostic significance, according to the BFM treatment protocol: day 15, day 33, day 78 and other time points. Half of the cases belonged to the group of other time points, followed by day 78, day 33 and day 15 with the latter representing 10% of the cases (Fig. 1).

Methods

1. Conventional approach

Methods for analysis of FC data included classical manual analysis using DIVA software version 8, and sample collection was performed using FACSAria III flow cytometer (BD Biosciences, USA). Bone marrow aspirates were stained using a standardized BCP panel consisting of the following fluorochrome-conjugated antibodies: SYTO41 Pacific Blue/ CD45 BV510/ CD58 FITC/ CD10 PE/ CD34 PerCP-Cy5.5/ CD38 PE-Cy7/ CD19 APC/ CD20 APC-Cy7 (BD Biosciences, USA). All samples were processed within 24 to 48 hours of collection.

Table 1. Comparison between the sensitivity of the different methods available for MRD assessment

Sensitivity of different methods for evaluation of MRD				
Standard 4–8 colors, flow cytometry	Real-time quantitative polymerase chain reaction (RQ-PCR)	Reverse transcription polymerase chain reaction with (RT-PCR)	Digital droplet polymerase chain reaction	Next-generation sequencing
10^{-4*}	10^{-5}–10^{-6}	10^{-5}–10^{-6}	10^{-5}–10^{-6}	10^{-6}

*one blast cell in 10 000 bone marrow cells

2. Manual multidimensional approach

The third approach to analyze the 8-colour panel data was with Infinicyt multi-dimensional software using manual analysis, version 2.0.4. The developed algorithm for FC analysis using this software is thoroughly demonstrated (Fig. 2).

After exporting the FC data in fcs. format and importing it into Infinicyt, a new workspace was created. The raw data was cleaned from "debris"

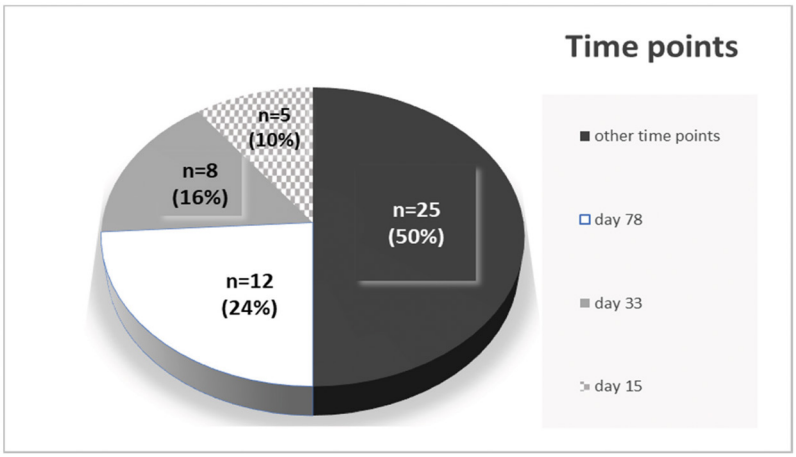

Fig. 1. Distribution of patients according to time point of flow cytometry assessment.

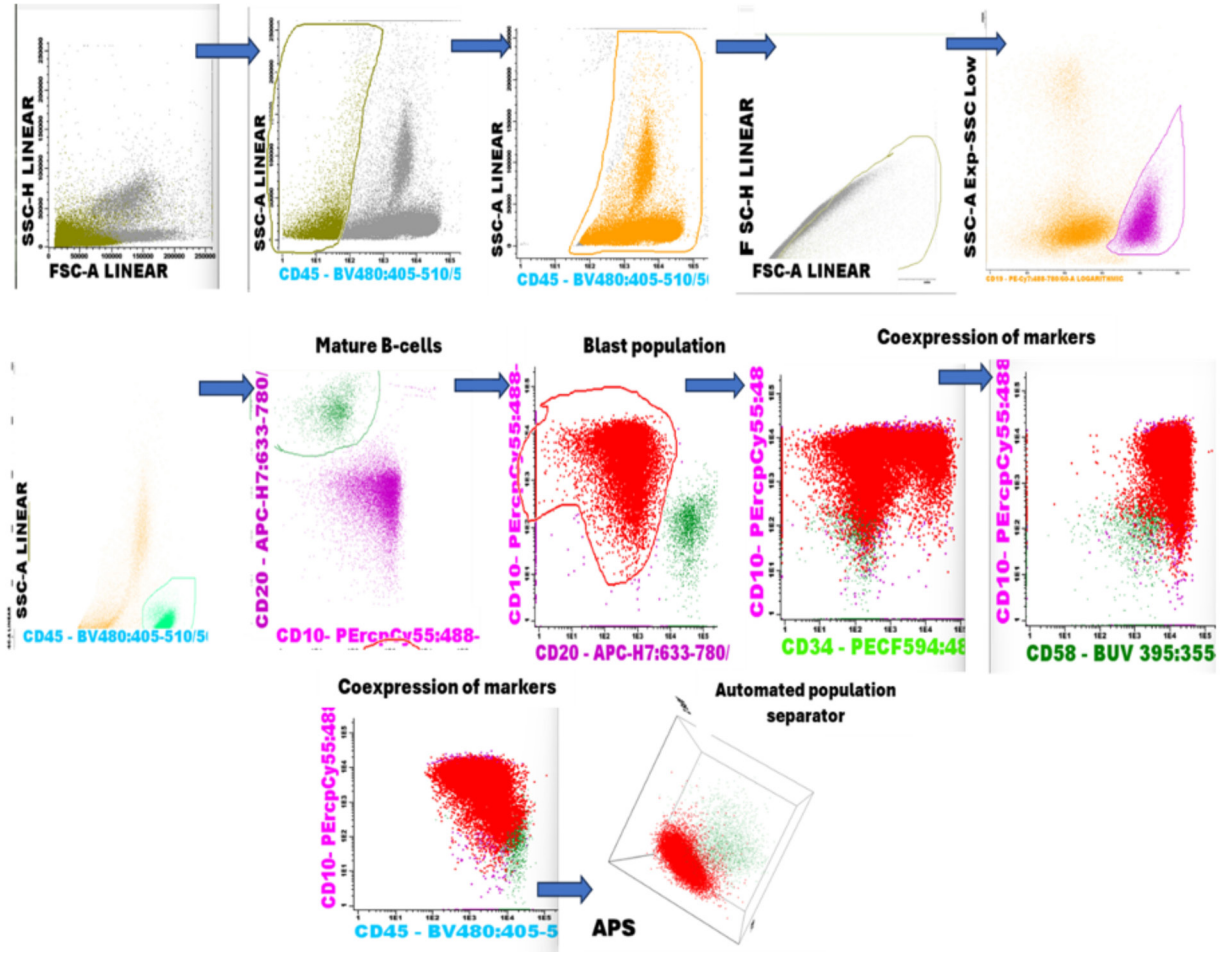

Fig. 2. Analysis algorithm with Infinicyt software.

and non-nucleated events by selecting CD45 negative events, then only nucleated CD45+ events were selected on CD45/SSC dot plot. This was followed by removal of doublets and selection of single cells only. The B-cell population was delineated based on CD19 expression, and T cells served as a negative control. Analysis of normal B-cell subpopulations was performed as well as identification of blasts based on aberrant marker expression within the B-cell population. This was followed by presentation of dot plots with co-expression of the respective markers and finally visualization using an automated cell separator (APS).

3. Semi-automated approach

The second approach was by using FlowJo semi-automated software version 10.8.1 as well as its corresponding plugins – FlowAI, flowClean, tSNE, UMAP, FlowSOM, Xshift, Phenograph, ClusterExplorer. The developed algorithm for semi-automated FC analysis is thoroughly demonstrated (Fig. 3).

A) The bivariate plot illustrates a variation in the quality of collected events. B) FlowAI plugin was applied in the first cleaning step to select only the good events (C). D) A gate based on FSC/SSC removed "debris" in the lower left corner. E) Another gate excluded doublets and selected single cells. F) CD19/SSC gating was employed to choose CD19+ events representing the B-cell population. G) FlowJo's tSNE or UMAP plugins reduced the fluorescence parameters to a bivariate plot, with individual subpopulations marked in different colors. H) Automated clustering of individual subpopulations with any of the FlowSOM, Phenograph and Xshift plugins was done. I) Subsequent visualization of phenotypic characterization using ClusterExplorer. At this stage, the cluster corresponding to the malignant population was determined by the combination of phenotypic markers.

4. Statistical Analysis

To test the equality of frequency distributions between results from conventional software and

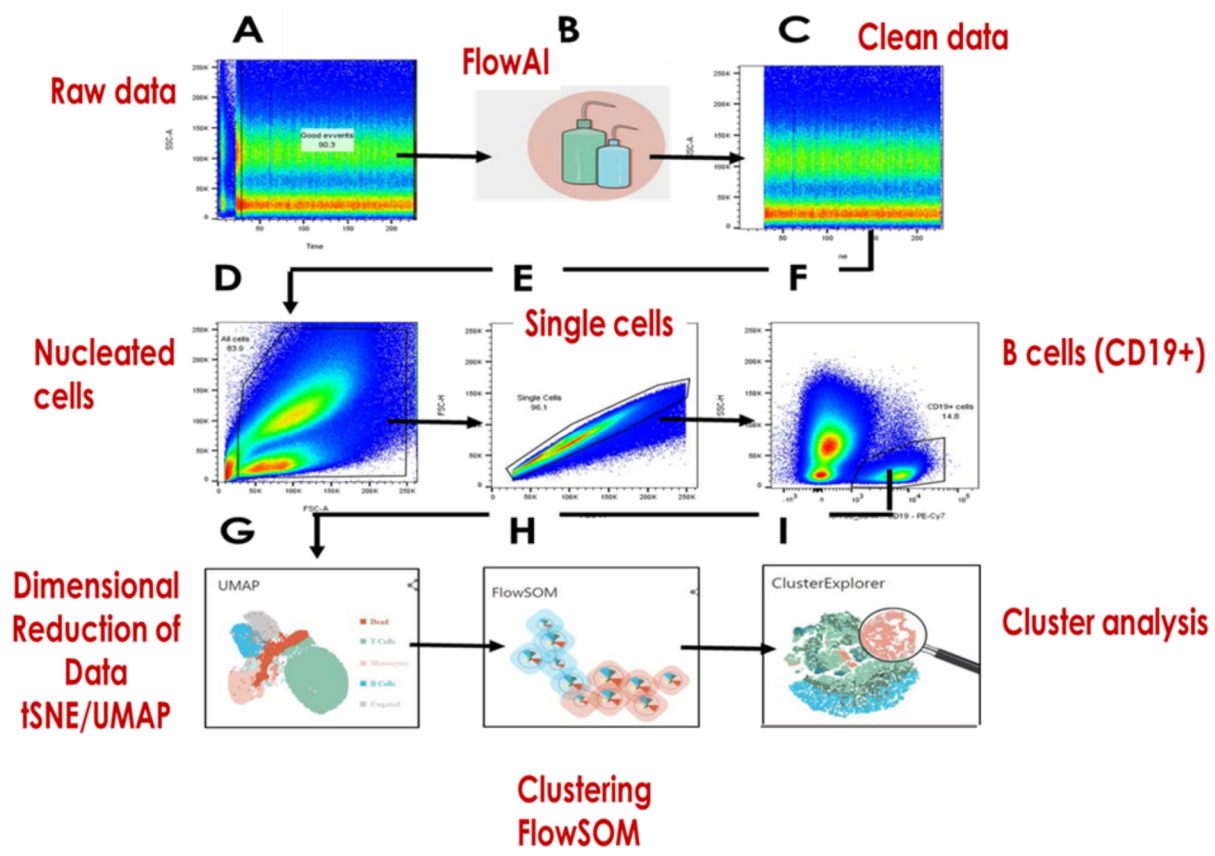

Fig. 3. Analysis algorithm with FlowJo software.

multivariate tools (Infinicyt and FlowJo), Friedman's correlated samples test was applied.

RESULTS

Friedman's test revealed no statistically significant difference ($p > 0.05$) between conventional software and multidimensional tools (Infinicyt and FlowJo) in the assessment of blast cell percentages (Fig. 4). Interestingly, the semi-automated cluster analysis tools not only identified the main cell populations but also successfully detected small subpopulations that proved challenging to discern with manual tools. This observation underscores the enhanced capability of semi-automated methods to detect cellular heterogeneity, presenting a valuable advantage in the comprehensive analysis of cell populations in comparison to conventional approaches.

Moreover, our findings provide evidence that populations appearing homogeneous on conventional two-dimensional dot plots can be further subdivided into distinct subclones through the application of semi-automated tools (Figs 5 and 6). This subclonal dissection not only gives additional information for the individual patient but also serves as a valuable strategy to mitigate the risk of subjective errors associated with manual analysis. The ability to distinguish subclonal diversity within seemingly homogeneous populations is a significant advancement, enhancing the precision of cellular characterization. This is crucial for a more comprehensive understanding of hematologic malignancies. This insight underscores the potential of semi-automated tools, such as FlowJo, to provide a more detailed perspective on cellular populations, thereby contributing to the refinement of diagnostic and therapeutic approaches for individualized patient level.

DISCUSSION

The progression of software capabilities has ushered in a transformative era in the realm of multidimensional analysis of FC data. The integration of unsupervised approaches has notably elevated the reproducibility of analyses, mitigating the reliance on manual gates through the implementation of automated identification processes for distinction of cell populations [18, 19]. The potential of automated FC approaches, particularly in the context of standardized sample analysis for hematologic malignancies, stands as a promising advancement. The ability of such tools to streamline the analysis process positions them as valuable complementary resources, particularly in cases demanding a more detailed examination of data. Furthermore, the incorporation of

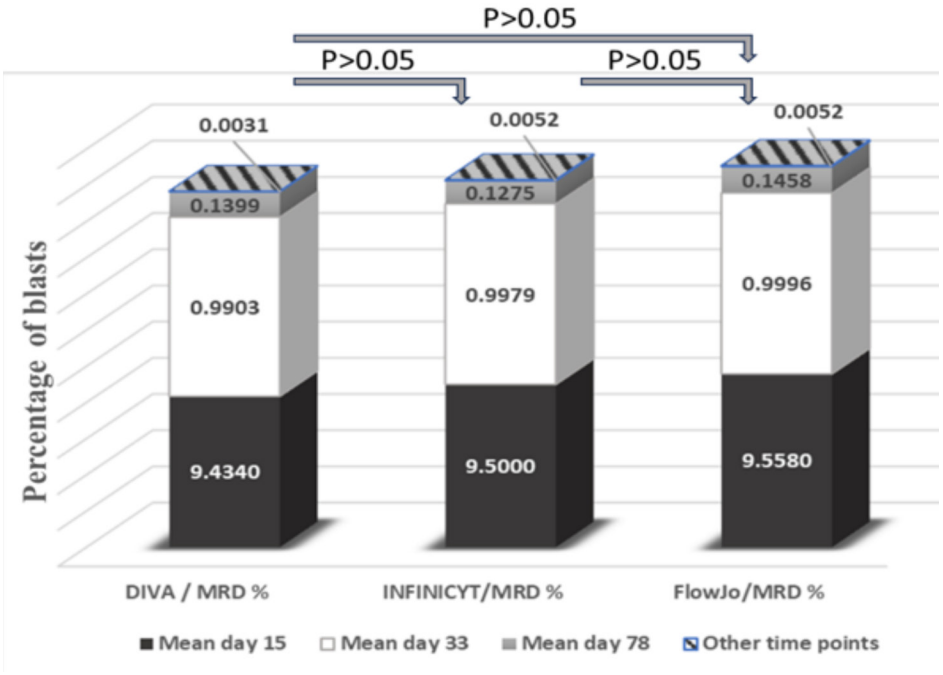

Fig. 4. Comparison between the mean values of the different time points assessed by DIVA, Infinicyt and FlowJo software.

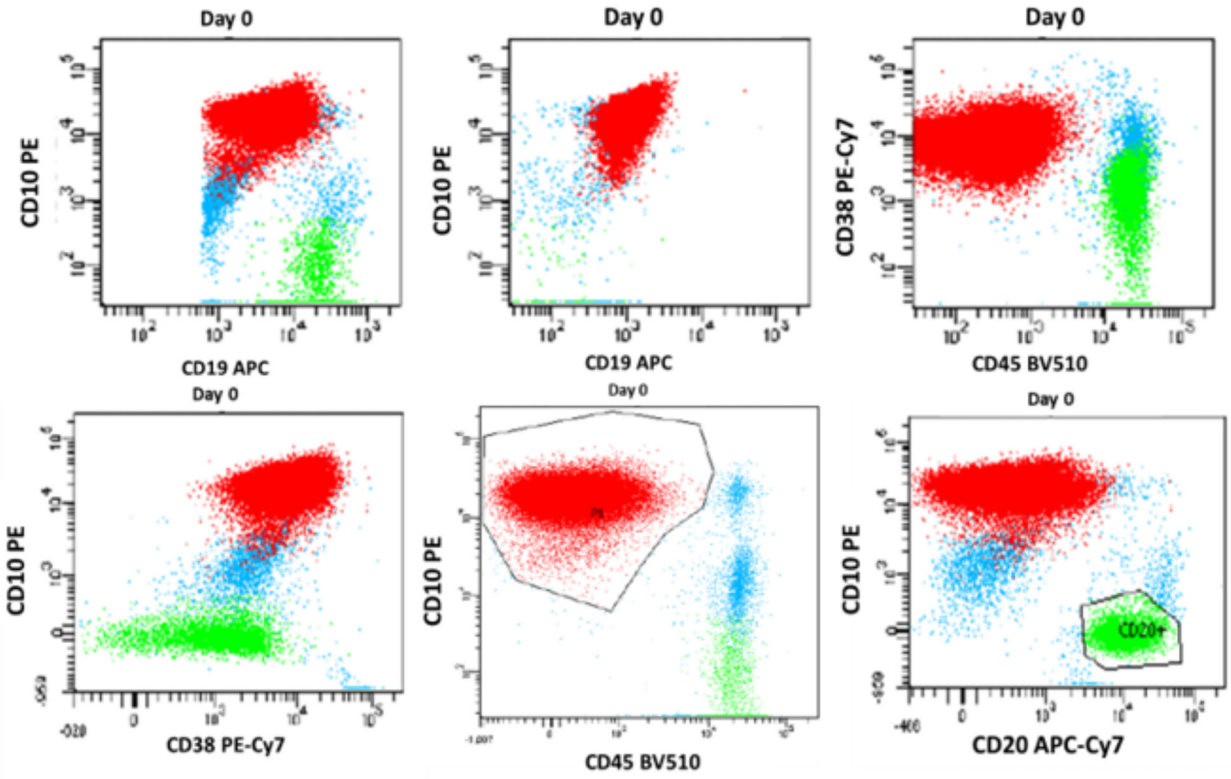

Fig. 5. Result at diagnosis (Day 0) of BCP-ALL using conventional DIVA software (93% blasts). The blast population in red has a homogeneous appearance.

semi-automated tools serves a crucial role in minimizing the risk of subjective mistakes, a potential pitfall in manual analyses. Integration of semi-automated tools emerges not only as an approach for validation of conventional results but also against interpretive errors, highlighting the importance they play in advancing the field of flow cytometry. This paradigm shift towards semi-automation not only reinforces the foundations of FC analysis but also holds promise for future developments in the understanding of cellular dynamics and heterogeneity in onco-hematological diseases [20]. Notably, the application of automated cluster analysis, underpinned by principal component analysis and regression mathematical models, extends its reach beyond the identification of major populations. It allows characterization of smaller subpopulations (e.g. FlowSOM plugin). This approach not only facilitates the identification of homogenous populations on bivariate diagrams but also unveils the capacity to detect subclones within visibly homogeneous groups [21]. The noteworthy concordance observed between results derived from conventional analyses and those employing multidimensional tools in patients with childhood ALL further attests to the efficacy and reliability of automated FC methodologies [21]. Despite these advantages, a pertinent challenge remains the requirement for standardized antibody combinations [21]. As technology continues to evolve, addressing such limitations and looking for a more comprehensive standardization will be imperative for realizing the full potential of automated FC in enhancing the understanding and management of hematologic malignancies.

CONCLUSIONS

In conclusion, the usage of semi-automated tools (FlowJo) in FC analysis marks a substantial stride towards enhancing the robustness and efficiency of conventional FC methodologies. Notably, these tools not only corroborate the findings derived from traditional FC analyses but also introduce a layer of simplification to the analytical process.

Acknowledgments: *This research was funded by the projects: Project BG05M2OP001-1.002-0005 – Competence Center "Personalized Innovative Med-*

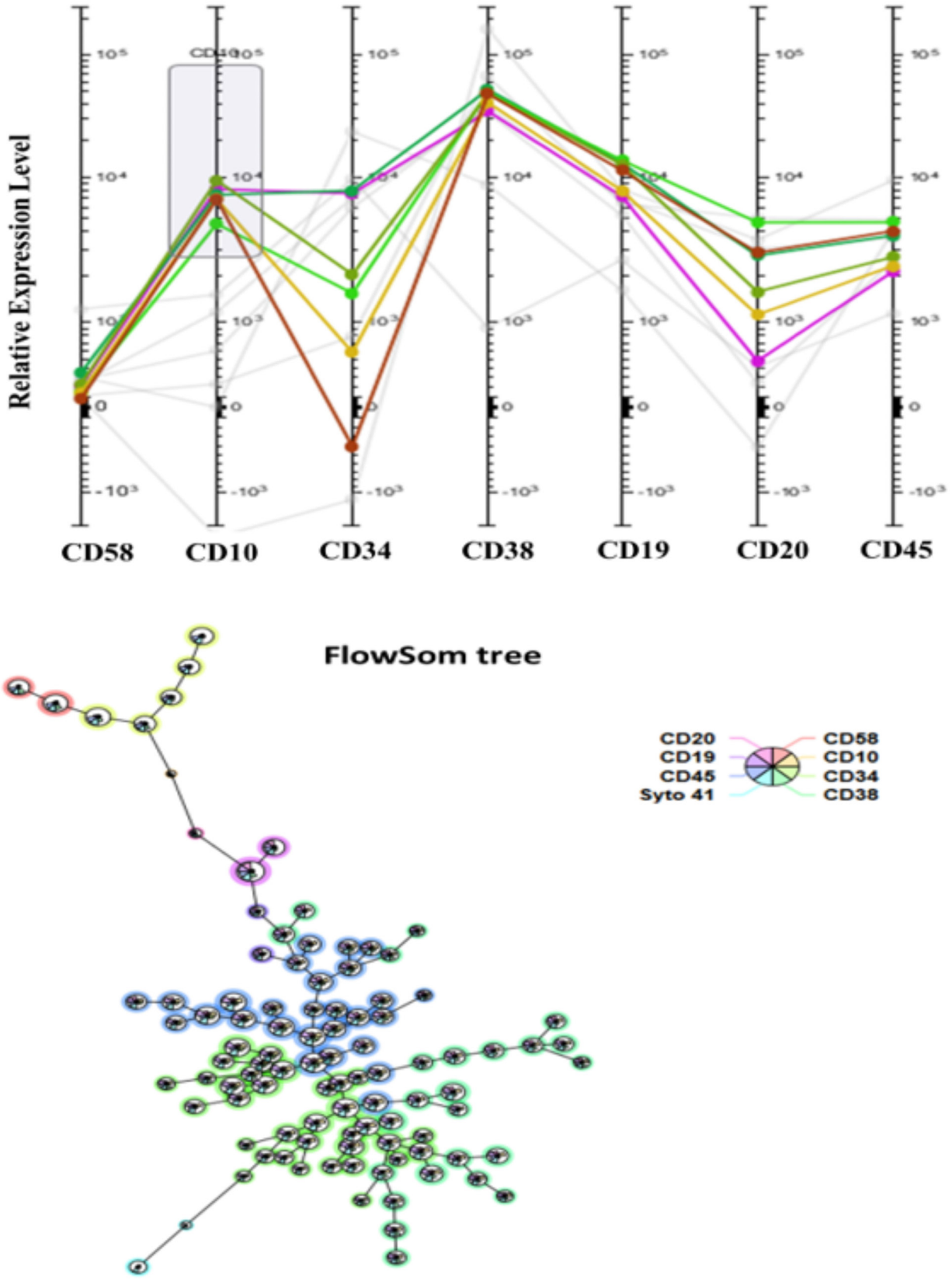

Fig. 6. Result of the same patient with BCP-ALL at diagnosis (day 0) using FlowJo software and its plugin FlowSOM (93,6% blasts). The division of the same population into several subclones is visible.

icine (PERIMED)", financed by Operational Program "Science and Education for Smart Growth", EU, ESIF; The European Union – NextGenerationEU, via the National Recovery and Resilience Plan of the Republic of Bulgaria, project no. BGRRP-2.004-0007-C01; Project "National University Complex for Biomedical Applied Research, linked to participation in BBMRI-ERIC" (NUKB-PI-BBMRI.BG), Contracts D01-285/17.12.2019 and D01-395/18.12.2020, within the National Road Map of scientific infrastructure (2020–2027) and Project of Medical University Plovdiv: ∂n/∂n-01/23 Development of an algorithm for automated analysis of multiparameter flow cytometric data on B-lymphocyte subpopulations.

REFERENCES

1. T. Szczepański, M. J. Willemse, W. A. Kamps, E. R. van Wering, A. W. Langerak, J. J. van Dongen, *Med. Pediatr. Oncol.,* **36**(3), 352 (2001).
2. A. S. Rosenberg, A. Brunson, J. K. Paulus, J. Tuscano, T. Wun, T. H. M. Keegan et al., *Blood Cancer Journal*, **7**(9), e605 (2017).
3. C. S. Hourigan, R. P. Gale, N. J. Gormley, G. J. Ossenkoppele, R. B. Walter, *Leukemia*, **31**(7), 1482 (2017).
4. B. D. Smith, A. W. Roberts, G. J. Roboz, M. DeWitte, A. Ferguson, L. Garrett et al., *Blood*, **126**(23), 3819 (2015).
5. T. Prebet, S. Bertoli, J. Delaunay, A. Pigneux, E. Delabesse, M. J. Mozziconacci et al., *Haematologica*, **99**(10), e185 (2014).
6. J. Lambert, J. Lambert, O. Nibourel, C. Pautas, S. Hayette, J.-M. Cayuela, et al., *Oncotarget*, **5**(15), 6280 (2014).
7. H. Cavé, J. van der Werff ten Bosch, S. Suciu, C. Guidal, C. Waterkeyn, J. Otten, et al., *New England Journal of Medicine*, **339**(9), 591 (1998).
8. A. Kruse, N. Abdel-Azim, H.N. Kim, Y. Ruan, V. Phan, H. Ogana, W. Wang, R. Lee, E. J. Gang, S. Khazal, Y. M. Kim, *Int. J. Mol. Sci*., **21**(3), 1054 (2020).
9. I. S. Kim, *Blood Res*., **55**(S1), S19 (2020).
10. D. Campana, C.-H. Pui, *Blood*, **129**(14), 1913 (2017).
11. T. Szczepański, *Leukemia*, **21**(4), 622 (2007).
12. I. Abou Dalle, E. Jabbour, N. J. Short, *Ther. Adv. Hematol*., **11**, (2020).
13. M. J. Pongers-Willemse, O. J. Verhagen, G. J. Tibbe, A. J. Wijkhuijs, V. de Haas, E. Roovers, C. E. van der Schoot, J. J. van Dongen, *Leukemia*, **12**(12), 2006 (1998).
14. T. Terwilliger, M. Abdul-Hay, *Blood Cancer*, **J7**(6), e577 (2017).
15. K. Hein, N. Short, E. Jabbour, M. Yilmaz, *Blood Lymphat Cancer*, **12**, 7 (2022).
16. I. Della Starza, S. Chiaretti, M. S. De Propris, L. Elia, M. Cavalli, L. A. De Novi, et al., *Frontiers in Oncology*, **9**, 726 (2019).
17. J. J. M. van Dongen, V. H. J. van der Velden, M. Brüggemann, A. Orfao, *Blood*, **125**(26), 3996 (2015).
18. M. C. Béné, F. Lacombe, A. Porwit, *Int. J. Lab. Hematol*., **43**, 54 (2021).
19. L. Lhermitte, E. Mejstrikova, A. J. van der Sluijs-Gelling, G. E. Grigore, L. Sedek, A. E. Bras, G. Gaipa, E. Sobral da Costa, M. Novakova, E. Sonneveld, C. Buracchi, T. de Sá Bacelar, J. G. Te Marvelde, A. Trinquand, V. Asnafi, T. Szczepanski, S. Matarraz, A. Lopez, B. Vidriales, J. Bulsa, O. Hrusak, T. Kalina, Q. Lecrevisse, M. Martin Ayuso, M. Brüggemann, J. Verde, P. Fernandez, L. Burgos, B. Paiva, C.E. Pedreira, J. J. M. van Dongen, A. Orfao, V. H. J. van der Velden, *Leukemia*, **32**(4), 874 (2018).
20. E. S. Costa, C. E. Pedreira, S. Barrena, Q. Lecrevisse, J. Flores, S. Quijano, J. Almeida, M. del Carmen García-Macias, S. Bottcher, J. J. Van Dongen, A. Orfao, *Leukemia*, **24**(11), 1927 (2010).
21. B. Kárai, K. Tisza, O. Eperjesi, A. C. Nagy, A. Ujfalusi, Á. Kelemen, I. Szegedi, C. Kiss, J. Kappelmayer, Z. Hevessy, *Cancers*, **13**, 5044 (2021).

Bulgarian Chemical Communications, Volume 55, Special Issue C (pp. 25–32) 2023 *DOI: 10.34049/bcc.55.C.0002*

Molecular genetic research in oncology – when, what and why

H. Ivanov[1], V. Popov[2], G. Raycheva[2], A. Linev[1], N. Miteva-Marcheva[1], D. Dimitrov[1], M. Topalov[1], V Stoyanova[1], V. Goranova-Marinova[3], Zh. Grudeva-Popova[2]

[1] *Department of Pediatrics and Medical Genetics, Medical University Plovdiv*
[2] *Department of Clinical Oncology, Medical University Plovdiv*
[3] *First Department of Internal Medicine, Section of Hematology, Medical University Plovdiv*

Received: November 2023; Revised: December 2023

Molecular tests, integral to clinical oncology, are routinely employed for diagnosing hereditary cancer syndromes. Healthy carriers of cancer-predisposing mutations can avail rigorous medical surveillance and preventive measures. Germ-line mutation-induced cancers often necessitate significant treatment strategy modifications. Personalized cancer drug selection, based on actionable mutations, is now a therapy cornerstone. The administration of inhibitors like EGFR, BRAF, ALK, ROS1, PARP, and other cytotoxic/targeted drugs is guided by molecular tests. Tumors invariably shed fragments (single cells, clusters, DNA, RNA, proteins) into various body fluids. The liquid biopsy, analyzing circulating DNA or other tumor-derived molecules, offers potential for non-invasive cancer monitoring, drug-sensitizing mutation analysis, and early cancer detection. Specific mutations and expression markers can effectively diagnose cancers of unknown primary origin (CUPs). Systematic tumor molecular portrait cataloging is likely to reveal new medically relevant DNA- and RNA-based markers. Pharmacogenetics understands how genetic variations influence individual drug responses. This knowledge aids in predicting positive patient responses to specific drugs, contributing to cancer therapy personalization. Integrating molecular tests, including pharmacogenetics, into clinical oncology has opened new diagnosis and treatment avenues. It has enabled cancer therapy personalization, improved early detection, and provided valuable tumor biology insights. As our cancer genetics understanding continues to grow, these tools will undoubtedly play an increasingly important role in improving patient outcomes.

Keywords: pharmacogenetics, oncology, liquid biopsy, cancer therapy personalization.

INTRODUCTION

Molecular genetic diagnostics, has revolutionized oncology by facilitating the detection of individual biological molecules. This approach has enabled a more precise and personalized treatment strategy, shifting the paradigm from a one-size-fits-all model to targeted therapies. The potential of molecular genetic tools was first acknowledged by oncohematologists, who recognized the diagnostic value of specific chromosomal translocations in various leukemias and lymphomas. For instance, the Philadelphia chromosome, a specific chromosomal abnormality that results from a translocation between chromosome 9 and 22, is a well-known hallmark of chronic myeloid leukemia [1]. Similarly, the translocation t(14;18), resulting in the overexpression of the BCL2 gene, is commonly observed in follicular lymphomas [2]. The advent of user-friendly methods of molecular analysis has revolutionized the field of molecular oncology. A significant breakthrough in this regard was the invention of the Polymerase Chain Reaction (PCR) by Kary Mullis in 1983 [3]. This technique, which allows for the amplification of specific DNA sequences, has had a profound impact on clinical DNA testing. PCR-based techniques are highly compatible with clinical routines. They can be used for a wide range of applications, including the detection of specific gene mutations associated with cancer, the identification of minimal residual disease, and the prediction of response to therapy [4]. Immunohistochemistry (IHC), a technique that enables the visualization of specific antigens within tissue, has played a pivotal role in the field of personalized oncology.

* To whom all correspondence should be sent:
E-mail: doctorhristoivanov@yahoo.com

One of the most significant applications of IHC is in the determination of the level of expression of the estrogen receptor (ER) in breast cancer tissues [5]. The ER status of a breast cancer, determined by IHC, is a critical factor in guiding the treatment strategy. ER-positive breast cancers, which express the estrogen receptor, are typically sensitive to endocrine therapy. Thus, IHC has revolutionized the treatment of breast cancer by enabling the tailoring of endocrine therapy based on the ER status of the tumor, determined through a laboratory test [6]. In addition to its role in breast cancer, IHC has also been instrumental in other areas of oncology. For instance, in colorectal cancer, IHC is used to test for Microsatellite Instability (MSI), a condition that leads to an increased mutation rate within the cancer cells. MSI status, determined by IHC, can influence the choice of therapy. Colorectal cancers with high MSI (MSI-H) have been found to respond well to immunomodulating therapy with immune checkpoint inhibitors [7].

Molecular tests have become an indispensable component of standard patient management in oncology, particularly in two key areas. Firstly, the identification of individuals with hereditary cancers, such as BRCA1 and BRCA2 mutations linked to breast and ovarian cancer, has become a routine practice in clinical oncology. This allows for early detection and preventive measures in individuals at high risk [8]. Secondly, numerous molecular tests, help select the most effective treatment based on the molecular characteristics of tumor tissues or other biological parameters of malignant disease. These tests can predict the likelihood of disease recurrence and guide decisions about whether chemotherapy is necessary in addition to hormone therapy [9].

There are also additional applications of molecular diagnostics in the developmental stage. For instance, modern molecule-oriented techniques, such as liquid biopsy, which virtually have no sensitivity limit, are being intensively explored for monitoring residual cancer disease and early tumor detection. This technique analyzes circulating tumor DNA (ctDNA) in the blood to detect minimal residual disease following treatment, monitor response to therapy, and detect relapse at the earliest possible stage [10]. Moreover, DNA and RNA assays, such as next-generation sequencing (NGS), can assist in differentiating between tumors of distinct histologic origin. This is particularly useful for diagnosing cancers of unknown primary site (CUPs), a condition where metastatic cancer is identified, but the location of the primary tumor is unknown [11].

Lastly, we underscore the role of Pharmacogenetic studies in predicting drug toxicity and effectiveness. These studies, conducted on DNA and/or tumor cells, have emerged as a powerful tool in the field of personalized medicine [12]. By examining specific genes that encode for drug-metabolizing enzymes, transporters, or targets, pharmacogenetic studies can help predict an individual's response to a particular drug, both in terms of its therapeutic effect and potential toxicity [13].

The aim of this article is to provide a comprehensive overview of the role and impact of molecular-genetic research in oncology. It seeks to elucidate the 'when', 'what', and 'why' of various investigative techniques, their practical applications, and their implications for patient management. The article will delve into key areas such as hereditary cancer syndromes, predictive markers, circulating tumor fragments, carcinoma of unclear primary origin, and pharmacogenetic studies. The ultimate goal is to enhance understanding and stimulate further research and discussion in this critical area of oncology.

Hereditary cancer syndromes

Hereditary cancer syndromes are characterized by a collection of genetic abnormalities that significantly increase the risk of cancer. Notably, this risk is often organ-specific, enabling the implementation of targeted diagnostic and preventive measures for individuals carrying these germ-line mutations. Compared to traditional genetic diseases, hereditary cancers are considerably more prevalent. For instance, the population frequency of breast or ovarian cancers linked to BRCA1/2 gene defects is approximately 1:500 and can even reach 1:40 in certain founder populations [14]. In the Ashkenazi Jewish population, the incidence of BRCA1/2 mutation status is particularly noteworthy. Approximately 2.0% of individuals of Ashkenazi Jewish descent carry a pathogenic variant in one of these two genes, usually one of three specific variants (BRCA1: c.68_69del AG; BRCA1:c.5266dupC; BRCA2:c.5946delT), called founder mutations [15]

There are several hereditary cancer syndromes, each associated with specific types of cancer. Hereditary Breast & Ovarian Cancer Syndrome (HBOC) is associated with mutations in the BRCA1 and BRCA2 genes, leading to a significantly increased risk of developing breast and ovarian cancer [16]. Lynch Syndrome (Hereditary Non-polyposis Colorectal Cancer Syndrome) is characterized by an

increased risk of colorectal cancer and other types of cancer at a young age, and is associated with mutations in several genes, including MLH1, MSH2, MSH6, PMS2, and EPCAM [17]. Familial Adenomatous Polyposis (FAP) is associated with mutations in the APC gene, leading to the development of numerous polyps in the colon and rectum at a young age, significantly increasing the risk of colorectal cancer [18]. Cowden Syndrome (CS) is associated with mutations in the PTEN gene, leading to an increased risk of developing several types of cancer, including breast, thyroid, and endometrial cancer [19]. Peutz-Jeghers Syndrome is associated with mutations in the STK11 gene, leading to the development of characteristic pigmented spots on the lips and in the mouth, as well as polyps in the digestive tract, and an increased risk of developing several types of cancer, including gastrointestinal, breast, and gynecological cancers [20].

Hereditary cancers often exhibit unique clinical features, including early onset, the presence of multiple neoplasms, and a preference for specific histological patterns. The advent of genetic testing has revolutionized the management of hereditary cancer syndromes, facilitating early detection, personalized treatment strategies, and improved patient outcomes.

According to the National Comprehensive Cancer Network (NCCN) guidelines, molecular genetic testing for hereditary cancer syndromes is indicated when there is: a personal or family history suggestive of a hereditary cancer syndrome; early-onset cancer; multiple primary tumors; rare cancers; or several family members with the same or related forms of cancer. The guidelines also recommend genetic testing when the results can potentially impact risk management and treatment [21].

Traditionally, genetic testing is focused on single-gene analysis of specific high-risk genes. However, the advent of next-generation sequencing (NGS) has revolutionized this approach. NGS allows for the simultaneous testing of multiple genes, thereby facilitating a comprehensive analysis of cancer susceptibility genes [22]. This is particularly beneficial in cases where several genes may be implicated in a hereditary cancer syndrome, or where the genetic cause of cancer is complex and multifactorial. Multi-gene panel tests, which use NGS technology, can identify pathogenic mutations across a range of genes in a single test [23]. This not only increases the efficiency of genetic testing but also broadens our understanding of the genetic basis of hereditary cancers. As such, NGS and multi-gene panels have become a frontline approach in the identification of individuals with cancer predisposing gene variants.

In addition to multi-gene panels, whole exome sequencing (WES) by NGS is another powerful tool in the study of hereditary cancers [24]. WES involves sequencing all the protein-coding genes in a genome (known as the exome), allowing for a comprehensive analysis of cancer susceptibility genes [24]

Importantly, the use of NGS in genetic testing has the potential to identify new genes associated with hereditary cancers. As our understanding of the genetic landscape of cancer continues to grow, it is likely that more genes associated with hereditary cancer syndromes will be discovered. This underscores the clinical significance of NGS and multi-gene panel and WES analysis in hereditary cancer predisposition.

Effective treatment based on the genetic characteristics of the tumor

The advent of precision oncology has underscored the importance of tailoring cancer treatment based on the genetic characteristics of the tumor. Specific genetic alterations within the tumor, such as mutations, amplifications, or translocations, can drive cancer growth and progression [25]. These genetic aberrations can be identified through techniques such as NGS, allowing for a comprehensive genomic profile of the tumor.

Tumors harboring mutations in the KRAS, NRAS, or BRAF genes have been shown to respond to specific targeted therapies [26]. KRAS mutations are among the most common oncogenic alterations in human cancers. For a long time, these mutations were considered ‘undruggable’ due to the molecular structure of the KRAS protein, which made it difficult for drugs to bind effectively. However, recent advances in drug development have led to the creation of effective inhibitors against specific KRAS mutations [26]. One such mutation is the G12C mutation, which is common in lung and colorectal cancers. The development of KRAS G12C inhibitors represents a significant breakthrough in the treatment of cancers with this mutation. AMG 510 (Sotorasib) is the first FDA-approved specific KRAS G12C inhibitor that works irreversibly. It blocks KRAS in an inactive GDP-bound state. Preclinical studies of AMG 510 have shown that it inhibits phosphorylation of extracellular signal-regulated kinase (ERK), a critical downstream effector of KRAS, and induces

long-lasting complete tumor regression in mice bearing KRAS p.G12C tumors [27].

Similarly, BRAF mutations, particularly the V600E mutation, can be targeted by BRAF inhibitors. The V600E mutation results in a constitutively active BRAF kinase that promotes cell growth and proliferation. BRAF inhibitors work by selectively inhibiting the activity of the mutated BRAF kinase, thereby slowing down tumor growth [28].

NRAS mutations, on the other hand, can be targeted indirectly through MEK inhibitors. The NRAS protein is part of the RAS/RAF/MEK/ERK signaling pathway, which regulates cell growth and survival [29]. Mutations in NRAS can lead to the continuous activation of this pathway, promoting uncontrolled cell proliferation. MEK inhibitors work by blocking the activity of MEK, a protein downstream of NRAS in the signaling pathway, thereby inhibiting the growth of tumors with NRAS mutations. Research has shown that AML cells with NRAS mutations are dependent on continued oncogene expression, both in vitro and in vivo [30]. MEK inhibitors, such as PD0325901 or trametinib, have been used in preclinical studies to treat primary Nras-mutant AMLs. These treatments significantly prolonged survival and reduced proliferation but did not induce apoptosis, promote differentiation, or drive clonal evolution.

In the context of melanoma, studies have also shown the potential of MEK inhibitors in treating NRAS mutant melanoma [31]. However, all these findings are from preclinical studies and more research is needed to validate these results in clinical settings.

Rearrangements in the anaplastic lymphoma kinase (ALK) and c-ros oncogene 1 receptor tyrosine kinase (ROS1) genes have emerged as significant actionable targets in cancer therapy [32]. These genetic rearrangements are frequently observed in non-small cell lung carcinoma (NSCLC), a common type of lung cancer [33].

The presence of these rearrangements is associated with distinct clinical and pathological features. Patients with these rearrangements are often younger, have a milder or no history of smoking, and exhibit adenocarcinoma histology (34). Moreover, these rearrangements have been found to contribute to the metastasis of NSCLC by promoting cell migration and invasion [34].

Targeted therapies, such as ALK inhibitors (Crizotinib; Ceritinib; Alectinib Brigatinib; Ensartinib; Lorlatinib), have been developed to specifically act against tumors harboring these genetic rearrangements. The use of ALK inhibitors has led to significantly improved survival benefits [35]. However, the clinical benefits of ALK inhibitors are almost universally limited by the emergence of drug resistance. Therefore, continued research into new drugs and combination therapies is required to improve outcomes in NSCLC. The ultimate goal is to enhance the efficacy of these targeted therapies and improve the prognosis for patients.

Furthermore, mutations in the BRCA1/2 genes, particularly in the context of Hereditary Breast and Ovarian Cancer Syndrome (HBOC), have been effectively targeted by Poly (ADP-ribose) polymerase (PARP) inhibitors [36]. These inhibitors, such as olaparib (Lynparza), rucaparib (Rubraca), and niraparib (Zejula), are particularly effective against tumors carrying mutations in the BRCA1 and BRCA2 tumor suppressor genes [37]. PARP inhibitors work by blocking the activity of PARP, a protein that helps cells repair damaged DNA. In the presence of BRCA1/2 mutations, cells are already deficient in one mechanism of DNA repair. By blocking PARP, these drugs further hinder the cell's ability to repair DNA damage, leading to the accumulation of DNA damage and, ultimately, cell death [37]. The FDA has approved four PARP inhibitors to treat cancers with BRCA1/2 mutations [38]. These drugs have shown significant clinical outcomes in treating BRCA1/2 deficient cancers. Treatment with rucaparib improves how long some people with metastatic prostate cancer live without their cancer getting worse. Among patients whose tumors had BRCA mutations, progression-free survival was 11.2 months in those treated with rucaparib and 6.4 months in those who were treated with any of three other commonly used drugs for this form of prostate cancer [39]. Ongoing preclinical and clinical studies are exploring how to combine the PARPi with immuno-oncology drugs to further improve clinical outcomes [38]

The use of genetic testing and targeted therapies based on the genetic characteristics of the tumor represents a paradigm shift in cancer treatment. By matching the treatment to the genetic makeup of the tumor, precision oncology aims to improve the efficacy of therapy, minimize side effects, and ultimately, enhance patient outcomes. However, challenges remain, including the development of resistance to targeted therapies and the need for ongoing monitoring of the tumor's genetic landscape to capture the emergence of new alterations. As our understanding of the genetic basis of cancer continues to grow, so too will the potential of precision oncology to transform cancer treatment.

Liquid biopsy

Liquid biopsy, a non-invasive diagnostic tool, has emerged as a revolutionary technique in the field of oncology [40]. It involves the analysis of bodily fluids, primarily blood, to detect circulating tumor cells (CTCs) or circulating tumor DNA (ctDNA) [41]. As tumors grow, they shed cells and DNA fragments into the bloodstream, which can be detected and analyzed using liquid biopsy. This technique provides a comprehensive snapshot of the tumor's genetic landscape, enabling the detection of specific genetic alterations that can guide personalized treatment strategies [41]

This method, has shown promise in various clinical scenarios:

1. *Early Cancer Detection:* Liquid biopsy can detect cancer at an early stage, which is crucial for improving quality of life, survival rates, and reducing the financial burden of cancer treatments [42]. It has been utilized for the early detection of solid cancers and concentration of tumor DNA in the bloodstream can provide an indication of the cancer's advancement [43].

2. *Monitoring Treatment Response:* Liquid biopsies can be used to monitor cancer progression, track a patient's response to treatment [44], or as a surveillance method for individuals who have completed treatment but are at high risk of disease recurrence [45]. For instance, in individuals with non-metastatic pancreatic cancer, liquid biopsies have been demonstrated to diagnose surgically removable tumors [46].

3. *Tracking Minimal Residual Disease (MRD):* MRD refers to the presence of disease undetectable by conventional clinical and imaging methods [40]. Liquid biopsies can detect MRD, enabling the detection of circulating tumor DNA (ctDNA), circulating tumor cells (CTC), or tumor-specific microRNA. These liquid biopsy markers not only enhance our understanding of the disease but also pave the way for personalized medicine, where treatment decisions are tailored to the individual patient's disease profile.

Despite its potential, several challenges need to be addressed to fully realize the clinical utility of liquid biopsy:

1. *Sensitivity and Specificity*: Many liquid biopsy strategies being developed for early detection of cancer lack the sensitivity required to detect early-stage cancers. Additionally, the small amounts of tumor-derived components shed into the circulation can limit the detection of cancer at early stages (47].

2. *Standardization and Reproducibility:* There is a lack of preclinical and clinical standardization, which has so far hindered the development of an algorithm for precise tumor profiling [48].

3. *Technical Challenges:* Isolating circulating tumor cells (CTCs) can be technically more challenging than isolating cfDNA [48].

Liquid biopsy is a powerful tool, and significant advances in this technology have impacted multiple aspects of precision oncology, from early diagnosis to management of refractory metastatic disease [48]. The goal is not to select and refine a single approach to liquid biopsy. In fact, the synergy of multiple circulating biomarkers can reveal the specifics of a cancer. Future research may focus on fluids beyond blood, such as ascites, effusions, urine, and cerebrospinal fluid, as well as methylation patterns and elements such as exosomes. The FDA has approved several liquid biopsy tests, such as Guardant360 CDx and FoundationOne Liquid CDx, which check for multiple cancer-related genetic changes [41]. These tests can assist doctors in selecting the best treatments for some people with cancer. Liquid biopsy tests are currently used for non-small cell lung cancer, advanced breast cancer, colorectal cancer, and prostate cancer [41].

Liquid biopsy holds great promise for both healthy individuals and those diagnosed with cancer. For healthy individuals, it could serve as a routine prescreening method to identify those who may have early-stage cancer. For cancer patients, it provides valuable information about cancer cells that can help healthcare providers plan treatment and management.

Carcinoma of unclear primary origin (CUP)

The diagnosis of carcinoma of unclear primary origin (CUP) remains a significant challenge in oncology. Approximately 3–5% of patients with newly diagnosed metastatic disease have an unknown organ or tissue origin for these metastases [49]. In many cases, the inability to make the correct diagnosis is solely due to limitations in tumor imaging techniques. Even autopsy fails to identify the primary tumor in 15–45% of cases [49].

The diagnostic approach in patients with CUP largely relies on common clinical judgment, anatomical localization of metastases, gender of the patient, and habits such as smoking [50]. Immunohistochemistry, which uses a spectrum of tissue-specific markers, is the gold standard for the clinical analysis of CUP. However, it has several

limitations. Many expression-based markers are not sufficiently specific for a given tumor type. Some proteins are expressed at low levels and therefore cannot be detected by conventional antibody-based methods [51]. The range of diagnostic antibodies is limited to those marketed by biotechnology companies, and interpretation of immunohistochemistry results is subject to interlaboratory variation.

DNA- and RNA-based tests may offer advantages over immunohistochemistry. Certain mutations are highly characteristic of specific types of cancer. For instance, the presence of a TKI-sensitizing somatic mutation in EGFR in tumor tissue aids in diagnosing lung cancer [52], and detection of a BRCA1/2 germline mutation in a patient with adenocarcinoma of unknown primary site prompts consideration of breast or ovarian cancer as the most likely tumor variety [53].

RNA expression markers can outperform some immunohistochemical tests. The development of personalized PCR diagnostic tests, which can be performed in any molecular genetics laboratory without the need for industrial facilities, opens up new avenues for the diagnosis and management of CUP [54]. This advancement brings us closer to the era of personalized medicine, offering hope for improved patient outcomes.

Despite the challenges posed by CUP, these innovative methods offer a beacon of hope. They not only enhance the accuracy of diagnosis but also pave the way for personalized treatment strategies, thereby bringing us closer to the era of personalized medicine. However, the journey is far from over. The field continues to evolve, and further research is needed to overcome the existing limitations and to fully harness the potential of these advanced techniques.

Pharmacogenetic studies

Pharmacogenetic studies have emerged as a powerful tool in the field of personalized medicine, underscoring the role of genetic variations in predicting drug toxicity and effectiveness [55]. These studies, conducted on DNA and/or tumor cells, provide insights into how an individual's unique genetic makeup influences their response to drugs [55]. By examining specific genes that encode for drug-metabolizing enzymes, transporters, or targets, pharmacogenetic studies can help predict an individual's response to a particular drug, both in terms of its therapeutic effect and potential toxicity [53]. In the realm of cancer genomics, many studies have traditionally focused on acquired, somatic mutations [54;55]. These are mutations that are unique to tumor cells and occur in genes encoding proteins that play a central role in the hallmark processes that dictate malignant growth. They are acquired randomly following exposure to agents that have the potential to damage DNA in cells [54]. In the context of cancer, these somatic mutations accumulate in the cancer cells and are commonly used as drug targets [54].

However, increasing evidence shows that inherited germline genetic variations also play a key role in cancer risk and treatment outcome [56]. For example, variations in the DPYD gene can affect the metabolism of 5-fluorouracil, a commonly used drug in the treatment of various cancers. Patients with certain DPYD variants may experience severe toxicity when treated with standard doses of 5-fluorouracil [56].

These examples underscore the importance of pharmacogenetics in oncology, as understanding these genetic variations can lead to more personalized and effective treatment strategies, thereby improving patient outcomes and reducing adverse drug reactions.

CONCLUSION

We are currently in the midst of a transformative era in medical research. The advent of Next-Generation Sequencing has revolutionized the field, enabling the analysis of germline variants in DNA, somatic mutations, and RNA profiles. This has led to a continuous accumulation of data, paving the way for the identification of new hereditary syndromes, molecular targets for targeted cancer therapy, tumor-specific diagnostic markers, and pharmacogenetic options for a personalized approach.

However, it is important to acknowledge the challenges that come with this progress. The clinical integration of even relatively simple and straightforward assays, such as BRCA1/2 analysis or EGFR mutation testing, took years, and many questions remain unresolved. The complexity of these processes underscores the intricacies involved in translating research findings into clinical practice. Furthermore, the management of the huge influx of new candidate markers poses a significant challenge. These markers, represented by multiple rare and diverse molecular events, cannot be clinically validated on an individual basis due to their rarity and diversity. This raises questions about how clini-

cal medicine will adapt to accommodate this wealth of information. Despite these challenges, the potential benefits of these advancements are immense. They hold the promise of transforming patient care by enabling more precise diagnoses, more effective treatments, and ultimately, better patient outcomes. The profound impact of molecular diagnostics in oncology is undeniable, providing clinicians with invaluable tools for accurate diagnosis, prognosis, and therapeutic decision-making. As our understanding of the molecular underpinnings of cancer continues to grow, so too will the role of molecular diagnostics in guiding cancer management. This ongoing evolution underscores the dynamic nature of medical research and its potential to shape the future of oncology.

Acknowledgments: *Project BG05M2OP001-1.002-0005 – Competence Center "Personalized Innovative Medicine (PERIMED)", financed by Operational Program "Science and Education for Smart Growth", EU, ESIF.*

REFERENCES

1. F. Mitelman, B. Johansson, F. Mertens, *Nat. Rev. Cancer*, **7**(4), 233 (2007).
2. 2. Y. Tsujimoto, J. Cossman, E. Jaffe, C. M. Croce, *Science*, **228**(4706), 1440 (1985).
3. K. Mullis, F. Faloona, S. Scharf, R. Saiki, G. Horn, H. Erlich, *Cold Spring Harb Symp Quant Biol.*, **51**, 263 (1986).
4. F. Diehl, M. Li, D. Dressman, Y. He, D. Shen, S. Szabo, L. A. Jr. Diaz, S. N. Goodman, K. A. David, H. Juhl, K. W. Kinzler, B. Vogelstein, *Proc. Natl. Acad. Sci.*, **102**(45), 16368 (2005).
5. S. Magaki, S. A. Hojat, B. Wei, A. So, W. H. Yong, *Methods Mol Biol*., **1897**, 289 (2019)
6. L. Saya, L. Jacob, L. A. Huppert, H. S. Rugo, *J. Oncol. Pract.*, **19**(4), 167 (2023).
7. K. Li, H. Luo, L. Huang et al., *Cancer Cell Int.*, **20**, 16 (2020).
8. A. P. Sokolenko, E. N. Imyanitov, *Front. Mol. Biosci.*, **5**, 76 (2018).
9. M. Kittaneh, A.J. Montero, S. Glück, *Biomark. Cancer*, **5**, 61 (2013).
10. A. Pulumati, A. Pulumati, B. S. Dwarakanath, A. Verma, R. V. L. Papineni, *Cancer Rep*, **6**(2), 1764 (2023).
11. D. Qin, *Cancer Biol. Med.*, **16** (1), 4 (2019).
12. S. Ball, N. Borman, *Nat. Biotechnol.*, **16**(2), 4 (1998).
13. A. Alfirevic, M. Pirmohamed, *Medical and Health Genomics*, 121 (2016).
14. J. M. Satagopan, K. Offit, W. Foulkes, M. E. Robson, S. Wacholder, C. M. Eng et al., *Cancer Epidemiol. Biomarkers Prev*., **10** (5), 467 (2001).
15. https://www.cdc.gov/cancer/breast/young_women/bringyourbrave/hereditary_breast_cancer/jewish_women_brca.htm
16. N. Petrucelli, M. B. Daly, T. Pal. BRCA1- and BRCA2-Associated Hereditary Breast and Ovarian Cancer. 1998 Sep 4 [Updated 2023 Sep 21]. In: M. P. Adam, J. Feldman, G. M. Mirzaa et al. (eds). GeneReviews® [Internet]. Seattle (WA): University of Washington, Seattle; 1993–2023.
17. G. Idos, L. Valle. Lynch Syndrome. 2004 Feb 5 [Updated 2021 Feb 4]. In: M. P. Adam, J. Feldman, G. M. Mirzaa et al. (eds). GeneReviews® [Internet]. Seattle (WA): University of Washington, Seattle; 1993–2023.
18. T. Yen, P. P. Stanich, L. Axell et al. APC-Associated Polyposis Conditions. 1998 Dec 18 [Updated 2022 May 12]. In: M. P. Adam, J. Feldman, G. M. Mirzaa et al. (eds). GeneReviews® [Internet]. Seattle (WA): University of Washington, Seattle; 1993–2023.
19. L. Yehia, C. Eng. PTEN Hamartoma Tumor Syndrome. 2001 Nov 29 [Updated 2021 Feb 11]. In: M. P. Adam, J. Feldman, G. M. Mirzaa et al. (eds). GeneReviews® [Internet]. Seattle (WA): University of Washington, Seattle; 1993–2023.
20. T. J. McGarrity, C. I. Amos, M. J. Baker. Peutz-Jeghers Syndrome. 2001 Feb 23 [Updated 2021 Sep 2]. In: M. P. Adam, J. Feldman, G. M. Mirzaa et al. (eds). GeneReviews® [Internet]. Seattle (WA): University of Washington, Seattle; 1993–2023.
21. M. B. Daly et al., *J. Natl. Compr. Canc. Netw.*, **18**(4), 380 (2020).
22. W. Chan, M. Lee, Z. X. Yeo et al., *Hered. Cancer Clin. Pract.*, **18**, 9 (2020).
23. G. N. Tsaousis, E. Papadopoulou, A. Apessos et al., *BMC Cancer*, **19**, 535 (2019).
24. T. Shen, S. H. Pajaro-Van de Stadt, N. C. Yeat, J. C. Lin, *Front. Genet.*, **6**, 215 (2015).
25. X. Chang, Z. Liu, S. Man, A. Roys, Z. Li, D. Zuo, Y. Wu, *RSC Adv.*, **9**(31), 17921 (2019).
26. K. Parikh, G. Banna, S. V. Liu et al., *J. Hematol. Oncol.*, **15**, 152 (2022).
27. J. Canon, K. Rex, A. Y. Saiki et al., *Nature*, **575**(7781), 217 (2019).
28. R. J. Sullivan, J. R. Infante, F. Janku et al., *Cancer Discov.*, **8**(2), 184 (2018).
29. M. Dillon, A. Lopez, E. Lin et al., *Cancers*, **13**(20), 5059 (2021).
30. M. R. Burgess, E. Hwang, A. J. Firestone et al., *Blood*, **124**(26), 3947 (2014).
31. M. Salzmann, J. Loquai, C. Schadendorf et al., *Eur. J. Cancer*, **166**, 24 (2022).
32. C. Zhou, M. Li, Z. Guo, *J. Genet.*, **99**, 78 (2020).
33. E. Conde, F. Rojo, J. Gómez et al., *J. Clin. Pathol.*, **75**, 145 (2022).
34. X. Chang, Z. Liu, S. Man, A. Roys, Z. Li, D. Zuo, Y. Wu, *RSC Adv.*, **9**(31), 17921 (2019).
35. Y. Pan, C. Deng, Z. Qiu, C. Cao, F. Wu, *Front. Oncol.*, **11**, 713530 (2021).
36. M. Rose, J. T. Burgess, K. O'Byrne et al., *Front. Cell Dev. Biol.*, **8**, 564601 (2020).
37. T. Inoue, S. Sekito, T. Kageyama et al., *Cancers*, **15**(9), 2662 (2023).

38. A. Ragupathi, M. Singh, A. M. Perez, D. Zhang, *Front. Cell Dev. Biol.*, **11**, 1133472 (2023).
39. https://www.cancer.gov/news-events/cancer-currents-blog/2020/fda-olaparib-rucaparib-prostate-cancer
40. S. Connal, J. M. Cameron, A. Sala et al., *J. Transl. Med.*, **21**(1), 118 (2023).
41. D. Biswas, J. Ganeshalingam, J. C. M. Wan, *Lancet Oncol.*, **21**(12), 550 (2020).
42. P. Pinzani, V. D'Argenio, M. Del Re et al., *Clin. Chem. Lab. Med.*, **59**(7), 1181 (2021).
43. S. N. Lone, S. Nisar, T. Masoodi et al., *Mol. Cancer*, **21**, 79 (2022).
44. M. Nikanjam, S. Kato, R. Kurzrock, *J. Hematol. Oncol.*, **15**, 131 (2022).
45. Y. Liu, H. Xu, T. Li, W. Wang, *Lab Chip*, **21**(6), 994 (2021).
46. Y. Bai, H. Zhao, *Ann. Transl. Med*., **6**(1), 89 (2018).
47. M. S. Lee, H. K. Sanoff, *BMJ*, **371**, m4050 (2020).
48. D. M. Mohamed, H. A. Kamel, *Egypt J. Radiol. Nucl. Med.*, **52**, 65 (2021).
49. E. Y. Kim, A. Kim, G. Lee et al., *BMC Cancer*, **18**, 1221 (2018).
50. K. J. Eoh, H. M. Kim, J. Y. Lee et al., *BMC Cancer*, **20**, 204 (2020).
51. B. M. Paisley, Y. Liu, *Front. Genet.*, **12**, 763431 (2021).
52. N. N. Miteva-Marcheva, H. Y. Ivanov, D. K. Dimitrov et al., *Biomark Res.*, **8**, 32 (2020).
53. D. Z. Mhandire, A. K. L. Goey, *Mol. Diagn. Ther.*, **26**, 137 (2022).
54. H. T. Chan, Y. M. Chin, S. K. Low, *Oncol. Ther.*, **7**, 1 (2019).
55. P. F. Przytycki, M. Singh, *Genome Med.*, **9**(1), 79 (2017).
56. N. Oak, A. D. Cherniack, R. J. Mashl et al., *Genome Med.*, **12**, 51 (2020).

Bulgarian Chemical Communications, Volume 55, Special Issue C (pp. 33–36) 2023 *DOI: 10.34049/bcc.55.C.0003*

Environmentally acceptable synthesis of magnesium bearing fertilizers. 2. Mechanochemical preparation

G. G. Velyanova[1], K. S. Kossev[1*]

Institute of Mineralogy and Crystallography, Bulgarian Academy of Sciences, 1113, Sofia, "Akad. G. Bonchev" str., bl. 107.

Received: November 2023; Revised: December 2023

Mechanochemical synthesis of magnesium bearing fertilizer by using magnesium sulphate and magnesium sulphate hydrates is reported. The use of mechanochemical synthesis methods has a number of advantages. Solvent-free synthesis, low-temperature operation, high yields, and the absence of by-products make these methods the most environmentally acceptable. Based on widely used fertilizer compounds, magnesium salts and urea, a new compound with chemical formula $MgSO_4$•$6OC(NH_2)_2$•$0.5H_2O$ is obtained. The high ratio of urea to magnesium sulphate corresponds to the use of nitrogen as a major bioelement, and sulphur and magnesium as trace elements, which meets the requirements for the fertilizer products and mixtures. The new product implies smaller losses of nitrogen and its low hygroscopicity supposes good storage stability.

Keywords: mechanochemistry, fertilizers.

INTRODUCTION

Magnesium is the eighth most common element in the Earth's crust. Its content in the crust is about 2.4% (Patnaik, 2003) [1] and is mainly associated with the carbonate minerals magnesite and dolomite. The richest source of bioavailable magnesium, is the hydrosphere. In seawater, the concentration of magnesium is about 55 mmol/L, and smaller, but also significant, amounts of magnesium are found in river environments and surface waters [2]. Magnesium is one of the main bioelements and performs important functions for the development of living organisms – animals and plants. Maintaining effective intensive agriculture requires suitable soils and the application of large amounts of fertilizers that provide the bioelements needed by plants [3–4]. Magnesium is part of the chlorophyll structure and it is most commonly associated with plant growth, which is why magnesium salts find wide application in agrochemistry. Natural (kieserite, epsomite) and synthetic crystal hydrates of magnesium sulphate are used as stand-alone preparations or in the composition of microfertilizers, because in addition to magnesium, they contain another important bioelement – sulphur. Urea, on the other hand, is a commonly used nitrogen fertilizer. Approximately 60% of the bound nitrogen used for fertilization is applied as urea [5]. This is determined both by its high bound nitrogen content of the order of 46% and by its convenient use. There are two main problems facing the use of urea as fertilizer. The concomitant production of biuret which is toxic to plants and the loss of bound nitrogen after application to the soil. While the former is being addressed by controlling the production process and introducing an additional purification stage, the latter still lacks an effective solution. The loss of fixed nitrogen depends on many factors: soil type and moisture, temperature, pH, type of crop sown, rate of fertilizer applied, etc. In practice, it is very difficult to estimate what the losses will be for a particular application. However, there are published models concerning specific cases [6]. The most significant losses are related to volatilization of nitrogen derivatives, the majority in the form of NH_3. Published data on nitrogen losses under different application conditions are contradictory, but it is accepted that losses when urea is used are relatively high and between 10 and 40% of the nitrogen applied as urea is lost, mainly as ammonia [7].

* To whom all correspondence should be sent:
E-mail: kossev@yahoo.com

Various methods have been developed to reduce the losses of bound nitrogen when fertilizing with nitrogen fertilizers, such as coating the urea particles with a polymer shell [8]. More sophisticated techniques such as mixing urea with rice husk ash with or without the addition of magnesium sulphate, produces also a slow-release urea product [9–11]. Other additives to urea have been investigated in search of ammonia emission reduction – phosphogypsum, $(NH_4)_2HPO_4$, $ZnSO_4$, NH_4Cl or KCl [12]. Wang and co-authors [13] in 2022 reported on the effect of magnesium sulphate, borax and zeolite additions to urea as fertilizer and showed that although there was a slight increase in losses of bound nitrogen as N_2O from 0.7 to 1.7%, losses as ammonia decreased from 39 to18%.

There are a considerable number of studies devoted to the interaction of magnesium sulphate with urea [14–15]. The presence of urea in the aqueous solutions of magnesium sulphate results of magnesium sulphate complexes where the magnesium ion coordinates urea molecules and depending on the synthetic conditions, compounds of different compositions and physicochemical characteristics are obtained – $MgSO_4•5OC(NH_2)_2•2H_2O$ and $MgSO_4•6OC(NH_2)_2•2H_2O$, $MgSO_4•OC(NH_2)_2•3H_2O$ and $MgSO_4•OC(NH_2)_2•2H_2O$. The studies of the crystallohydrates of magnesium salts revealed that urea molecule effectively replaces water molecules, which in turn, leads to an increase of the resistance and thermal stability of the new compounds thus suggests slower release properties (Georgieva et al., 2022; Kossev et al., 2021; Rusev et al., 2018) [16–18]. Later research on the interaction of magnesium sulfate and urea has been presented mainly in patent developments, which is conditioned by the interest they represent for use as agrochemical preparations (Patents WO 098367, 2013; WO 036494A1, 2021 and US20200189987A1, 2020). The characteristic feature of all these patents is that they describe the preparation of mixtures of urea complexes of magnesium sulphate and/or their mixtures with urea and crystal hydrates of magnesium sulphate, rather than individual defined chemical compounds. In our laboratory we have obtained two new complexes $MgSO_4•4OC(NH_2)_2•2H_2O$ and $MgSO_4•6OC(NH_2)_2•0.5H_2O$ the latter one of particular interest for agrochemistry because with its high urea to magnesium ratio, low hygroscopicity and good storage stability [19].

In this work, we present a mechanochemical synthesis of $MgSO_4•6OC(NH_2)_2•0.5H_2O$ from magnesium hydrates, commonly used as a fertilizes. The use of mechanochemical synthesis methods has a number of advantages, such as solvent-free processes, low-temperature operation, high yields, absence of by-products est.

MATERIALS AND METHODS

The substances used in the experiments were the commercial products magnesium $MgSO_4•7H_2O$ and $CO(NH_2)_2$ with correspondingly 99.0 and 99.5% purity. The other magnesium salts were obtained after thermal treatment of $MgSO_4•7H_2O$ at 110 °C for 24 h for $MgSO_4•H_2O$, and at 340 °C for 2 h for $MgSO_4$.

For the mixing of the reagents, a planetary ball mill "Pulverisette 7 Premium line" was used. The operating conditions for all of the experiments were as follows: capacity of one mortar 45 ml – loading 5 g; size and number of agate balls – Ø10 mm, 18 pcs. The ratios 1:1; 1:2; 1:3; 1:4; 1:5; 1:6; 1:7; 2:1 between $MgSO_4•\ xH_2O$ (x = 0, 1, 7) and $CO(NH_2)_2$ were applied respectively. Additional syntheses, with time and speed variations, were performed for the systems with reagents rations 1:6 and 1:1. The time and speed for those experiments were in the range of 3–120 min and 100–750 rpm.

Powder diffraction analyses were used to verify the purity of reagents and the resulting products. The powder diffraction patterns were obtained by X-ray diffractometer "D2 Phaser", Cu-Kα radiation

Fig. 1. Measurement system.

(1.54 Å), 2θ range from 3° at 70°, 0.05 step size and measuring time 1 s per step.

The measurement of ammonia volatilization after the application of urea and the newly obtained urea complex ($MgSO_4 \cdot H_2O \cdot 6[OC(NH_2)]$) on a commercial organic substrate was carried out by GT-903 Series Gas Detector. The used organic substrate has the following characteristics (NH_4+NO_3) 25–50 mg/100 g; P (P_4O_5) 30–50 mg/100 g; pH 5.5–6.5; EC (mS/cm) 0.6–1.0; bulk density (kg/L) 0.45–0.55; moisture (%) 40–50). Two samples containing organic substrate and pure urea or newly obtained urea compound were prepared. Amounts of 100 g organic substrate, 10 ml of water and 0.17 mol Urea were applied for both systems. The samples were placed in a desiccator and measurements were performed ones per day. The measurement system is presented on the Fig. 1.

RESULTS AND DISCUSSION

The XRD analyses show that within the parameters used for the mechanochemical synthesis, a single-phase product was not obtained when $MgSO_4$ or $MgSO_4 \cdot 7H_2O$ were applied as reagents. In the case of $MgSO_4$ no reaction between the reagents was observed, unless some water was added to the vessel which allows the magnesium sulphate to be dissolved and consequently urea adducts to be formed. A mixture of urea complex and reactants in all of the studied rations. In difference when $MgSO_4 \cdot 7H_2O$ was used, a very dense mass is formed. It adheres to the walls of the vessel and was difficult to separate. The results reveal formation of $MgSO_4 \cdot 6OC(NH_2)_2 \cdot 0.5H_2O$, but within the used grinding parameters (temperature, revolutions, size of the balls) a single phase product was not obtained. For all ratios of the reagents, the final product was a mixture of two or three phases, and relatively the highest yield of the desired product was obtained at a ratio $MgSO_4 \cdot 7H_2O$: $1OC(NH_2)_2$. It should also be noted that even for a short time (2–3 min) of tribochemical treatment a liquefied product was formed and that's why it was applied a secondary heat treatment. The trials of a series of short grinding, drying, and regrinding did not lead to a significantly different result. The best results were obtained in the system $MgSO_4 \cdot H_2O$ – Urea. The received products were with high degree of crystallinity and easily removable from the vessel. All of them contain $MgSO_4 \cdot 6OC(NH_2)_2 \cdot 0.5H_2O$ confirming that this is the most stable urea complex of magnesium sulphate. Using of magnesium sulphate monohydrate as a reagent allowed obtaining of single phase product of $MgSO_4 \cdot 6OC(NH_2)_2 \cdot 0.5H_2O$ and almost 100% yield is achieved for the ratio of $MgSO_4 \cdot H_2O$:$6OC(NH_2)$ and 120 minutes grinding time (Fig. 2). The precise parameters of the synthesis are patent pending.

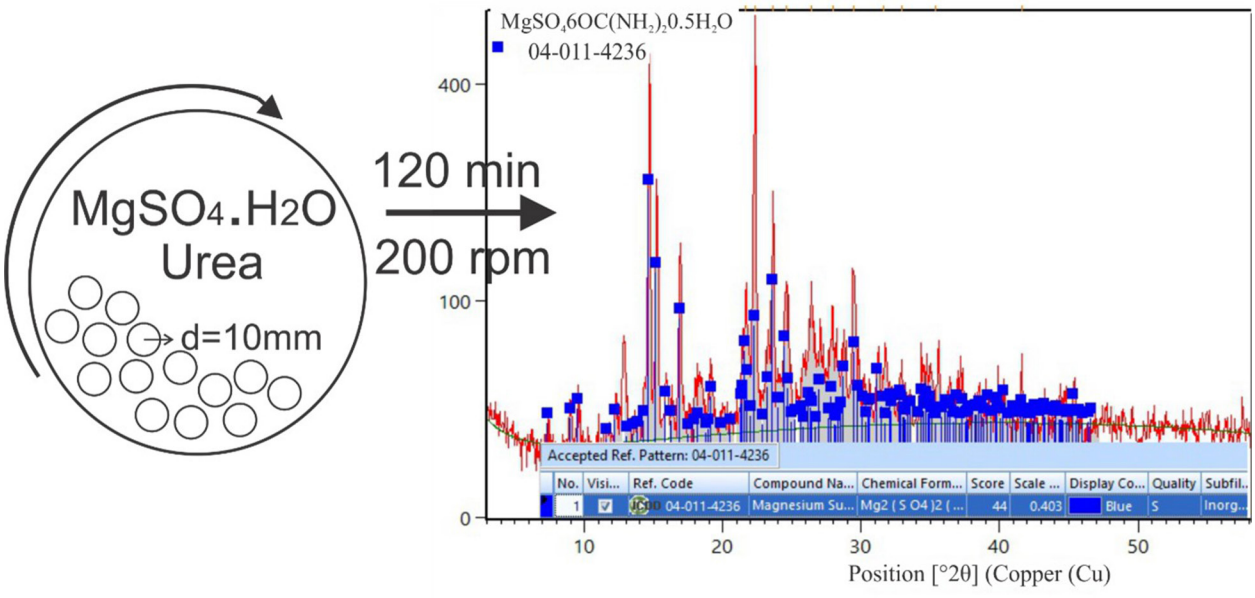

Fig. 2. Schematic presentation of machanochemical synthesis of $MgSO_4 \cdot 6OC(NH_2)_2 \cdot 0.5H_2O$.

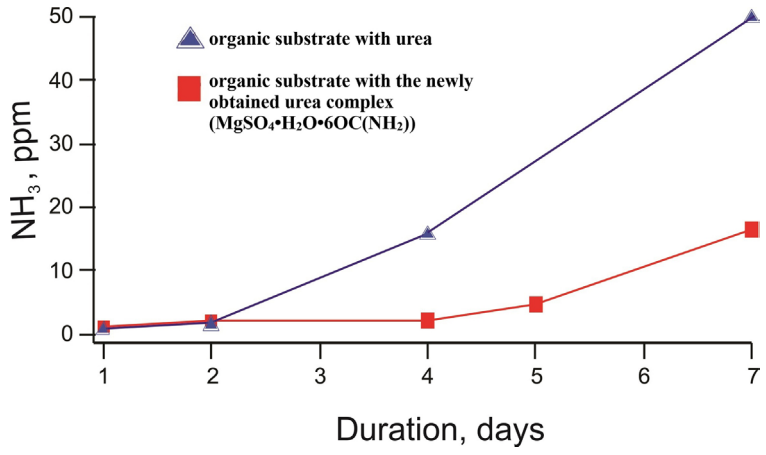

Fig. 3. Ammonia volatilisations for the studied systems.

The ammonia volatilizations for the studied systems are presented in Fig. 3. The results show different tendencies for the urea and the newly obtained urea complex ($MgSO_4$•H_2O•6OC(NH_2)), proving that the nitrogen release is slower in the case of the urea complex and that it stays in the soil for a longer time.

CONCLUSIONS

The tribochemical method is suitable for obtaining of $MgSO_4$•6OC(NH_2)$_2$•0.5H_2O. The method allows this product to be obtained systematically, simply, selectively and without obtaining secondary products. Being single-phase, the discussed product is easy to be characterized and has strictly defined properties. The high ratio of urea to magnesium sulphate corresponds to the use of nitrogen as a major bioelement, and sulfur and magnesium as trace elements. This meet the requirements for the fertilizer products and mixtures. Longer-term measurements in the presence of plants should be performed.

Acknowledgments: *The authors thanks to the Bulgarian National Science Fund (grant agreement КП-06-Н64/4, 15.12.2022) for the financial support of the presented study and to the project PERIMED BG05M2OP001–1.002–0005/29.03.2018 for the technical support.*

REFERENCES

1. P. Patnaik, Handbook of inorganic chemicals, McGraw-Hill, New York, 2003.
2. H. J. M. Bowen, Trace Elements in Biochemistry, Academic Press, New York, 1966.
3. P. A. Sanchez, *Science*, **295**(5562), 2019 (2002).
4. J. J. Stoorvogel, E. M. Smaling, B. H. Janssen, *Fertilizer Res.*, **35**(3), 227 (1993).
5. M. Prud'homme, *IFA Strategic Forum, Dubai*, Dubai, UAE: International Fertilizer Association (IFA) (2016).
6. M. L. C. D. Vale, R. O. D. Sousa, W. B. Scivittaro, *Revista Brasileira de Ciência do Solo*, **38**, 223 (2014).
7. F. E. Allison, *Adv. Agron.*, **18**, 219 (1966).
8. F. C. Siman, F. V. Andrade, R. R. Passos, *Commun. Soil Sci. Plant Anal.*, **51**(10), 1283 (2020).
9. M. Adlim, R. F. I. Ramayani, I. Khaldun, F. Muzdalifah, *Rasayan J. Chem.*, **14**(3), 1851 (2021).
10. S. V. Vassilev, C. G. Vassileva, D. Baxter, *Fuel*, **129**, 292 (2014).
11. Z. Sha, T. Lv, M. Staal, X. Ma, Z. Wen, Q. Li, G. Pasda, T. Misselbrook, X. Liu, *J. Soils Sediments*, **20**(4), 2130 (2020).
12. T. J. Purakayastha, J. C. Katyal, *Nutr. Cycling Agroecosyst.*, **51**(2), 107 (1998a), **51** (2), 117 (1998b).
13. H. Wang, L. Oertelt, K. Dittert, *Sci. Total Environ.*, **803**, 149902 (2022).
14. C. W. Whittaker, F. O. Lundstrom, J. H. Shimp, *J. Am. Chem. Soc.*, **58**(10), 1975 (1936).
15. J. Y. Yee, R. O. E. Davis, S. B. Hendricks, *J. Am. Chem. Soc.*, **59**(3), 570 (1937).
16. I. Georgieva, K. Kossev, R. Titorenkova, N. Petrova, T. Zahariev, R. Nikolova, *J. Solid State Chem.*, **312**, 123263 (2022).
17. K. Kossev, N. Petrova, I. Georgieva, R. Titorenkova, R. Nikolova, *J. Mol. Struct.*, **1224**, 129009 (2021).
18. R. Rusev, L. Tsvetanova, B. Shivachev, K. Kossev, R. Nikolova, *Bulg. Chem. Commun.*, **50**, 79 (2018).
19. T. Todorov, R. Petrova, K. Kossev, J. Macicek, O. Angelova, *Acta Crystallogr. C: Crystal Structure Communications*, **54**(12), 1758 (1998a), **54** (4), 456 (1998b).

Bulgarian Chemical Communications, Volume 55, Special Issue C (pp. 37–43) 2023 *DOI: 10.34049/bcc.55.C.0004*

Colorectal cancer and probiotics

Y. Zh. Gvozdeva[1,2]*, R. A. Staynova[1], M. I. Kassarova[2]

[1] *Department of Pharmaceutical Sciences, Faculty of Pharmacy, Medical University of Plovdiv, 15A Vassil Aprilov Blvd., 4002 Plovdiv, Bulgaria*
[2] *Research Institute at Medical University of Plovdiv, Plovdiv, Bulgaria*

Received: November 2023; Revised: December 2023

The colorectal cancer (CRC) ranks as the third most common cause of death among various cancer types globally, with the highest occurrence observed in developed nations. In recent times, there has been an acknowledgment that the composition of the intestinal microbiota serves as a risk factor in the onset of CRC. The intestinal microbiota exerts influence over various facets of intestinal health, encompassing cellular characteristics, physiology, metabolism, development, and immune homeostasis. The aim of this review is to explore the potential mechanisms by which probiotics act in preventing colorectal cancer. Research indicates that consistent probiotic consumption has the potential to thwart the onset of colorectal cancer.

Keywords: colorectal cancer, intestinal microbiota, probiotics.

INTRODUCTION

The intestinal microbiota plays a crucial role in facilitating the absorption of nutrients, bolstering the host's resilience against infections, fortifying the immune system within the intestines, and regulating the host's metabolic processes [1]. The alteration or dysbiosis of the gut microbiota is widely acknowledged for its significant role in triggering and promoting chronic inflammatory pathways. Moreover, it is implicated in profound genetic and epigenetic alterations that culminate in dysplasia, clonal expansion, and malignant transformation. Probiotic bacteria exhibit antitumor activity through diverse mechanisms, including nonspecific physiological and immunological pathways [2].

The term 'probiotic' is derived from the literal meaning 'for life.' According to the Food and Agriculture Organization (FAO) and the World Health Organization (WHO) of the United Nations, probiotics are living microorganisms that, when applied in appropriate quantities, confer health benefits to the host [3]. Primarily belonging to the genera *Lactobacillus, Bifidobacterium*, and *Streptococcus*, they contribute to the restoration and maintenance of the balance of the human gut microbiome [4].

Probiotics can exert a range of favorable effects on the human body when consumed in the form of functional foods and dietary supplements containing high levels of viable bacteria, denoted by at least 10^6–10^7 CFU per gram of the product at the time of consumption. The efficacy of probiotics is also contingent on their ability to reach the small intestine of the human gastrointestinal tract in an active state [5]. Numerous investigations, both in animal models and human populations, have underscored the efficacy of probiotic consumption in addressing diverse medical conditions such as gastroenteritis, lactose intolerance, constipation, antibiotic-induced diarrhea and genitourinary tract infections [6]. Furthermore, many studies indicate the anti-tumor effect of probiotics and their capacity to inhibit the progression of cancerous conditions, particularly highlighting a specific correlation between colorectal cancer and probiotics [7].

Colorectal cancer ranks as the second most prevalent cause of cancer-related morbidity and mortality on a global scale. The incidence rates are notably increasing among younger populations, underscoring the imperative for enhanced and cost-effective interventions and adequate treatment [8].

This review aims to offer a broad overview of the potential mechanisms through which probiotics might exert their positive effects in preventing colorectal cancer.

* To whom all correspondence should be sent:
E-mail: yana.gvozdeva@mu-plovdiv.bg

Intestinal microflora

From the moment of birth, an individual's gastrointestinal tract becomes a habitat for a diverse array of microorganisms that persists throughout their lifetime. This assemblage of microorganisms, commonly referred to as the 'normal' gut microflora, comprises bacterial species endowed with genetic, physiological and morphological characteristics that enable them to establish and proliferate under specific conditions at designated sites. These microbes coexist harmoniously with other colonizing microorganisms and exert a competitive influence, impeding the growth of potentially harmful bacteria [9].

Each person possesses a distinct microbiota, and the specific counts of bacterial phyla and species differ among individuals. The intestinal microbiota encompasses a diverse community of viruses, bacteria, archaea, fungi, helminths and protists that symbiotically inhabit the human digestive system. Among these, the predominant microorganisms in the gut belong to five bacterial phyla: *Actinobacteria, Bacteroidetes, Firmicutes, Proteobacteria* and *Verrucomicrobia* [10]. The term "microbiome" collectively refers to the entire genome of these microbes.

Remarkably, the colon contains one million times more bacteria than the small intestine, and intriguingly, it encounters around 12 times more malignancies than the latter. This proves the possibility that the gut microbiota may play a significant role in the initiation of colorectal carcinogenesis [11, 12].

However, the equilibrium of this complex microbial community is susceptible to alterations induced by various environmental factors, including but not limited to diet and medications. Such external influences can lead to shifts in the composition of the resident microbiota, giving rise to a state of dysbiosis [13]. Nutrition is the primary controller of intestinal microbial function. Typically, individuals adhering to a Western-style diet exhibit a higher *Firmicutes/Bacteroidetes* phyla ratio, while those on a subsistence diet show an increased quantity of the Prevotella genus, which is part of the *Bacteroidetes* phylum [14]. This imbalance carries adverse implications for the individual's health, emphasizing the intricate interplay between environmental factors and the delicate symbiosis within the gastrointestinal ecosystem [13].

Factors Potentially Contributing to Colon Cancer Development

Colorectal cancer does not seem to have a specific, singular cause. Instead, there are multiple risk factors associated with its development. The mechanisms underlying how these risk factors contribute to colorectal cancer carcinogenesis remain unclear. Exceptions to this general pattern include Lynch Syndrome and familial adenomatous polyposis, both genetic conditions, although they represent a minority of global colorectal cancer cases [15].

Specific bacterial strains and an imbalance in gut microbiota, known as dysbiosis, have been linked to the onset of colorectal cancer [16]. Dysbiosis in the gastrointestinal tract has the potential to disturb the balance of the immune system and the homeostasis of the mucosal barrier, triggering inflammation and heightened mucosal barrier permeability. This persistent state of inflammation can activate cytokines and some growth factors, including vascular endothelial growth factor (VEGF), tumor necrosis factor (TNF), tumor growth factor beta (TNF-β) and IL-6. This cascade of events may contribute to the proliferation and viability of abnormal cells [17].

There are suspicions that *Bacteroides fragilis, Enterococcus faecalis, Streptococcus bovis, Escherichia coli* and *Fusobacterium spp*. may play a role in colorectal carcinogenesis. The disruption in microbial phyla balance is frequently heightened by oxidative stress driven by leukocytes, the secretion of bacteriocins by harmful bacteria, and the prevalence of bacteriophages in the population [18]. In a comprehensive review, Song *et al.* explored the intricate relationship between the occurrence of colorectal cancer and environmental factors, dietary habits, and the composition of the gut microbiome [19].

Prolonged use of antibiotics is connected to a heightened risk of colorectal cancer, establishing a link between gut microbiota and CRC [20]. As individuals age, there is a decline in CD4 T-cells and a transition in the microbiota towards a pro-inflammatory profile. This diminishes the capacity of immune cells to restrain inflammation in the colon. Moreover, there is a decrease in butyrate-producing bacteria, leading to an elevation in intracolonic pH. This, combined with dysbiosis and inflammation, contributes to CRC [21]. Additionally, smoking has been identified to alter the composition of the gut microbiota.

Moreover, the potential exposure of colon mucosa to toxins from *Bacteroides fragilis* has been proposed as a risk factor for the development of colorectal cancer [22]. The *B. fragilis* toxin induces tumorigenesis in colonic epithelial cells through mechanisms reliant on signal-transducer-and-activator-of-transcription 3 (STAT3) and interleukin-17 (IL-17) activity [23]. Oxidative stress is

pivotal in the onset of colorectal cancer. Reactive oxygen species (ROS), generated as by-products of normal cell metabolism in the gastrointestinal tract, are implicated in this process. The toxin produced by *Bacteroides fragilis* stimulates the generation of ROS in intestinal epithelial cells (IECs) and dendritic cells [24].

Peptostreptococcus and *Fusobacterium* contribute to colorectal cancer pathogenesis and, as such, can serve as biomarkers for the early detection of the disease [25]. Notably, *F. nucleatum* has recently surfaced as a potential contributor to colorectal cancer susceptibility, acting during the initial stages of promoting colorectal carcinogenesis [26]. The heightened presence of *Fusobacterium nucleatum* in individuals with CRC appears to play a potential role in the progression from adenoma to cancer [27]. Castellarin *et al.* documented the over-representation of these microbes in colorectal tumor tissue, establishing their invasive nature [28]. Additionally, Kostic *et al*. provided further evidence by demonstrating the presence of these species in human colonic adenomas [29]. Regarding the mechanisms through which *Fusobacterium* contributes to carcinogenesis, it has been suggested that its interaction with E-cadherin enhances the malignant potential of CRC by increasing inflammation and antagonizing the immune function of T cells. Another proposed mechanism is that Fusobacteria may promote colorectal cancer by activating Wnt/β-catenin signaling, inducing DNA damage through ROS production, and activating oncogenes [30].

Boleij *et al*. demonstrated that the distinct association of *S. gallolyticus* with colonic malignancy is attributed to tumor cell metabolites that support the survival of *S. gallolyticus*. This bacterium produces virulence factors, such as a pilus protein featuring a collagen-binding domain, enabling its growth in the microenvironment of colon tumors. Additionally, it exhibits heightened inflammatory signals, including Ptgs2 (COX-2) [31].

In the context of colonic polyp carcinogenesis (CPC), scientific evidence points to the involvement of *Clostridium perfringens* and species within the *Atopobium* cluster, notably *Enterobacteriaceae* and *Staphylococcus sp*., highlighting their association with colon tumorigenesis [27].

The pathogenesis of CRC has been linked to two strains of *E. coli*, characterized as genotoxic and tightly adherent. The prevalence of mucosa-associated *E. coli* was notably higher in colon tissue from individuals with adenocarcinomas compared to control samples. Furthermore, *E. coli* isolated from colon cancer patients demonstrated the ability to persist in the gut, triggering colon inflammation, causing epithelial damage, and promoting cell proliferation [32].

In cases of colorectal cancer, elevated oxidative and genotoxic levels have been noted in the gastrointestinal tract [16]. Notably, there were increased levels of bile acids in the aqueous phase of feces. Bile acids have the potential to induce cytotoxic effects on the colonic epithelium and enhance the proliferation of malignant cells [33].

Bacterial Influence and Defense Mechanisms in Colorectal Cancer Prevention

Eubiosis is characterized as the state of a well-balanced and harmonious gut microflora ecosystem [34]. Creating a eubiotic state holds potential in both preventing and treating colorectal cancer. Restoring balance to the gut ecosystem can be achieved through the administration of probiotics, prebiotics, and synbiotics. These interventions work to establish homeostasis by counteracting harmful pathogens, promoting the growth of beneficial indigenous bacteria, modulating immunological responses, and repairing the intestinal mucosa [35]. The composition of the intestinal microflora plays a pivotal role in influencing the response to treatments for colorectal cancer (Fig. 1).

Currently, research indicates that the normal microbiota consists of both beneficial and pathogenic bacteria. If pathogenic bacteria proliferate excessively, it can initiate an inflammatory process leading to the production of carcinogenic compounds. It is crucial to acknowledge the protective role that a healthy microbiota plays in preventing detrimental health conditions [15].

Probiotics present an appealing option as a potential adjunct to treatment due to their cost-effectiveness and minimal associated adverse effects. The existing evidence also indicates a substantial clinical impact of probiotics. For example, in a study involving 168 patients assessed post-colorectal cancer surgery, those who received probiotics demonstrated a significantly reduced rate of all major postoperative complications compared to the placebo group (28.6% vs. 48.8%, $p = 0.010$) [36].

Furthermore, probiotic microorganisms can diminish the population of pathogenic bacteria through various mechanisms, including competing for nutrients, growth factors, and adhesion receptors. Certain probiotics can generate antibacterial substances such as bacteriocins, reuterin, hydrogen

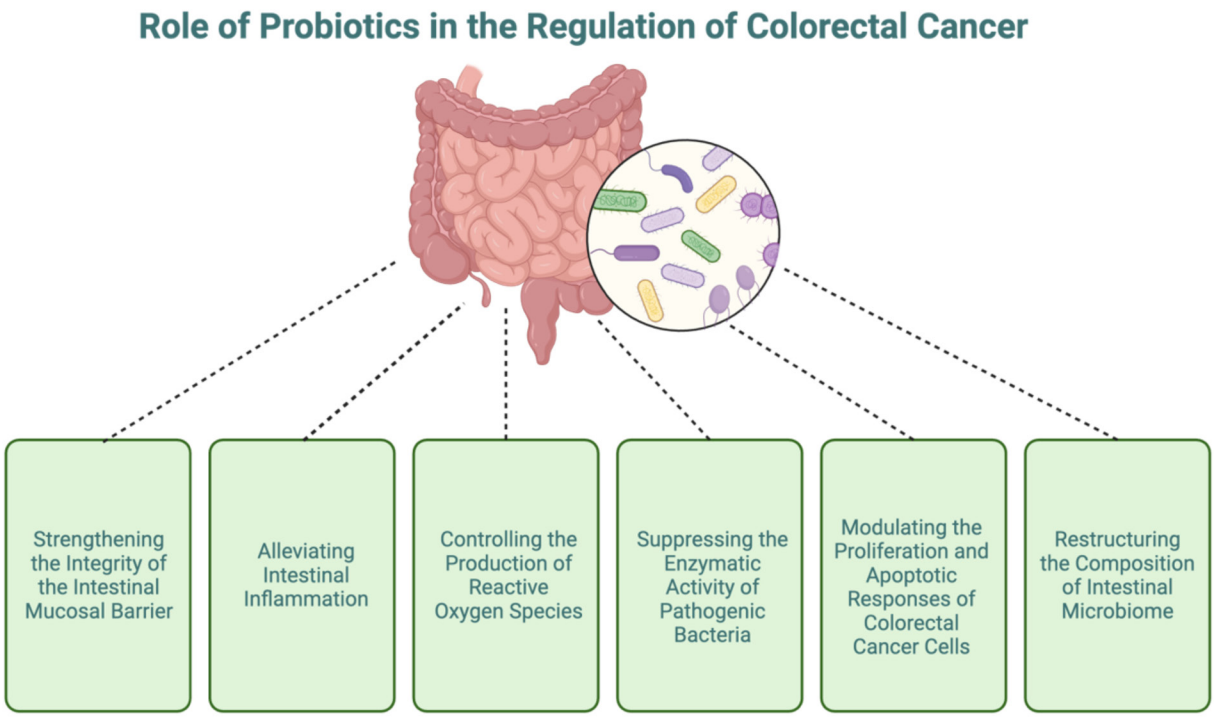

Fig. 1. Mechanisms Governing the Role of Probiotics in the Regulation of Colorectal Cancer. *Created with BioRender.com (accessed on 20 December 2023).*

peroxide, and lactic acid, effectively inhibiting the growth or eliminating pathogenic bacteria from the intestinal lumen. The positive alterations in the composition of the intestinal microbiota are directly linked to a reduced risk of developing colorectal cancer [37].

The anticancerous (ACA) and antimutagenic activity (AMA) of probiotics stems from specific mechanisms, including their capability for [33, 38]:

A) Inhibiting mutagenesis and binding or degrading of mutagens by probiotics.

B) Inhibition of the transformation of non-toxic procarcinogens into potent carcinogens is achieved by probiotics.

C) Acidification of the intestinal environment through the generation of short-chain fatty acids (SCFA) during the breakdown of non-digestible carbohydrates.

D) Augmentation and adjustment of the host's innate immune response through the secretion of anti-inflammatory molecules.

Probiotics boost the integrity of the intestinal barrier by influencing the expression of tight junction proteins, for example, claudin-1 and occludin. Additionally, they stimulate intestinal cells to produce mucin [24]. *Bifidobacterium infantis* and *Lactobacillus acidophilus* were identified as agents that safeguard intestinal permeability. They achieve this by controlling the expression of occludin and claudin-1 proteins while shielding against the activation of nuclear factor kappa-B (NF-kB) induced by IL-1β in Caco-2 cells [39]. One potential mechanism through which probiotics enhance the stability of the colonic environment is by influencing colonic macrophages. They engage in probiotic phagocytosis, mitigating deep tissue damage following infection by secreting anti-inflammatory mediators [2].

Evidence indicates a substantial decrease in the abundance of fecal putrefactive bacteria, such as coliforms, alongside an increase in commensal bacteria like *Lactobacillus* and *Bifidobacteria.* This shift has been linked to a reduced occurrence of colonic adenocarcinoma [40]. Several bacterial enzymes, including β-glucuronidase and nitroreductase, exert a pivotal role in cancer development by hydrolyzing carcinogenic compounds. Insights from animal studies suggest that the intake of yogurt starter bacteria has the potential to diminish the activity of these enzymes. This observation points towards a plausible mechanism through which probiotics may act to prevent colorectal cancer [41].

Beyond their implicated role in CRC prevention, probiotics exhibit anti-tumorigenic activity, hinting at a potential application in treating established tumors. A conceivable mechanism involves the modulation of both mucosal and systemic immune responses. Research has highlighted instances of probiotics enhancing anti-tumor immunity through processes such as cytokine production and the alteration of T-cell function [40].

The gut microbiota is pivotal in promoting the development of the immune system and establishing immune tolerance — a mechanism that modulates the immune system to safeguard the host organism against pathogens. Supplying an adequate amount of probiotics and cultivating a favorable microbiota for immune system support represents an approach to immunomodulation for the benefit of the host organism. The utilization of probiotics for immunomodulation is a widespread and expanding practice, facilitated through the interaction between immune cells in the gastrointestinal tract and probiotic microorganisms or their metabolites [42].

A newly identified protein, P8, derived from probiotics, demonstrates the ability to inhibit the progression of colorectal cancer. P8 exhibits the capacity to enter cell membranes through endocytosis, leading to the arrest of the cell cycle in DLD-1 cells. This effect is achieved by down-regulating CDK1/Cyclin B1 [43]. An *et al*.'s investigation unveiled the anti-cancer mechanisms underlying the actions of P8. Firstly, endocytosed P8 in the cytosol was observed to undergo translocation into the nucleus facilitated by KPNA3 and importin. Once in the nucleus, P8 directly bound to GSK3β introns, causing disruption in its transcription. Secondly, cytosolic P8 demonstrated a specific binding affinity to GSK3β, preventing its inactivation by protein kinases AKT/CK1ε/PKA. This active GSK3β, in turn, exhibited robust phosphorylation of β-catenin, leading to its degradation [44].

Probiotics contribute to the augmentation of dietary fiber fermentation, resulting in elevated levels of anti-tumor compounds, such as short-chain fatty acids (SCFAs), conjugated linoleic acids (CLAs), or phenols. These compounds have demonstrated potential therapeutic effects against colorectal cancer. SCFAs, in particular, serve as an energy source for colonocytes and contribute to the induction of acidosis and apoptosis in CRC cells [45]. Elevated concentrations of short-chain fatty acids in the colon appear to bring about several positive effects, including heightened synthesis of intestinal mucus, enhanced barrier function, diminished levels of pro-inflammatory mediators and stimulation of immunosuppressive cytokines like interleukin 10 (IL-10). Additionally, the increased presence of SCFAs appears to foster the preferential growth of beneficial bacteria while suppressing pathogenic strains [46]. The utilization of short-chain fatty acids derived from the gut microbiota holds promise for both the prevention and treatment of colorectal cancer [47].

In a clinical study involving patients with colorectal cancer, the oral intake of probiotics led to elevated levels of *Bifidobacterium, Lactobacillus*, and *Enterococcus,* while concurrently reducing the levels of *Escherichia coli* and *Staphylococcus aureus* [48].

Bifidobacterium longum has been documented to inhibit the incidence of colon cancer induced by the food mutagen 2-Amino-3-methylimidazo(4,5-f) quinoline [49].

Several other lactic acid bacteria (LABs) have demonstrated protective roles against colorectal cancer. These encompass *Lactobacillus rhamnosus, Lactobacillus acidophilus, Lactobacillus salivarius, Lactobacillus casei* and *Lactobacillus plantarum*. LABs inhibit CRC initiation and progression through various mechanisms, including the induction of metabolic antioxidant activity by producing antioxidants like glutathione, superoxide dismutase, and catalase. They also play a role in suppressing inflammation by activation of anti-tumor immune effectors, tumor cell apoptosis and reducing tumor size. LABs inhibit the expression of tumor-specific proteins and polyamine components and lead to anti-tumorigenic epigenetic modifications facilitated by metabolic products like short-chain fatty acids [50, 51].

The study of Budu *et al*. evidenced the distinctive antitumor properties of *Lacticaseibacillus rhamnosus* (LGG) against two colon cancer cell types, HCT-116 and HT29, elucidating the underlying mechanisms. The probiotic exhibited a targeted pro-apoptotic effect on mitochondria, inducing cytotoxicity in both colon cancer cell lines. Notably, HCT-116 displayed heightened sensitivity to LGG's anticancer activity. Nevertheless, the data presented implies that the use of probiotics, particularly LGG, either alone or in conjunction with 5FU, holds promise in triggering apoptosis in colon cancer cells. These findings may pave the path for the development of alternative chemopreventive and chemotherapeutic agents for diverse forms of colon cancer [52].

Bashir *et al.* prove in their study that the utilization of *Enterococcus faecium* strain as adjuvant

therapy alongside anticancer chemotherapy exhibits a dual benefit – it diminishes the proliferation of cancer cells and provides a protective effect against cancer [53].

Propionibacterium freudenreichii, a probiotic present in the human gut microbiota, has demonstrated the ability to suppress colorectal adenocarcinoma cells through apoptosis mediated by short-chain fatty acids. Specifically, butyric acid, one of the SCFAs, was identified as a preventive agent against colorectal cancer. It exerts its effects by modulating the cell cycle, differentiation, and apoptosis of colon cancer cell lines [24, 54].

It is logical to consider that various bacteria with anti-tumor effects might work synergistically when administered together. The use of probiotic strains with distinct and complementary mechanisms of action could potentially yield superior outcomes compared to any single strain alone. There could be additional cooperative mechanisms among commensal bacteria. Yet, it is equally plausible that combining specific probiotics may result in a scenario where their effectiveness is mutually constrained [51].

CONCLUSIONS

All the cited studies show the impact of probiotic administration on the modification of colonic microflora, influencing the intestinal environment and the development of preneoplastic or neoplastic lesions. Recent research indicates a noteworthy distinction in the microbiome composition between patients who have developed colorectal cancer and those who have not. These findings expand our understanding of the intricate interplay between gut microflora, the development of cancer, and the efficacy of cancer treatments. Researchers face the task of pinpointing strains with the most pronounced antitumoral characteristics. Subsequently, clinical investigators should develop studies that employ well-defined bacterial strains in predetermined quantities, carefully chosen for their specific characteristics. This approach is crucial for advancing our understanding of the potential clinical applications of probiotics in preventing or treating neoplastic conditions. Nevertheless, further research is imperative to ascertain whether the synergistic interplay between probiotics and anti-cancer drugs will indeed translate into enhanced oncologic outcomes.

Acknowledgments: *this work is published with the support of the Project № BG05M2OP001-1.002-0005-C 03, Center for Competence "Personalized Innovative Medicine (PERIMED)", work package – 8; funded by the Operational Program "Science and Education for Intelligent Growth" 2014–2020, co-financed by the European Union through the European Regional Development Fund.*

REFERENCES

1. J. K Nicholson, E. Holmes, J. Kinross, R. Burcelin, G. Gibson, W. Jia, S. Pettersson, *Science*, **336**(6086), 1262 (2012).
2. M. Eslami, B. Yousefi, P. Kokhaei, M. Hemati, Z. R. Nejad, V. Arabkari, A. Namdar, *J. Cell Phys.*, **234**(10), 17127 (2019).
3. http://www.fao.org/3/a-a0512e.pdf (2020).
4. D. R. Mack, *Can. Fam. Phys.*, **51**(11),1455 (2005).
5. V. Y. Marinova, I. K. Rasheva, Y. K. Kizheva, Y. D. Dermenzhieva, P. K. Hristova, *Biotechnol. Biotechnol. Equip.*, **33**(1), 834 (2019).
6. T. Iannitti, B. Palmieri, *Clin. Nutrit.*, **29**(6), 701 (2010).
7. K. Śliżewska, P. Markowiak-Kopeć, W. Śliżewska, *Cancers*, **13**(1), 20 (2020).
8. R. L. Siegel, K. D. Miller, A. Jemal, *CA: Cancer J. Clin.*, **68**(1), 7 (2018).
9. R. A. Rastall, *J. Nutr.*, **134**(8), 2022S-6S (2004).
10. H. E. Ho, S. Bunyavanich, *Curr. Allergy Asthma Rep.*, **18**, 1 (2018).
11. L. M. Proctor, *Cell Host Microbe*, **10**, 287 (2011).
12. S. Singh, P. Sharma, D. K. Sarma, M. Kumawat, R. Tiwari, V. Verma, R. Nagpal, M. Kumar, *Cancers*, **15**(6), 1913 (2023).
13. M. Uccello, G. Malaguarnera, F. Basile, V. D'agata, M. Malaguarnera, G. Bertino, M. Vacante, F. Drago, A. Biondi, *BMC Surg.*, **12**(1), 1 (2012).
14. K. R. Amato, C. J. Yeoman, G. Cerda, C. A Schmitt, J. D. Cramer, M. E. Miller, A. Gomez, T. R. Turner, B. A. Wilson, R. M. Stumpf, K. E. Nelson, *Microbiome*, **3**, 1 (2015).
15. P. Lamichhane, M. Maiolini, O. Alnafoosi, S. Hussein, H. Alnafoosi, S. Umbela, T. Richardson, N. Alla, N. Lamichhane, B. Subhadra, R. R. Deshmukh, *Cancers*, **12**(5), 1162 (2020).
16. A. Boleij, H. Tjalsma, *Biol. Rev.*, **87**(3), 701 (2012).
17. L. Klampfer, *Curr. Cancer Drug. Targets*, **11**, 451 (2011).
18. G. A. Weiss, T. Hennet, *Cell Molec. Life Sci.*, **74**, 2959 (2017).
19. M. Song, A. T. Chan, J. Sun, *Gastroenterology*, **158**(2), 322 (2020).
20. Y. Cao, K. Wu, R. Mehta, D. A. Drew, M. Song, P. Lochhead, L. H. Nguyen, J. Izard, C. S. Fuchs, W. S. Garrett, C. Huttenhower, *Gut*, **67**(4), 672 (2018).
21. H. Pandey, D. W. Tang, S. H. Wong, D. Lal, *Cancers*, **15**(3), 866 (2023).
22. A. Boleij, E. M. Hechenbleikner, A. C. Goodwin, R. Badani, E. M. Stein, M. G. Lazarev, B. Ellis, K. C. Carroll, E. Albesiano, E. C. Wick, E. A. Platz, *Clin. Infect. Dis.*, **60**(2), 208 (2015).

23. L. Chung, E. T. Orberg, A. L. Geis, J. L. Chan, K. Fu, C. E. Shields, C. M. Dejea, P. Fathi, J. Chen, B. B. Finard, A. J. Tam, *Cell Host Microbe*, **23**(2), 203 (2018).
24. S. Ding, C. Hu, J. Fang, G. Liu, *Oxid. Med. Cell. Longev.*, (2020).
25. Z. Gao, B. Guo, R. Gao, Q. Zhu, W. Wu, H. Qin, *Mol. Med. Rep.*, **12**, 6119 (2015).
26. A. Pino, M. De Angelis, M. Chieppa, C. Caggia, C. Randazzo, *WCRJ*, **7**, 1456 (2020).
27. P. Ambalam, M. Raman, R. K. Purama, M. Doble, *Best Pract. Res. Clin. Gastroenterol.*, **30**(1), 119 (2016).
28. M. Castellarin, R. L. Warren, J. D. Freeman, L. Dreolini, M. Krzywinski, J. Strauss, R. Barnes, P. Watson, E. Allen-Vercoe, R. A. Moore, R. A. Holt, *Genome Res.*, **22**(2), 299 (2012).
29. A. D. Kostic, E. Chun, L. Robertson, J. N. Glickman, C. A. Gallini, M. Michaud, T. E. Clancy, D. C. Chung, P. Lochhead, G. L. Hold, E. M. El-Omar, *Cell Host Microbe*, **14**(2), 207 (2013).
30. S. Zhou, J. Chen, H. Yao, H. Hu, *Front. Oncol.*, **8**, 371 (2018).
31. A. Boleij, B. E. Dutilh, G. A. Kortman, R. Roelofs, C. M. Laarakkers, U. F. Engelke, H. Tjalsma, *Mol. Cell. Proteomics*, **11**(10), 851 (2012).
32. H. M. Martin, B. J. Campbell, C. A. Hart, C. Mpofu, M. Nayar, R. Singh, H. Englyst, H. F. Williams, J. M. Rhodes, *Gastroenterology,* **127**(1), 80 (2004).
33. S. A. Dos Reis, L. L. da Conceição, N. P. Siqueira, D. D. Rosa, L. L. da Silva, G. P. Maria do Carmo, *Nutr. Res*., **37**, 1 (2017).
34. A. Tripathy, J. Dash, S. Kancharla, P. Kolli, D. Mahajan, S. Senapati, M. K. Jena, *Cancers*, **13**(13), 3178 (2021).
35. K. Kaźmierczak-Siedlecka, A. Daca, M. Fic, T. van de Wetering, M. Folwarski, W. Makarewicz, *Gut Microbes*, **11**(6), 1518 (2020).
36. K. Kotzampassi, G. Stavrou, G. Damoraki, M. Georgitsi, G. Basdanis, G. Tsaousi, E. J. Giamarellos-Bourboulis, *World J. Surg*., **39**, 2776 (2015).
37. D. E. Serban, *Cancer Lett.*, **345**(2), 258 (2014).
38. M. Raman, P. Ambalam, K. K. Kondepudi, S. Pithva, C. Kothari, A. T. Patel, R. K. Purama, J. M. Dave, B. R. Vyas, *Gut Microbes*, **4**(3), 181 (2013).
39. S. Guo, T. Gillingham, Y. Guo, D. Meng, W. Zhu, W.A. Walker, K. Ganguli, *J. Pediatr. Gastroenterol. Nutr.*, **64**(3), 404 (2017).
40. M. S. Geier, R. N. Butler, G. S. Howarth, *Cancer Biol. Ther.*, **5**(10), 1265 (2006).
41. A. De Moreno de LeBlanc, G. Perdigón, *Biocell*, **29**(1), 15 (2005).
42. I. Koboziev, C. R. Webb, K. L. Furr, *Free Radic. Biol. Med.*, **68**, 122 (2014).
43. B. C. An, Y. Ryu, Y. S. Yoon, O. Choi, H. J. Park, T. Y. Kim, S. I. Kim, B. K. Kim, M. J. Chung, *Mol. Cells*, **42**(11), 755 (2019).
44. B. C. An, J. Y. Ahn, D. Kwon, S. H. Kwak, J. Y. Heo, S. Kim, Y. Ryu, M. J. Chung. *Int. J. Mol. Sci.*, **24**(12), 9857 (2023).
45. I. Kahouli, C. Tomaro-Duchesneau, S. Prakash, *J. Med. Microbiol.*, **62**(8), 1107 (2013).
46. M. A. Looijer-Van Langen, L. A. Dieleman, *Inflamm. Bowel Dis.*, **15**(3), 454 (2009).
47. Z. Wang, W. Dan, N. Zhang, J. Fang, Y. Yang, *Gut Microbes*, **15**(1), 2236364 (2023).
48. J. W. Zhang, P. Du, D. W. Chen, L. Cui, C. M. Ying, *Chin. J. Gastrointest. Surg.*, **13**(1), 40 (2010).
49. B. S. Reddy, A. Rivenson, *Cancer Res.*, **53**, 3914 (1993).
50. L. Zhong, X. Zhang, M. Covasa, *World J. Gastroenterol.*, **20**, 7878 (2014).
51. R. Hendler, Y. Zhang, *Medicines*, **5**(3), 101 (2018).
52. O. Budu, C. D. Banciu, C. Soica, D. F. Lighezan, A. Milan, A. Prodea, A. Mioc, M. Mioc, G. Mardale, L. Sima, *Processes*, **11**(3), 781 (2023).
53. S. K. Bashir, G. M. El Moghazy, M. H. Abdel Aal, J. K. El Jakee, *Egypt J. Vet. Sci.*, **55**(3), 817 (2023).
54. L. Pattayil, H. T. Balakrishnan-Saraswathi, *Anti-cancer Res.*, **39**(7), 3795 (2019).

Bulgarian Chemical Communications, Volume 55, Special Issue C (pp. 45–55) 2023 *DOI: 10.34049/bcc.55.C.0005*

Pharmacogenetic markers associated with drug metabolism in patients with oncological diseases

N. Miteva-Marcheva[1,2], H. Ivanov[1,2], A. Linev[1,2], M. Topalov[1], V. Popov[3,5], G. Raycheva[3,6], Z. Grudeva-Popova[3,4], V. Stoyanova[1,2]

[1] *Department of Pediatrics and Medical Genetics, Faculty of Medicine, Medical University of Plovdiv, Plovdiv, Bulgaria*
[2] *Department of Medical Genetics, University Hospital "Sveti Georgi" – Plovdiv, Plovdiv, Bulgaria*
[3] *Department of Clinical Oncology, Faculty of Medicine, Medical University of Plovdiv, Plovdiv, Bulgaria*
[4] *Clinic of Clinical Hematology, University Hospital "Sveti Georgi" - Plovdiv, Plovdiv, Bulgaria*
[5] *Clinic of Radiation Oncology, University Hospital "Sveti Georgi" - Plovdiv, Plovdiv, Bulgaria*
[6] *Clinic of Medical Oncology, University Hospital "Sveti Georgi" - Plovdiv, Plovdiv, Bulgaria*

Received: November 2023; Revised: December 2023

Pharmacogenetics is the field of genetics that investigates how an individual's genetic variations can impact their metabolism and response to pharmaceutical agents, aiming to identify genetic markers that predict drug efficacy and safety. Personalized medicine is an approach that utilizes an individual's genetic, genomic, and clinical information to tailor medical treatments and interventions, with the goal of optimizing therapeutic outcomes and minimizing adverse effects. The objective of our investigation is to ascertain specific pharmacogenetic markers, particularly single nucleotide polymorphisms (SNPs), linked to the metabolism of chemotherapy agents within a cohort of cancer patients. The study consisted of 19 patients with colorectal cancer (CRC), 12 patients with non-small cell lung cancer (NSCLC) and 9 women with breast cancer (BC). Circulating tumor DNA (ctDNA) was extracted from blood plasma and sequenced. We identified 23 germline pharmacogenetic variants within 16 genes that are potentially associated with the metabolism of the chemotherapy drugs administered to the subjects, and all patients experienced varying degrees of adverse drug reactions. These pharmacogenetic markers can be employed for preemptive testing in cancer patients prior to initiating treatment regimens, facilitating the selection of the most optimal medication at the precise dosage with minimal associated side effects. Pharmacogenetic markers are the modern approach to individualize therapy with minimal risk of toxicity.

Keywords: pharmacogenetics, colorectal cancer, non-small cell lung carcinoma, breast cancer.

INTRODUCTION

In the ever-evolving landscape of oncological treatment, precision and efficacy are paramount for improved patient outcomes. Personalized medicine, a transformative approach, tailors interventions to individual genetic makeup, with pharmacogenetic markers playing a central role. These genetic variations significantly influence drug metabolism, response, and toxicity. Understanding these markers is crucial in oncology, where individual genetic profiles shape treatment success. This article explores the intersection of pharmacogenetics and oncological drug metabolism, unraveling genetic nuances to optimize treatment strategies, minimize adverse effects, and enhance care quality for oncology patients. The investigation's primary aim is to discern pharmacogenetic markers, especially single nucleotide polymorphisms (SNPs), intricately linked to the metabolic processes of chemotherapeutic agents in the demographic of cancer patients.

EXPERIMENTAL

We conducted a study involving 40 patients, consisting of 19 individuals diagnosed with colorectal cancer (three of them were subsequently excluded from the study due to the imperative requirement for exclusive radiotherapy), 12 with non-small cell lung carcinoma, and 9 women with breast cancer. The cell-free DNA was extracted from the blood samples using the QIAamp MinElute ccfDNA Midi

* To whom all correspondence should be sent:
E-mail: miteva_md@abv.bg

Kit, adhering to the established protocol outlined in BioChain's cfPure® Cell Free DNA Extraction Kit (1). To assess the quality and quantity of the extracted DNA, we employed Agarose Gel Electrophoresis and the Qubit DNA Assay Kit in a Qubit 3.0 Fluorimeter (Life Technologies, CA, USA). The subsequent step involved Next-generation sequencing (NGS) utilizing a targeted assay, NovoPMTM 2.0, designed to identify genomic alterations in a comprehensive panel of 484 genes. These genes were specifically selected based on their paramount relevance for the accurate diagnosis and treatment of solid tumors, aligning with current medical literature and clinical guidelines. Additionally, an in-house bioinformatic algorithm, developed by Novogene (Cambridge, United Kingdom), was applied to predict the origin of short variant mutations (germline or somatic) exclusively through the sequencing and analysis of tumor samples.

RESULTS

Our principal focus centered on the identification of germline mutations that may constitute a risk factor for heightened chemotherapy toxicity in cohorts of patients diagnosed with colorectal cancer (Table 1), non-small cell lung cancer (Table 2), and breast cancer (Table 3). Through our meticulous analysis, we successfully pinpointed 23 germline pharmacogenetic variants distributed across 16 genes, each implicated in precipitating adverse effects. These variants include MTHFR 1286A>C, MTHFR c.665C>T, DPYD c.2194G>A, DPYD 1627A>G, DPYD c.496A>G, DPYD c.85T>C, CYP1B1 c.1294G>C, XPC c.2815C>A, XPC c.1496C>T, ABCG2 c.421C>A, SLC22A2 c.808T>G, SOD2 c.47T>C, EGFR c.1562G>A, ABCB1 2677T>G, ABCC2 c.1249G>A, GSTP1 c.313A>G, ATM c.5557G>A, SLCO1B3 c.334T>G, SLCO1B3 c.699G>A, TP53 c.215C>G, XRCC1 1196A>G, ERCC2 c.2251A>C, and ERCC2 c.934G>A.

Noteworthy adverse effects from 1st to 5th degree according to Common Terminology Criteria for Adverse Effects (CTCAE) observed within our patient cohorts encompassed a spectrum of manifestations, including but not limited to anaemia, leukopenia, thrombocytopenia, gastrointestinal toxicity, hepatotoxicity, neurotoxicity, nephrotoxicity, cardiotoxicity, alopecia, rash, lymphangitis, and bone/joint pain.

Owing to the congruence in the administered chemotherapy regimens across the sampled patient cohort, a systematic regrouping was conducted, resulting in the categorization of individuals into six distinct groups. These groups encompassed patients subjected to specific therapeutic interventions: platinum-based chemotherapeutics (comprising 27 patients), pyrimidine analogues (involving 17 patients), EGFR inhibitors (encompassing 11 patients), taxanes (including 15 patients), anthracyclines (comprising 6 patients), and Cyclophosphamide (involving 6 patients).

In the cohort comprising the initial patient group subjected to platinum-based chemotherapeutics, our investigation revealed the presence of 11 distinct variants distributed across seven genes that exhibited significant associations with drug toxicity (Table 4). Notably, within this cohort, 11 individuals manifested heterozygosity for the MTHFR c.1286A>C variant, 14 individuals carried the MTHFR c.665C>T variant, and 17 individuals bore the XPC c.2815C>A variant, with near-universal prevalence observed for the XPC c.1496C>T variant, barring only two exceptions.

Furthermore, within this patient population, 8 out of 27 patients demonstrated carriage of the SLC22A2 c.808T>G variant, while for the ABCC2 c.1249G>A variant, all patients, save for two, exhibited carrier status. The GSTP1 c.313A>G variant was identified in 26 patients, underscoring its substantial representation.

Turning our attention to the SLCO1B3 gene, two distinct variants, namely c.334T>G and c.699G>A, were identified, with 23 and 26 patients exhibiting carrier status, respectively. Additionally, the ERCC2 gene featured prominently, with the c.2251A>C variant identified in 19 carriers and the c.934G>A variant in 22 carriers within the patient cohort.

Within the cohort of patients subjected to pyrimidine analogues, encompassing a total of 17 individuals, our comprehensive genetic analysis revealed the presence of 14 distinct variants distributed across 10 genes, all of which demonstrated significant associations with drug toxicity (Table 5). Notably, the MTHFR gene exhibited two discernible variants: the c.1286A>C variant was identified in 8 heterozygous patients, while the c.665C>T variant was observed in 8 patients.

Further genetic scrutiny of the DPYD gene uncovered a spectrum of 4 variants: c.2194G>A was detected in 7 patients, c.1627A>G in 4 patients, c.496A>G in 3 patients, and c.85C>T in 14 patients. Additionally, the CYP1B1 gene featured the c.1294G>C variant in 11 patients, whereas the ABCG2 gene harbored the c.421C>A vari-

Table 1. Colorectal Cancer Patients: Chemotherapeutics and Adverse Drug Reactions (ADRs) Graded from 1st to 5th Degree According to CTCAE

Patient	Age	Sex	Treatment	ADRs from 1st to 5th degree						
				anaemia	leukopenia	thrombocytopenia	hepatotoxicity	nephrotoxicity	neurotoxicity	GIT toxicity
1	48	male	Oxaliplatin, Leucovorin, 5-Fluorouracil, Irinotecan, Bevacizumab	1			3			
2	68	male	Oxaliplatin, Capecitabine, Irinotecan Bevacizumab	2			3			
3	70	male	Oxaliplatin, Leucovorin, 5-Fluorouracil, Irinotecan, Panitumumab	1			3	1		
4	65	male	Oxaliplatin, Leucovorin, 5-Fluorouracil, Irinotecan, Bevacizumab, Ramucirumab	2			1		2	
5	62	female	Oxaliplatin, Leucovorin, 5-Fluorouracil, Irinotecan, Bevacizumab, Ramucirumab	1						
6	67	male	Oxaliplatin, Leucovorin, 5-Fluorouracil, Panitumumab	2	1	1	1			
7	75	male	Oxaliplatin, Leucovorin, 5-Fluorouracil, Panitumumab	1			3			
8	73	female	Oxaliplatin, Leucovorin,, 5-Fluorouracil	1					2	
9	75	male	Oxaliplatin, Leucovorin,, 5-Fluorouracil, Panitumumab	1			3			
10	64	female	Oxaliplatin, Leucovorin, 5-Fluorouracil	1	2	2	1			
11	70	male	Oxaliplatin, Leucovorin, 5-Fluorouracil, Irinotecan, Capecitabine, Panitumumab, Cetuximab	1	3	3				
12	63	male	Oxaliplatin, Irinotecan, Capecitabine, Bevacizumab	1	3	3				
13	74	male	Oxaliplatin, Leucovorin, 5-Fluorouracil	2	3	3				
14	63	male	Oxaliplatin, Leucovorin, 5-Fluorouracil, Irinotecan, Panitumumab, Ramucirumab	3			3	1		2
15	46	female	Oxaliplatin, Leucovorin, 5-Fluorouracil	3	2	2	3			
16	61	female	Oxaliplatin, Leucovorin, 5-Fluorouracil, Irinotecan, Capecitabine, Panitumumab	2			1			

ant in 3 patients. The ABCB1 gene exhibited the c.2677T>G variant in 15 patients, and both the ABCC2 c.1249G>A and GSTP1 c.313A>G variants were prevalent in 15 and all but one patients, respectively.

Furthermore, the TP53 gene displayed the c.215C>G variant in 14 patients, XRCC1 exhibited the c.1196A>G variant in 16 patients, and the ERCC2 gene demonstrated the c.2251A>C variant in 14 patients.

Table 2. Non-Small Cell Lung Cancer Patients: Chemotherapeutics and Adverse Drug Reactions (ADRs) Graded from 1st to 5th Degree According to CTCAE

Patient			Treatment	ADRs from 1st to 5th degree					
	Age	Sex		anaemia	leukopenia	thrombocytopenia	hepatotoxicity	nephrotoxicity	rash
1	56	male	Pembrolizumab	**1**					
2	53	female	Paclitaxel, Carboplatin, Bevacizumab, Erlotinib, Atezolizumab	**1**					
3	64	male	Etoposid, Carboplatin, Atezolizumab	**1**			**1**		
4	54	male	Etoposid, Cisplatin, Docetaxel, Ramucirumab, Nivolumab	**1**			**3**	**1**	
5	59	female	Paclitaxel, Carboplatin, Pembrolizumab	**1**			**1**		**2**
6	72	male	Etoposid, Carboplatin, Atezolizumab	**2**	**2**	**1**	**4**		
7	74	male	Gemcitabine, Carboplatin, Atezolizumab, Docetaxel	**2**	**4**	**3**		**2**	**2**
8	64	male	Gemcitabine, Cisplatin, Docetaxel, Ramucirumab, Nivolumab, Erlotinib	**1**					
9	63	male	Gemcitabine, Cisplatin, Pembrolizumab	**2**			**1**		
10	53	female	Alectinib	**2**					
11	52	male	Paclitaxel, Carboplatin, Pembrolizumab	**1**	**2**				
12	65	male	Cisplatin, Vinorelbin, Erlotinib, Docetaxel, Atezolizumab	**1**				**2**	

Table 3. Breast Cancer Patients: Chemotherapeutics and Adverse Drug Reactions (ADRs) Graded from 1st to 5th Degree According to CTCAE

Patient			Treatment	ADRs from 1st to 5th degree											
	Age	Sex		**A***	**B**	**C**	**D***	**E**	**F**	**G**	**H**	**J**	**K**	**L**	**M**
1	34	female	Farmorubicin, Cyclophosphamide, Docetaxel	**1**							**2**		**2**		
2	51	female	Paclitaxel, Carboplatin, Docetaxel	**2**			**1**						**1**		
3	53	female	Farmorubicin, Cyclophosphamide, 5-Fluoro uracil, Paclitaxel							**2**			**2**	**2**	**2**
4	63	female	Pertuzumab, Trastuzumab, Docetaxel				**2**						**1**		
5	31	female	Farmorubicin. Docetaxel, Cyclophosphamide	**1**			**1**						**2**		
6	58	female	Farmorubicin, Docetaxel, Cyclophosphamide	**2**	**2**	**1**							**2**		
7	87	female	Arimidex	**1**											
8	37	female	Farmorubicin, Cyclophosphamide, Trastuzuma, Docetaxel, Tamoxifen, Zolendronic acid, Zoladex, Letrozole, Xgeva, Exemestane, Lapatinib	**1**	**1**	**1**	**2**		**2**	**2**	**2**	**2**	**2**		
9	67	female	Farmorubicin, Docetaxel, Cyclophosphamide				**2**			**2**	**2**	**2**	**2**		

***A** anaemia, **B** leukopenia, **C** thrombocytopenia, **D** hepatotoxicity, **E** nephrotoxicity, **F** neurotoxicity, **G** cardiotoxicity, **H** GIT toxicity, **J** rash, **K** alopecia, **L** lymphangitis, **M** bone/joint pain.

Exclusive identification of a singular variant within the EGFR gene was discerned within the patient cohort subjected to EGFR inhibitors, denoted as c.1562G>A (Table 6). Remarkably, the entire patient ensemble unequivocally exhibited carrier status for this specific genetic variant, as delineated in Table 6.

Within the cohort of patients subjected to taxane-based treatments, comprising a total of 15 individuals, our comprehensive genetic analysis unveiled the presence of six distinct variants distributed across five genes, each exhibiting significant associations with drug toxicity (Table 7). Specifically, the c.47T>C variant of the SOD2 gene was identified in

Table 4. Patients Treated with Platinum-Based Chemotherapeutics and Genes Associated with the Metabolism of These Agents (HMZ – homozygote; HTZ – heterozygote)

Patient			Disease	Treatment	Genes, associated with the metabolism of platinum-based chemotherapeutics										
	Age	Sex			MTHFR	MTHFR	XPC	XPC	SLC22A2	ABCC2	GSTP1	SLCO183	SLCO183	ERCC2	ERCC2
					c.1286A>C	c.665C>T	c.2815C>A	c.1496>T	c.808T>G	c.1249G>A	c.313A>G	c334T>G	c.699G>A	c.2251A>A	c.934G>A
					rs1801131	rs1801133	rs2228001	rs2228000	rs316019	rs2273697	rsl695	rs4149117	rs7311358	rs13181	rs1799793
1	48	male	CRC	Oxaliplatin			HTZ(CA)	HMZ(CC)		HTZ(AG)	HTZ(AG)	HTZ(GT)	HTZ(AG)		HMZ(GG)
2	68	male	CRC	Oxaliplatin			HTZ(CA)	HMZ(CC)		HMZ(GG)	HMZ(AA)		HMZ(AA)	HTZ(CA)	
3	70	male	CRC	Oxaliplatin		HTZA(TC)				HMZ(GG)	HTZ(AG)		HMZ(AA)		HMZ(GG)
4	65	male	CRC	Oxaliplatin		HTZA(TC)	HMZ(CC)	HMZ(CC)			HMZ(AA)	HMZ(GG)	HMZ(AA)	HTZ(CA)	HTZ(GA)
5	62	female	CRC	Oxaliplatin	HTZ(CA)		HTZ(CA)	HTZ(CT)	HTZ(TG)	HMZ(GG)	HMZ(AA)		HMZ(AA)	HTZ(CA)	
6	67	male	CRC	Oxaliplatin		HTZA(TC)		HMZ(CC)	HTZ(TG)	HMZ(GG)	HMZ(AA)	HMZ(GG)	HMZ(AA)		HTZ(GA)
7	75	male	CRC	Oxaliplatin		HMZ(TT)		HTZ(CT)		HMZ(GG)	HMZ(AA)	HMZ(GG)	HMZ(AA)	HTZ(CA)	HTZ(GA)
8	73	female	CRC	Oxaliplatin	HTZ(CA)	HTZA(TC)	HTZ(CA)	HMZ(CC)	HTZ(TG)		HTZ(AG)	HMZ(GG)	HMZ(AA)	HTZ(CA)	HMZ(GG)
9	75	male	CRC	Oxaliplatin		HTZA(TC)		HTZ(CT)		HMZ(GG)	HMZ(AA)	HMZ(GG)	HMZ(AA)	HTZ(CA)	HTZ(GA)
10	64	female	CRC	Oxaliplatin			HTZ(CA)	HTZ(CT)		HMZ(GG)	HMZ(AA)	HMZ(GG)	HMZ(AA)	HMZ(CC)	
11	70	male	CRC	Oxaliplatin	HTZ(CA)		HTZ(CA)	HTZ(CT)	HTZ(TG)	HMZ(GG)		HMZ(GG)	HMZ(AA)	HTZ(CA)	HTZ(GA)
12	63	male	CRC	Oxaliplatin		HTZA(TC)		HMZ(CC)		HMZ(GG)	HTZ(AG)	HMZ(GG)	HMZ(AA)	HTZ(CA)	HTZ(GA)’
13	74	male	CRC	Oxaliplatin	HTZ(CA)		HTZ(CA)	HMZ(CC)		HMZ(GG)	HMZ(AA)	HMZ(GG)		HTZ(CA)	HTZ(GA)
14	63	male	CRC	Oxaliplatin	HTZ(CA)			HTZ(CT)		HTZ(AG)	HTZ(AG)	HMZ(GG)	HMZ(AA)	HTZ(CA)	HMZ(GG)
15	46	female	CRC	Oxaliplatin	HTZ(CA)	HTZA(TC)	HTZ(CA)	HTZ(CT)	HTZ(TG)	HMZ(GG)	HMZ(AA)	HMZ(GG)	HMZ(AA)	HTZ(CA)	HTZ(GA)
16	61	female	CRC	Oxaliplatin	HTZ(CA)		HTZ(CA)	HMZ(CC)	HTZ(TG)	HMZ(GG)	HTZ(AG)	HMZ(GG)	HMZ(AA)	HTZ(CA)	HTZ(GA)
17	53	female	NSCLC	Carboplatin	HTZ(CA)		HTZ(CA)	HMZ(CC)	HTZ(TG)	HMZ(GG)	HTZ(AG)	HTZ(GT)	HTZ(AG)	HMZ(CC)	
18	64	male	NSCLC	Carboplatin		HTZA(TC)	HMZ(CC)	HMZ(CC)		HTZ(AG)	HTZ(AG)	HMZ(GG)	HMZ(AA)		HMZ(GG)
19	54	male	NSCLC	cisPlatin		HTZA(TC)		HTZ(CT)		HMZ(GG)	HMZ(AA)	HMZ(GG)	HMZ(AA)	HTZ(CA)	HTZ(GA)
20	59	female	NSCLC	Carboplatin		HMZ(TT)		HTZ(CT)		HTZ(AG)	HMZ(AA)	HMZ(GG)	HMZ(AA)		
21	72	male	NSCLC	Carboplatin			HMZ(CC)	HMZ(CC)	HTZ(TG)	HMZ(GG)	HTZ(AG)		HMZ(AA)	HMZ(CC)	HMZ(GG)
22	74	male	NSCLC	Carboplatin	HTZ(CA)					HMZ(GG)	HTZ(AG)	HMZ(GG)	HMZ(AA)	HTZ(CA)	HMZ(GG)
23	64	male	NSCLC	cisPlatin	HTZ(CA)	HTZA(TC)	HMZ(CC)	HMZ(CC)		HTZ(AG)	HMZ(AA)	HTZ(GT)	HTZ(AG)	HTZ(CA)	HTZ(GA)
24	63	male	NSCLC	cisPlatin			HTZ(CA)	HTZ(CT)		HTZ(AG)	HMZ(AA)	HMZ(GG)	HMZ(AA)	HTZ(CA)	HTZ(GA)
25	52	male	NSCLC	Carboplatin		HMZ(TT)		HMZ(CC)		HMZ(GG)	HTZ(AG)	HMZ(GG)	HMZ(AA)		HMZ(GG)
26	65	male	NSCLC	cisPlatin	HTZ(CA)	HTZA(TC)		HTZ(CT)		HMZ(GG)	HMZ(AA)	HTZ(GT)	HTZ(AG)		HTZ(GA)
27	51	female	BC	Carboplatin			HTZ(CA)	HMZ(CC)		HTZ(AG)	HTZ(AG)	HTZ(GT)	HTZ(AG)		HTZ(GA)

Table 5. Patients Treated with Pyrimidine Analogues and Genes Associated with the Metabolism of These Agents (HMZ – homozygote; HTZ – heterozygote)

	Patient		Disease	Treatment	Genes associated with the metabolism of 5-FU/ Capecitabine												
	Age	Sex			MTHFR	MTHFR	DPYD	DPYD	DPYD	DPYD	CYP1B1	ABCC2	ABCC2	GSTP1	TPS3	XRCC1	ERCC2
					c.1286A>C	c.665C>T	c.2194G>A	C.1627A>G	c.496A>G	c.85C>T	c.1294G>C	c.421C>A	c.1249G>A	c.313A>G	c.215C>G	c.1196A>G	c.2251A>C
					rsl801131	rsl801133	rsl801160	rsl801159	rs2297595	rsl801265	rsl056836	rs2231142	rs273697	rs1695	rs10425222	rs25487	rs13181
1	48	male	CRC	5-Fluoro uracil					HTZ(GA)	HTZ(TC)	HTZ(CG)		HTZ(AG)	HTZ(AG)	HMZ(GG)	HTZ(AG)	
2	68	male	CRC	Capecitabine						HMZ(TT)	HTZ(CG)		HMZ(GG)	HMZ(AA)	HTZ(GC)	HTZ(AG)	HTZ(CA)
3	70	male	CRC	5-Fluoro uracil		HTZ(TC)				HTZ(TC)			HMZ(GG)	HTZ(AG)	HMZ(GG)	HMZ(AA)	
4	65	male	CRC	5-Fluoro uracil		HTZ(TC)	HTZ(AG)	HTZ(GA)		HMZ(TT)	HTZ(CG)			HMZ(AA)	HMZ(GG)	HTZ(AG)	HTZ(CA)
5	62	female	CRC	5-Fluoro uracil	HTZ(CA)		HTZ(AG)			HMZ(TT)			HMZ(GG)	HMZ(AA)		HTZ(AG)	HTZ(CA)
6	67	male	CRC	5-Fluoro uracil		HTZ(TC)				HTZ(TC)	HTZ(CG)		HMZ(GG)	HMZ(AA)	HTZ(GC)	HTZ(AG)	
7	75	male	CRC	5-Fluoro uracil		HMZ(TT)	HMZ(AA)						HMZ(GG)	HMZ(AA)	HMZ(GG)	HMZ(AA)	HTZ(CA)
8	73	female	CRC	5-Fluoro uracil	HTZ(CA)	HTZ(TC)	HTZ(AG)			HTZ(TC)	HMZ(CC)			HTZ(AG)	HTZ(GC)	HMZ(AA)	HTZ(CA)
9	75	male	CRC	5-Fluoro uracil		HTZ(TC)	HTZ(AG)	HTZ(GA)		HTZ(TC)			HMZ(GG)	HMZ(AA)	HTZ(GC)	HMZ(AA)	HTZ(CA)
10	64	female	CRC	5-Fluoro uracil			HMZ(AA)			HMZ(TT)	HMZ(CC)		HMZ(GG)	HMZ(AA)	HTZ(GC)	HTZ(AG)	HMZ(CC)
11	70	male	CRC	5-Fluorouracil, Capecitabine	HTZ(CA)					HMZ(TT)	HTZ(CG)	HTZ(AC)	HMZ(GG		HTZ(GC)	HMZ(AA)	HTZ(CA)
12	63	male	CRC	Capecitabine					HMZ(GG)		HMZ(CC)		HMZ(GG	HTZ(AG)	HTZ(GC)	HTZ(AG)	HTZ(CA)
13	74	male	CRC	5-Fluoro uracil	HTZ(CA)		HTZ(AG)	HMZ(GG)		HMZ(TT)			HMZ(GG	HMZ(AA)		HMZ(AA)	HTZ(CA)
14	63	male	CRC	5-Fluoro uracil	HTZ(CA)					HTZ(TC)	HTZ(CG)		HTZ(AG)	HTZ(AG)		HMZ(AA)	HTZ(CA)
15	46	female	CRC	5-Fluoro uracil	HTZ(CA)	HTZ(TC)		HTZ(GA)		HTZ(TC)	HTZ(CG)	HTZ(AC)	HMZ(GG	HMZ(AA)	HMZ(GG)		HTZ(CA)
16	61	female	CRC	5-Fluorouracil, Capecitabine	HTZ(CA)				HTZ(GA)	HTZ(TC)		HTZ(AC)	HMZ(GG	HTZ(AG)	HMZ(GG)	HMZ(AA)	HTZ(CA)
17	53	female	BC	5-Fluoro uracil	HTZ(CA)					HTZ(TC)	HTZ(CG)		HMZ(GG	HTZ(AG)	HMZ(GG)	HTZ(AG)	HTZ(CA)

Table 6. Patients Treated with EGFR Inhibitors and Genes Associated with the Metabolism of These Agents (HMZ – homozygote; HTZ – heterozygote)

Patient			Disease	Treatment	Genes, associated with the metabolism of EGFR Inhibitors
	age	sex			
					EGFR, c.1562G>A, rs 2227983
1	70	male	CRC	Panitumumab	HMZ(GG)
2	67	male	CRC	Panitumumab	HMZ(GG)
3	75	male	CRC	Panitumumab	HMZ(GG)
4	75	male	CRC	Panitumumab	HMZ(GG)
5	70	male	CRC	Panitumumab, Cetuximab	HMZ(GG)
6	63	male	CRC	Panitumumab	HMZ(GG)
7	61	female	CRC	Panitumumab	HMZ(GG)
8	53	female	NSCLC	Erlotinib	HMZ(GG)
9	64	male	NSCLC	Erlotinib	HTZ(GA)
10	65	male	NSCLC	Erlotinib	HTZ(GA)

Table 7. Patients Treated with Taxanes and Genes Associated with the Metabolism of These Agents (HMZ – homozygote; HTZ – heterozygote)

Patient			Disease	Treatment	Genes associated with the metabolism of 5-FU/ Capecitabine					
	Age	Sex			SOD2	ABCB1	ABCC2	SLCO1B3	SLCO1B3	ERCC2
					c.47T>C	c.22677T>G	c.1249G>A	c.334T>G	c.699G>A	c.2251A>C
					rs4880	rs2032582	rs2273697	rs4149117	ra7311358	rs131814
1	34	female	BC	Docetaxel	HTZ(AC)	HTZ(TG)	HMZ(GG)	HTZ(GT)	HTZ(AG)	HTZ(AC)
2	51	female	BC	Paclitaxel, Docetaxel	HTZ(AC)	HTZ(TG)	HTZ(GA)	HTZ(GT)	HTZ(AG)	HMZ(AA)
3	53	female	BC	Paclitaxel	HMZ(AA)	HTZ(TG)	HMZ(GG)	HMZ(GG)	HMZ(AA)	HTZ(AC)
4	63	female	BC	Docetaxel	HTZ(AC)	HMZ(TT)	HMZ(GG)	HMZ(GG)	HMZ(AA)	
5	31	female	BC	Docetaxel		HTZ(TG)	HMZ(GG)	HMZ(GG)	HMZ(AA)	HMZ(AA)
6	58	female	BC	Docetaxel	HMZ(AA)	HTZ(TG)	HMZ(GG)	HMZ(GG)	HMZ(AA)	HTZ(AC)
7	37	female	BC	Docetaxel	HTZ(AC)	HTZ(TG)	HTZ(GA)	HTZ(GT)	HTZ(AG)	HTZ(AC)
8	67	female	BRCA	Docetaxel			HMZ(GG)	HTZ(GT)	HTZ(AG)	HTZ(AC)
9	53	female	NSCLC	Paclitaxel			HMZ(GG)	HTZ(GT)	HTZ(AG)	
10	54	male	NSCLC	Docetaxel	HTZ(AC)			HMZ(GG)	HMZ(AA)	HTZ(AC)
11	59	female	NSCLC	Paclitaxel		HMZ(TT)	HTZ(GA)	HMZ(GG)	HMZ(AA)	HMZ(AA)
12	74	male	NSCLC	Docetaxel	HTZ(AC)		HMZ(GG)	HMZ(GG)	HMZ(AA)	HTZ(AC)
13	64	male	NSCLC	Docetaxel	HTZ(AC)		HTZ(GA)	HTZ(GT)	HTZ(AG)	HTZ(AC)
14	52	male	NSCLC	Paclitaxel		HTZ(TG)	HMZ(GG)	HMZ(GG)	HMZ(AA)	HMZ(AA)
15	65	male	NSCLC	Docetaxel		HTZ(TG)	HMZ(GG)	HTZ(GT)	HTZ(AG)	HMZ(AA)

10 patients, underscoring its substantial representation. Furthermore, the ABCB1 c.2677T>G variant and the ABCC2 c.1249G>A variant were each identified in 10 and all but one patients, respectively.

The intricate genetic landscape also revealed the presence of two variants within the SLCO1B3 gene—c.334T>G and c.699G>A—both universally present across the entire patient cohort. Lastly, the ERCC2 c.2251A>C variant was identified in 13 patients.

Both patient cohorts, namely those treated with Cyclophosphamide and Farmorubicin, exhibit an

identical composition of six individuals (Table 8). Our meticulous genetic investigation identified six genes harboring variants intricately associated with the metabolism and manifestation of adverse drug reactions within this shared patient subset. Notably, the CYP1B1 c.1294G>C variant was prevalent in 5 patients, while the ABCG2 c.421C>A and ATM c.5557G>A variants were identified in 2 patients each. Additionally, the ABCC2 c.1249G>A and GSTP1 c.313A>G variants were uniformly present across the entirety of both patient groups. Moreover, the TP53 c.215C>G and XRCC1 c.1196A>G variants were identified in all but one patient.

DISCUSSION

The study aimed to identify germline pharmacogenetic variants associated with increased chemotherapy-related toxicity risk. The MTHFR gene, encoding methylenetetrahydrofolate reductase involved in DNA and RNA synthesis, features the c.1286A>C variant linked to reduced enzyme activity. Kristensen et al. associated the CC genotype with heightened toxicity risk in colorectal neoplasm patients treated with Capecitabine, Fluorouracil, Leucovorin, and Oxaliplatin (2). In our cohort, c.1286A>C was detected in 11 of 27 platinum-treated patients (allele frequency 0.2037) and 8 of 17 pyrimidine analogue-treated patients (allele frequency 0.2353). Another MTHFR variant, c.665C>T, correlated with increased adverse effects in colorectal cancer patients (3). In our study, c.665C>T occurred in 14 platinum-treated patients (allele frequency 0.3148) and 8 pyrimidine analogue-treated patients (allele frequency 0.2647).

The DPYD gene, pivotal in pyrimidine metabolism, encodes dihydropyrimidine dehydrogenase, crucial for processing chemotherapy drugs like 5-Fluorouracil and Capecitabine. DPYD variants can diminish DPD activity, heightening toxic effects, particularly with 5-Fluorouracil (linked to DPD deficiency) (4). Four DPYD variants identified in our pyrimidine analogue-treated patients—c.2194G>A (7/17, allele frequency 0.2647), c.1627A>G (4/17, allele frequency 0.1471), c.496A>G (3/17, allele frequency 0.0294), and c.85C>T (all but two, allele frequency 0.6176) – may elevate the risk of adverse reactions to chemotherapy, aligning with previous research (5).

The CYP1B1 gene encodes cytochrome P450 1B1, pivotal in metabolizing various substances, including drugs and toxins. The c.1294G>C variant has been studied for its association with chemotherapeutic toxicity, notably Cyclophosphamide, Doxorubicin, and 5-Fluorouracil (6). In the pyrimidine analogue-treated group (n=17), 11 carriers were identified (allele frequency 0.4118). In the anthracyclines and Cyclophosphamide-treated group (n=6), carriers, all but one, exhibited the variant (allele frequency 0.5833). This highlights the potential role of the CYP1B1 variant in chemotherapy response across distinct patient groups.

Table 8. Patients Treated with Farmorubicin and Cyclophosphamide, and Genes Associated with the Metabolism of These Agents (HMZ – homozygote; HTZ – heterozygote)

Patient			Disease	Treatment	Genes associated with the metabolism of Farmorubicin						
	Age	Sex			CYP11B1	ABCG2	ABCC2	GSTP1	ATM	TP53	XRCC1
					c.1294G>C	c.421C>A	c.1246G>A	c.313A>G	c.5557G>A	c.215C>G	c.1196A>G
					rs1056836	rs2231142	rs2273697	rs1695	rs1801516	rs1042522	rs25487
1	34	female	BC	Farmorubicin, Cyclophosphamide	HMZ(CC)		HMZ(GG)	HTZ(AG)	HTZ(AG)	HTZ(GC)	HTZ(AG)
2	53	female	BC	Farmorubicin, Cyclophosphamide	HTZ(GG)		HMZ(GG)	HTZ(AG		HMZ(GG)	HTZ(AG)
3	31	female	BC	Farmorubicin, Cyclophosphamide	HTZ(GG)	HTZ(AC)	HMZ(GG)	HMZ(AA)		HTZ(GC)	HMZ(AA) GSTP1
4	58	female	BC	Farmorubicin, Cyclophosphamide	HTZ(GG)		HMZ(GG)	HMZ(AA)		HMZ(GG)	HTZ(AG)
5	37	female	BC	Farmorubicin, Cyclophosphamide	HMZ(CC)		HTZ(AG)	HMZ(AA)		HMZ(GG)	HTZ(AG)
6	67	female	BC	Farmorubicin, Cyclophosphamide		HTZ(AC)	HMZ(GG)	HTZ(AG)	HTZ(AG)		

DNA damage, implicated in cell death, aging, and cancer, is recognized and addressed by XPC, a crucial gene in damage removal. Commonly observed XPC gene variants among our patients are c.2815C>A and c.1496C>T. Studies suggest increased adverse reactions risk in individuals with AA and AC genotypes of c.2815C>A and CC and CT genotypes of c.1496C>T when treated with platinum-based chemotherapeutics (7). In our Cisplatin/Oxaliplatin-treated patients (n=27), c.2815C>A was found in 17 (allele frequency 0.4074), and c.1496C>T in all but two patients (allele frequency 0.7222), emphasizing potential implications for platinum-based chemotherapy responses.

The ABCG2 gene, linked to drug resistance in cancer cells, features the c.421C>A variant affecting the pharmacokinetics and toxicity of chemotherapy drugs. Research suggests increased toxicity risk, especially with Cyclophosphamide, Doxorubicin, and Fluorouracil (6). In the pyrimidine analogue-treated group (n=17), 3 carriers were identified (allele frequency 0.0882). In the Cyclophosphamide and Anthracyclines-treated group (n=6), carriers were 2 out of 6 (allele frequency 0.1667), highlighting the potential impact of the ABCG2 variant on chemotherapy responses.

The overexpression of the SLC22A2 gene, observed in various cancers, is linked to multidrug resistance, reducing chemotherapy efficacy (8). The SLC22A2 c.808T>G variant, associated with adverse chemotherapeutic effects, is implicated in increased toxicity in non-small cell lung and colorectal cancer patients receiving platinum-based compounds (9). In our patient group, 8 carriers were identified (allele frequency 0.1667), emphasizing the potential impact of the SLC22A2 variant on platinum-based chemotherapy responses.

In cancer research, the SOD2 gene has been scrutinized for its involvement in tumorigenesis and malignancy progression. The c.47T>C variant is linked to heightened sensitivity to chemotherapy-induced adverse reactions, particularly with taxanes, where T allele homozygotes and heterozygotes face increased risks compared to CC homozygotes (10). In our Docetaxel/Paclitaxel-treated patient group (n=15), 10 carriers were identified (allele frequency 0.4333), highlighting the potential impact of the SOD2 variant on taxane chemotherapy responses.

EGFR signaling inhibitors, including tyrosine kinase inhibitors (TKIs) and monoclonal antibodies, are pivotal targeted therapies for cancer. Recent studies reveal an association between the EGFR c.1562G>A variant and cytotoxicity with EGFR inhibitors (11). In our EGFR inhibitor-treated patient cohort, all individuals were carriers of the variant, yielding an allele frequency of 0.9091, underscoring the potential impact of the EGFR variant on treatment outcomes.

ABCB1 overexpression in tumors is linked to multidrug resistance in cancer chemotherapy (12). Gonzalez-Haba et al. found increased adverse drug reactions in homozygous mutant or heterozygous carriers of the c.2677T>G polymorphism during 5-FU/Capecitabine therapies (13). In our pyrimidine analogue-treated group, all but two were carriers (allele frequency 0.5588). Taxane-treated patients with the wild-type allele, in homozygous or heterozygous state, are at heightened risk of adverse reactions (14). In our taxane-treated group (n=15), carriers were 10 patients (allele frequency 0.4). This underscores the potential impact of ABCB1 polymorphisms on chemotherapy outcomes.

In cancer research, ABCC2 is extensively examined for its role in drug resistance, where overexpression can actively expel drugs from cancer cells, reducing intracellular concentrations. The c.1249G>A variant is associated with increased susceptibility to adverse reactions induced by chemotherapeutics like 5-Fluorouracil, Cyclophosphamide, and Farmorubicin (6). In our pyrimidine analogue-treated group (n=17), all but two were carriers (allele frequency 0.8235). In the Cyclophosphamide and Farmorubicin-treated groups (n=6), all but one were carriers (allele frequency 0.8), highlighting the potential impact of ABCC2 variant on chemotherapy responses.

GSTP1 has been implicated in cancer, potentially contributing to chemotherapy and radiotherapy resistance or influencing carcinogenesis by regulating compound metabolism (15). Literature data suggest a higher risk of toxicity in cancer patients with the c.313A>G polymorphism (genotype AA/AG) receiving 5-Fluorouracil and platinum compounds (16). In our platinum-based chemotherapeutics group (n=27), carriers of the variant constituted the majority, with an allele frequency of 0.7407. Similarly, in the 5-Fluorouracil/Capecitabine group (n=17), carriers predominated, with an allele frequency of 0.7353. This underscores the potential role of the GSTP1 variant in influencing chemotherapy responses.

The ATM gene, vital for maintaining genome stability and DNA repair, plays a pivotal role in safeguarding against chemotherapy-induced DNA damage. Variants in the ATM gene, notably c.5557G>A, have been scrutinized for their asso-

ciation with chemotherapeutic toxicity. Individuals with AA and AG genotypes face a higher risk than those with the GG genotype (6). In our sample, the incidence of the c.5557G>A variant in patients treated with Cyclophosphamide and Farmorubicin was low—2 out of 6 with an allele frequency of 0.1667. This underscores the potential impact of the ATM variant on chemotherapy responses in this specific treatment context.

SLCO1B3 overexpression is noted in cancers like non-small cell lung carcinoma, breast cancer, and colorectal cancer, associated with poor prognosis and chemotherapy resistance, especially to taxanes and platinum-containing medications. The c.334T>G and c.699G>A variants of SLCO1B3 are linked to chemotherapeutic toxicity and drug resistance (17). In our taxane-treated patients (n=27), carriers of c.334T>G were 24 (allele frequency 0.7963), and for c.699G>A, all but one were carriers (allele frequency 0.8704). In the taxane-treated group, all 15 patients were carriers of both variants (allele frequency for both variants 0.7667). This emphasizes the potential impact of SLCO1B3 variants on chemotherapy responses.

The TP53 gene, pivotal in cell growth regulation and tumor suppression, is often disrupted in cancers due to its crucial role in maintaining genomic integrity. Studies on the TP53 c.215C>G variant indicate heightened susceptibility to chemotherapy-induced adverse reactions, including hematological, neurotoxicity, or gastrointestinal toxicity (6). In our pyrimidine analogue-treated group (n=17), carriers were 14 patients with an allele frequency of 0.6471, while in the Farmorubicin and Cyclophosphamide-treated group (n=6), carriers were 5 individuals with an allele frequency of 0.6667. This underscores the potential impact of the TP53 variant on chemotherapy responses in specific treatment contexts.

The XRCC1 gene, crucial in DNA repair, features the c.1196A>G variant associated with chemotherapeutic toxicity, particularly haematological or gastrointestinal toxicity, when treated with 5-Fluorouracil/Capecitabine, Farmorubicin, or Cyclophosphamide (6). In our pyrimidine analogue-treated group, the allele frequency is 0.7059, with carriers constituting all but one individual. Similarly, in the Farmorubicin and Cyclophosphamide-treated group, the allele frequency is 0.5, with all but one individual being carriers. This emphasizes the possible influence of the XRCC1 variant on how chemotherapy is responded to in these particular treatment scenarios.

The ERCC2 gene, alias XPF, encodes the ERCC2 protein, a vital element in the nucleotide excision repair (NER) pathway, countering DNA damage from UV radiation. Studies link the c.2251A>C variant to elevated drug toxicity risk in colorectal neoplasm patients treated with 5-Fluorouracil and Leucovorin or 5-Fluorouracil, Leucovorin, and Oxaliplatin (18). In our pyrimidine analogue-treated group, carriers of the variant were all but three (allele frequency 0.4412), while in the platinum-based chemotherapeutics group, 19 individuals were carriers (allele frequency 0.4074). Another ERCC2 variant, c.934G>A, linked to XPD protein function in DNA repair, may increase drug toxicity risk with platinum-containing chemotherapeutics (19). In our Carboplatin/Oxaliplatin-treated group, carriers numbered 22 individuals, with an allele frequency of 0.5556.

CONCLUSIONS

In conclusion, our study delves into the realm of pharmacogenetics, investigating how genetic variations impact drug metabolism in patients with oncological diseases. The identified 23 germline pharmacogenetic variants within 16 genes present potential associations with the metabolism of chemotherapy drugs, revealing a complex interplay between genetic factors and adverse drug reactions in our cohort of colorectal cancer, non-small cell lung cancer, and breast cancer patients. These findings underscore the importance of personalized medicine in optimizing therapeutic outcomes and minimizing adverse effects. The incorporation of these pharmacogenetic markers into preemptive testing protocols offers a promising avenue for tailoring treatment regimens, ensuring the selection of the most effective medication at precise dosages, while minimizing the risk of toxicity. Embracing pharmacogenetic markers represents a modern and vital approach to individualizing therapy in oncology, paving the way for more effective and safer treatment strategies.

Acknowledgements: *The authors acknowledge support (financial, computational, logistic) from the project BG05M2OP001-1.002-0005 /29.03.2018 (2018-2023) - Center for Competence "Personalized Innovative Medicine (PERIMED)", funded by the Science and Education for Smart Growth Operational Programme, co-funded by the European Union through the European Structural and Investment Funds.*

REFERENCES

1. P. G. Bruce, A. R. West, *J. Solid State Chem*., **44**(3), 354 (1982).
2. E. Polatoglou, Z. Mayer, V. Ungerer, A. J. Bronkhorst, S. Holdenrieder, *Diagnostics* (Basel), **12**(10), 2550 (2022).
3. M. H. Kristensen, P. L. Pedersen, G. V. Melsen, J. Ellehauge, J. Mejer, *J. Int. Med. Res.*, **38**(3), 870 (2010).
4. W. H. Vogel, A. Minhas, S. Baumrucker, *J. Adv. Pract. Oncol*. **11**(1), 68 (2020).
5. N. Božina, I. Bilić, L. Ganoci, L. Šimičević, S. Pleština, L. Lešnjaković, V. Trkulja, *Br. J. Clin. Pharmacol*., **88**(5), 2190 (2022).
6. K. Tecza, J. Pamula-Pilat, J. Lanuszewska, D. Butkiewicz, E. Grzybowska, *Oncotarget*, **9**(10), 9114 (2018).
7. S. Sakano, Y. Hinoda, M. Sasaki, T. Wada, H. Matsumoto, S. Eguchi, A. Shinohara, Y. Kawai, T. Hara, K. Nagao, T. Hara, K. Naito, H. Matsuyama, *Pharmacogenomics*, **11**(10), 1377 (2010).
8. J. Chen, L. Wang, G. Tong, J. Ma, C. Liu, L. Wang, *Int. J. Clin. Pharmacol. Ther*., **61**(1), 1 (2023).
9. C. Y. Qian, Y. Zheng, Y. Wang, J. Chen, J. Y. Liu, H.H. Zhou HH, J. Y. Yin, Z. Q. Liu, *Chin. J. Cancer*, **35**(1), 85 (2016).
10. V. Bosó, M. J. Herrero, A. Santaballa, L. Palomar, J. E. Megias, H. de la Cueva, L. Rojas, M. R. Marqués, J. L. Poveda, J. Montalar, S. F. Aliño, *Pharmacogenomics*, **15**(15), 1845 (2014).
11. G. Liu, S. Gurubhagavatula, W. Zhou, Z. Wang, B. Y. Yeap, K. Asomaning, L. Su, R. Heist, T. J. Lynch, D. C. Christiani, *Pharmacogenomics*, **8**(2), 129 (2008).
12. H. Sui, Z. Z. Fan, Q. Li, *J. Int. Med. Res.*, **40**(2), 426 (2012).
13. E. Gonzalez-Haba, M. I. García, L. Cortejoso, C. López-Lillo, N. Barrueco, P. García-Alfonso, S. Alvarez, J. L. Jiménez, M. L. Martín, M. A. Muñóz-Fernández, M. Sanjurjo, L. A. López-Fernández, *Pharmacogenomics*, **11**(12), 1715 (2010).
14. H. S. Kim, M. K. Kim, H. H. Chung, J. W. Kim, N. H. Park, Y. S. Song, S. B. Kang, *Gynecol. Oncol.*, **113**(2), 264 (2009).
15. R. R. Singh, K. M. Reindl, *Antioxidants*, **10**(5), 701 (2021).
16. H. L. McLeod, D. J. Sargent, S. Marsh, E. M. Green, C. R. King, C. S. Fuchs, R. K. Ramanathan, S. K. Williamson, B. P. Findlay, S. N. Thibodeau, A. Grothey, R. F. Morton, R. M. Goldberg, *J. Clin. Oncol*., **28**(20), 3227 (2010).
17. H. S. Park, S. M. Lim, H. J. Shin, A. Cho, J. G. Shin, M. G. Lee, H. R. Kim, J. H. Kim, B. C. Cho, *Pharmacogenet. Genomics*, **26**(3), 116 (2016).
18. M. Y. Huang, W. Y. Fang, S. C. Lee, T. L. Cheng, J. Y. Wang, S. R. Lin, *BMC Cancer*, **12**(8), 50 (2008).
19. C. Pérez-Ramírez, M. Cañadas-Garre, A. Alnatsha, E. Villar, J. R. Delgado, M. J. Faus-Dáder, M. Ÿ. Calleja-Hernández, *Pharmacol. Res*., **111**, 877 (2016).

Bulgarian Chemical Communications, Volume 55, Special Issue C (pp. 57–63) 2023 *DOI: 10.34049/bcc.55.C.0006*

Specific protease- and aminopeptidase activity of potential bioactive peptide-producing lactobacilli in media with plant protein hydrolysates

T. M. Panayotova[1,2*], Z. L. Urshev[1], I. N. Iliev[2]

[1] *Centre of Technologies, Plovdiv University "Paisii Hilendarski", 21, "Kostaki Peev" Str., 4000, Plovdiv, Bulgaria*
[2] *LB-Bulgaricum Plc., R&D Center, 14, "Malashevska" Str., 1202 Sofia, Bulgaria*

Received: November 2023; Revised: December 2023

In this study selected strains of Lactobacillus, potential producers of bioactive peptides, were evaluated for their specific protease- and aminopeptidase activity after growth in milk, mMRS (MRS without peptone and meat extract) and mMRS with added pea protein hydrolysate, soy protein hydrolysate or whey protein 80 (WP 80). Five *Lactobacillus helveticus* strains (AB, h25, h48, h70, b244) and *Lacticaseibacillus casei* c1 (LB Bulgaricum PLC, Sofia, Bulgaria) were assayed. With minor exceptions the protease activity varied between strains to a much larger extent (> 10 fold) than it was influenced by the composition of each growth medium (up to 3 fold). This makes the selection of a highly proteolytic strains of primary importance. Although mMRS composition differed largely from milk, the protease activity of cells grown in mMRS remained high. Leucine- and lysine-aminopeptidase activities were highest in milk and mMRS, while as a rule the addition of plant hydrolysates or WP 80 resulted in lower values. As a whole the activities of these two aminopeptidases followed a constitutive pattern. On the contrary the arginine- and proline-aminopeptidase activities showed inducible character with measurable values obtained only in milk and mMRS with added pea protein hydrolysate. In the end of the study we selected two *L. helveticus* strains (b244 and h70) with high protease and aminopeptidase activity for further experiments.

Keywords: aminopeptidase activity, lactobacilli, plant protein hydrolysates, protease activity

INTRODUCTION

Products obtained after fermentation with selected lactobacilli can improve health, while dairy products are widely present in the daily life of every family. However, people suffering from allergy to milk proteins or lactose intolerance are recommended to consume alternative products [1]. A worldwide trend is the growing popularity of plant-based products [2]. On the other hand, with the exception of soy-products, alternative milk substituents and plant-based products contain less protein than dairy products [3, 4]. Also, plant proteins are more difficult for the human body to digest due to the presence of antinutritional factor compounds such as protease inhibitors and non-starch polysaccharides, as well as properties inherent to the protein structure such as cross-linking, hydrophobicity and secondary structure elements [5].

Pea and soy proteins are some of the most commonly used plant proteins for the production of dairy alternatives. The main components in pea (*Pisum sativum*) are protein (20–25%), fat (1.5–2.0%), starch (24–49%) and dietary fibers (60–65%), while vitamins, minerals, phytic acid, saponins, polyphenols, and oxalates are present as minor constituents [6]. The basic mineral elements contained in pea are potassium (1.04%), phosphorous (0.39%), magnesium (0.10%), and calcium (0.08%). Pea preparations also provide a large quantity of water-soluble vitamins, especially B-group vitamins, as well as essential amino acids such as lysine and threonine [7].

Unlike most legumes, soybeans have high protein content, making soybeans and their food derivatives excellent plant-based protein sources [8]. Soybeans contain protein (35–40%), lipids (20%) and dietary fibers (9%) based on the dry weight of mature raw seeds [9]. Soy and pea proteins are rich in sulphur-containing amino acids. According to Qin *et al.* [10] digestibility of these proteins is 95–98% and 83–90% for soy and pea, respectively.

* To whom all correspondence should be sent:
E-mail: tpanayotova87@gmail.com

Lactic acid bacteria (LAB) are one of the most well-studied microorganisms. Certain health-promoting properties of LAB strains are related to the production of bioactive peptides. These are well studied in milk media, but there are less reports of LAB-derived peptides in plant-based products. Bioactive peptides are final products of the activity of proteinases, peptidases and specific transport systems, all components of the proteolytic system of LAB [11, 12] (Fig. 1). All of these enzyme activities and cell functions are influenced by the composition of the growth medium and growth conditions. The present study investigates the effect of semi-defined growth media, containing pea or soy-protein hydrolysates, compared to milk on the specific protease activity and several aminopeptidase activities in cell preparations from strains of lactobacilli with potential to produce bioactive peptides.

MATERIALS AND METHODS

Five *Lactobacillus helveticus* strains (AB, h25, h48, h70, b244) and one *Lacticaseibacillus casei* (c1) all maintained in the LBB Culture Collection of LB Bulgaricum PLC, Sofia, Bulgaria, were used in the study. The selected lactobacilli were cultured for 16 hours at 37 °C in sterile 10% reconstituted skimmed milk (RSM), mMRS (containing glucose, Tween 80, sodium citrate, sodium-acetate, di-potassium hydrogen phosphate trihydrate, yeast extract, magnesium and manganese salts) and mMRS with added 1% pea protein hydrolysate (PPH), mMRS with 1% soy protein hydrolysate (SPH) and mMRS with 1% whey protein 80 (WP 80).

The pH of the strains was measured after 16 hours of cultivation. The number of microorganisms in milk medium was determined after plating suitable decimal dilutions on MRS agar and anaerobic incubation for 48 hours at 37 °C. Growth of bacteria in mMRS-based media was evaluated spectrophotometrically by measuring the optical density at 600 nm against uninoculated media. Then cells were harvested by centrifugation, washed three times with phosphate buffer (pH 7,5) and disrupted by sonification.

The specific protease activity (PA_{sp}) was determined with the Enzymatic Assay of protease casein as a substrate (SSCASE01.001, 04.02.99) method [13]. Protease activity (PA) was defined as the amount of enzyme that catalyzes the release of 1 µmol of tyrosine for 1 minute at pH 7,5 and 37 °C. PA was expressed in U/ml. PA_{sp} was calculated as the ratio of PA and the protein content in the sample determined by the Bradford method [14].

In order to assess aminopeptidase activity (APA) we used four chromogenic substrates L-leucine-p-

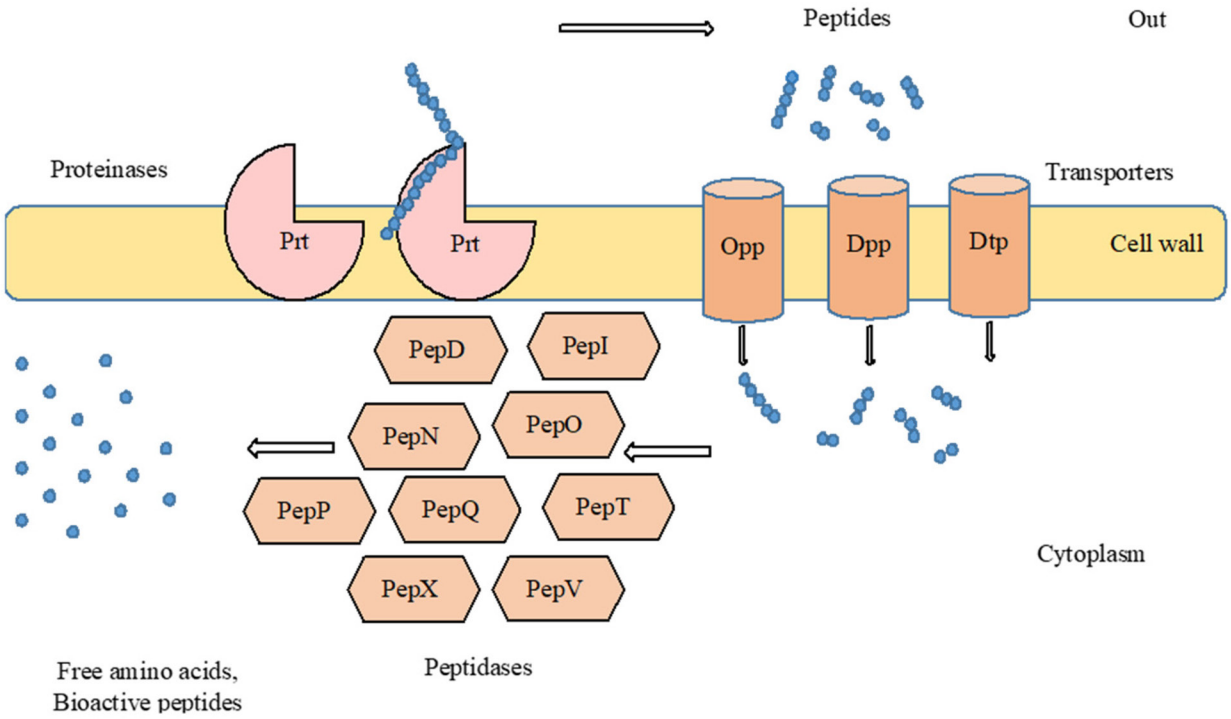

Fig. 1. Schematic representation of the proteolytic system of *Lactobacillus* ssp.

nitroanilide (L-leu-pNA), L-lysine-p-nitroanilide (L-lys-pNA), L-arginine-β-naphthylamide (L-arg-βNA) and L-proline-β-naphthylamide (L-pro-βNA) [15,16]. APA for the first two substrates was calculated using the formula:

$$\text{APA (pNA)} = \frac{(\Delta A405 \text{ nm Test Sample} - \Delta A405 \text{ nm Blank})(3)df}{(10{,}8)(0{,}1)} \quad (1)$$

where: ΔA_{405} nm Test Sample/Blank – maximal linear change in absorption at 405 nm per minute for the Test Sample or the Blank for a measurement period of 5 minutes; 3 – Total volume, ml; df – Dilution factor; 10,8 – Millimolar extinction coefficient of p-Nitroanilide at A405nm, $M^{-1}cm^{-1}$; 0,1 – Sample volume, ml.

The calculation of APA for the second two substrates was different. The APA of β-naphthylamides was measured indirectly by the reaction of released β-naphthylamines with a stabilized diazonium salt, Fast Garnet GBC and Brij35, producing a red azo dye which was evaluated spectrophotometrically at 550 nm. Absorptions were measured at the beginning (0 min) and at the end (60 min) of the enzymatic reaction. APA for the L-arg-βNA and L-pro-βNA was calculated using this formula:

$$\text{APA (βNA)} = \frac{(\Delta A550 \text{ nm})/(60)(5)}{(20)(0{,}1)} \quad (2)$$

where: $\Delta A_{550\ nm}$ – Change in absorption at 550 nm for a measurement period of 60 minutes; 60 min – Duration of enzyme reaction; 5 – Total volume, ml; 20 – Millimolar extinction coefficient of β-Naphthylamide at A550 nm, $M^{-1}cm^{-1}$; 0,1 – Sample volume, ml.

The specific APA (APA_{sp}) for all four substrates was calculated as a ratio between APA and the protein content.

RESULTS AND DISCUSSION

Growth of the cultures in the tested media

After 16 hours of cultivation, the strains showed a normal acidification process in all tested media. All strains with the exception of *Lc. casei* c1 coagulated RSM with a final pH in the range of 3,51–4,34 (pH for *Lc. casei* was 5,13). Viable cell counts in RSM for all strains were of the same order (1×10^8–$7{,}8 \times 10^8$ cfu/ml). In mMRS-derived media the final pH was in the interval of 3,5–4,0. The final optical density of the cultures was variable and strain-specific (Fig. 2). The addition of plant protein hydrolysates and whey protein (WP80) to mMRS had no significant effect on the measured final pH and optical density values.

Specific protease activity (PA_{sp})

The PA_{sp} of cells grown on different media was strictly strain-specific (Fig. 3). Regarding the different types of media, the highest values were observed in milk medium and mMRS without additives – 64,96 and 57,29 U/mg, respectively. The highest PA_{sp} values in RSM were measured with *L. helveticus* h70 followed by b244 and h25. Interestingly, all *L. helveticus* strains had comparable or higher PA_{sp} values in mMRS compared to RSM or mMRS media with additives. In mMRS *L. helveticus* b244

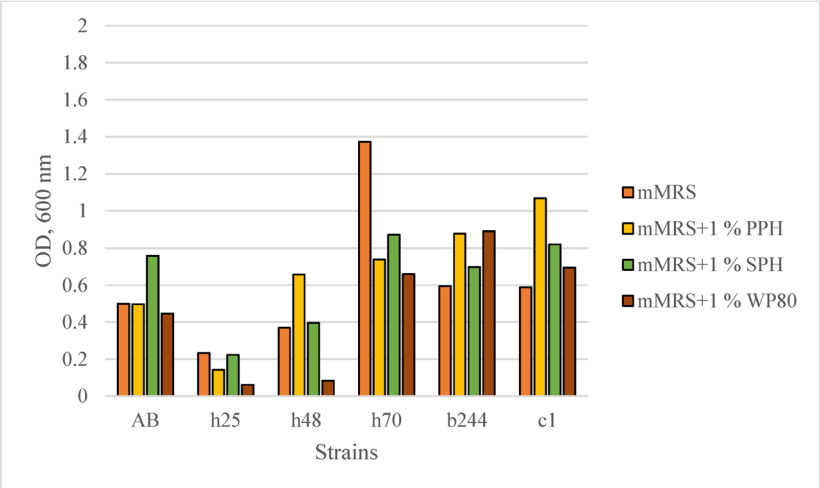

Fig. 2. Optical density in different growth media: mMRS – modified MRS without peptone and meat extract; PPH – pea protein hydrolysate; WP 80 – whey protein; SPH – soy protein hydrolysate * AB, h25, h48, h70, b244, c1 – LAB strains.

showed the highest PA_{sp} value followed by h70, h25 and h48. As a rule, the addition of plant protein hydrolysates reduced the protease activity for the most of the *L. helveticus* strains. For example, the addition of PPH to mMRS resulted in a 5-6-fold reduction in the PA_{sp} values compared to RSM and mMRS. Strain h25 had negligible PA_{sp} values on all mMRS media with additives. A notable exception was strain b244 with comparable PA_{sp} values on all tested media. Interestingly in mMRS with 1% PPH AB and h48 strains showed higher results compared to RSM and mMRS. As in the case of mMRS-PPH, mMRS with added SPH resulted in low PA_{sp} values of the *L. helveticus* cells. The addition of WP 80 to mMRS produced cells with PA_{sp} comparable to RSM and mMRS only for strains h70 and b244 – 30,26 U/mg and 53,71 U/mg, respectively. For other *L. helveticus* strains cultured in mMRS with WP 80 the values were minor. Compared to the *L. helveticus* strains, *Lc. casei* c1 showed low, but constant protease activity on all mMRS-derived media (not determined in milk). *L. helveticus* h70 and b244 proved to be the strongest proteolytic strains in the tested group.

Specific aminopeptidase activity (APA_{sp})

APA_{sp} with L-leu-pNA and L-lys-pNA as substrates

The results for APA_{sp} with L-leu-pNA and L-lys-pNA as substrates varied greatly between strains and growth media. For cells grown in RSM, the highest results were obtained for *L. helveticus* strains h70, h25 and b244 with values for the two substrates (L-leu-pNA/L-lys-pNA) of 350/344 U/mg, 299/356 U/mg and 224/195 U/mg, respectively (Fig. 4A). *L. helveticus* AB had negligible APA_{sp} for L-leu-pNA and L-lys-pNA in RSM, while RSM was not suitable for growth of *Lc. casei* c1.

Growth in mMRS without any additives resulted in cells with the highest APA_{sp} for L-leu-pNA and L-lys-pNA among all tested media (Fig. 4B). Values for all strains were significantly higher compared to RSM. This was especially well shown for *L. helveticus* strain h25 reached APA_{sp} of 696 U/mg and 816 U/mg for L-leu-pNA and L-lys-pNA, respectively. Unlike results for RSM, cells of *L. helveticus* AB grown in mMRS had APA_{sp} comparable to other tested *L. helveticus* strains. In mMRS *Lc. casei* c1 had detectable, although lower APA_{sp} compared to *L. helveticus* strains for L-leu-pNA and L-lys-pNA (Fig. 4B).

Similar to the observed decrease in the specific protease activity, the addition of plant protein hydrolysates to mMRS resulted in significant reduction in APA_{sp} measured with L-leu-pNA and L-lys-pNA (Figure 4C, D). In mMRS with 1% PPH APA_{sp} values varied between 28 to 119 U/mg and from 32 to 189 U/mg for L-leu-pNA and L-lys-pNA, respectively, with values for strains AB, h48, h70 and b244 being of the same order (Fig. 4C). Similar results were obtained in mMRS with 1 % SPH where for the cells of *L. helveticus* strains AB, h70 and b244 the measured APA_{sp} for the two substrates (L-

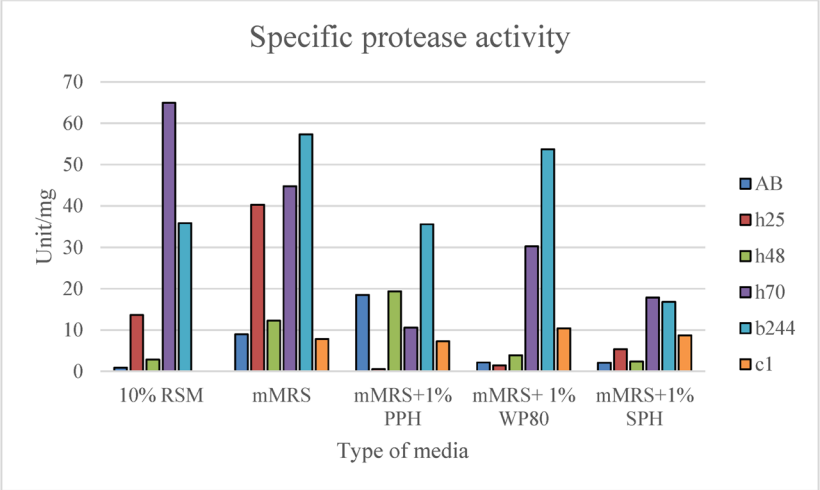

Fig. 3. Specific protease activity (PA_{sp})of cells grown in different growth media: RSM – 10 % reconstituted skimmed milk; mMRS – modified MRS without peptone and meat extract; PPH – pea protein hydrolysate; WP 80 – whey protein; SPH – soy protein hydrolysate
* AB, h25, h48, h70, b244, c1 – LAB strains.

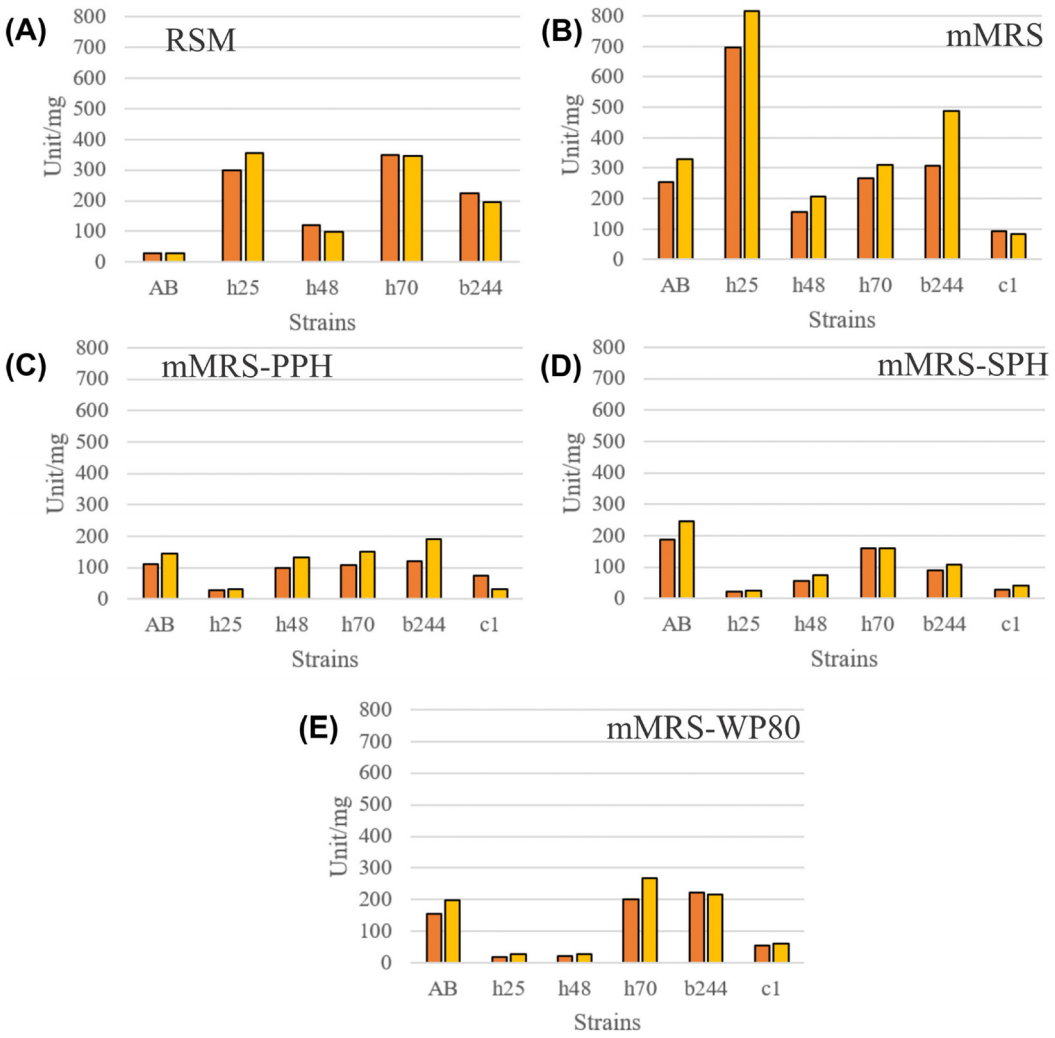

Fig. 4. Specific aminopeptidase activity (APA_{sp}) of cells grown in different media with L-leucine-p-nitroanilide (■) and L-lysine-p-nitroanilide (■) as substrates.

leu-pNA/L-lys-pNA) was 186/246 U/mg, 159/159 U/mg and 89/107 U/mg, respectively (Fig. 4D).

The results for strains cultivated in mMRS with WP 80 are shown in Fig. 4E. The APA_{sp} of cells grown in this medium were slightly higher than mMRS-PPH and mMRS-SPH media but still substantially below the high values measured for mMRS without additives. Cells of *L. helveticus* strains h70, b244 and AB harvested from mMRS-WP80 showed APA_{sp} values for the two substrates (L-leu-pNA/L-lys-pNA) of 201/269 U/mg, 222/215 U/mg and 154/196 U/mg, respectively (Fig. 4E).

On all mMRS media with or without the additives *Lc. casei* c1 showed low, but constant APA_{sp} for these two substrates (Fig. 4B-E). From the point of view of selection of strains with high APA_{sp} for L-leu-pNA and L-lys-pNA the best performing strains on all tested media were *L. helveticus* strains h70 and b244.

Notably, there was a clear correlation between the APA_{sp} values measured separately for L-leu-pNA and L-lys-pNA with all tested cultures (Fig. 4A-E). This might suggest that these two enzymatic activities are closely related, overlapping in substrate specificity and/or regulated in an identical manner.

APA_{sp} with L-arg- βNA and L-pro- βNA as substrates

Although units of specific enzyme activity for APA with the four chromogenic substrates were defined in an identical manner, values of APA_{sp} for the L-arg-βNA and L-pro-βNA substrates were of

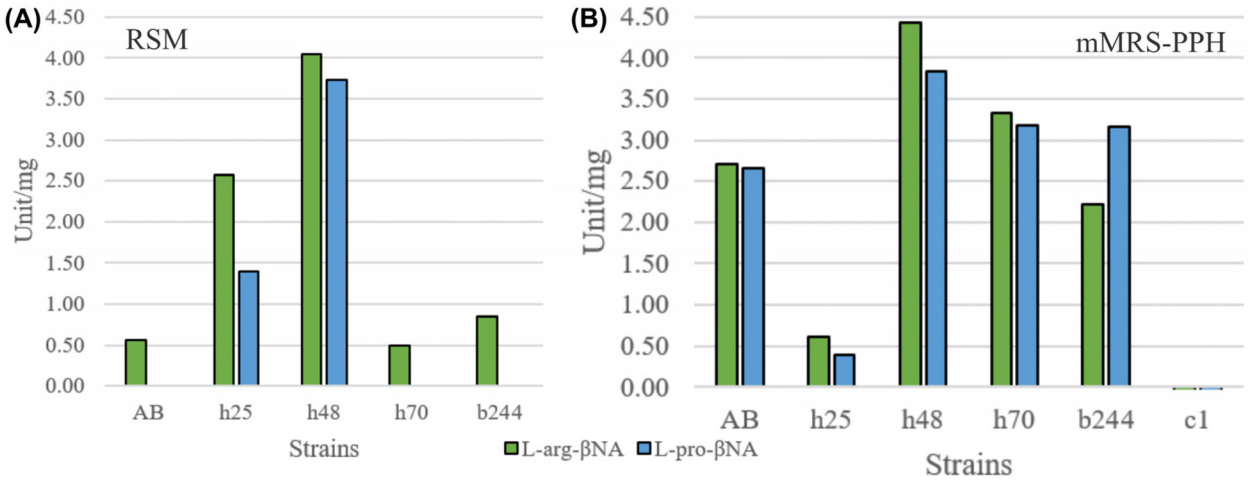

Fig. 5. (A–B) Specific aminopeptidase activity (APA_{sp}) of cells with L-arginine-β-naphthylamide and L-proline-β-naphthylamide substrates.

significantly lower scale compared to L-leu-pNA and L-lys-pNA (Fig. 5A, B). Moreover, detectable activity towards L-arg-βNA and L-pro-βNA was only measured in RSM and mMRS with addition of 1% PPH. Values of APA_{sp} for L-arg-βNA and L-pro-βNA were strain-specific with higher activity (> 1U/mg) measured for two of the five tested *L. helveticus* strains (h25 and h48) in RSM and for four of the same five cultures (AB, h48, h70 and b244) in mMRS-PPH. Cells of *Lc. casei* c1 showed no activity towards L-arg-βNA and L-pro-βNA on all tested media.

Unlike APA measured with L-leu-pNA and L-lys-pNA, activity towards the L-arg-βNA and L-pro-βNA substrates was practically very low or undetectable for the majority of strains and tested media (mMRS, mMRS-SPH, mMRS-WP80). These results suggest that peptidase activity for peptides with arginine or proline at their N-terminus is tightly regulated and specific for the composition of the growth medium, possibly related to the availability of these two amino-acids in the medium.

Values of specific protease activity and APA_{sp} for L-leu-pNA and L-lys-pNA both showed negative correlation with the addition of plant protein hydrolysates and WP80. The ready availability of low-molecular nitrogen source in the growth medium (peptides from protein hydrolysates) seems to lower the pressure on the proteolytic system of the culture, resulting in lower values of the tested enzyme activities.

CONCLUSIONS

The highest levels of specific protease activity were observed in mMRS, comparable to RSM, while lower values were obtained with the addition of plant protein hydrolysates and WP80. The response to the growth medium of each culture with respect to specific aminopeptidase activity with L-leu-pNA and L-lys-pNA substrates was strain-dependent with highest values in mMRS and RSM and a decrease with the addition of plant protein hydrolysates and WP80 to the medium. Specific aminopeptidase activity with L-arg-βNA and L-pro-βNA as substrates was barely detectable and only in RSM and mMRS with added PPH. The best performing strains with constant protease and aminopeptidase activity on all tested media were *L. helveticus* h70 and b244.

Acknowledgements: *This participation is financed by the operational program "Science and education for smart growth" 2014–2020, grant number BG-05M2OP001-1.002-0005-C01, Personalized Innovative Medicine Competence Center (PERIMED).*

REFERENCES

1. M. Montemurro,E. Pontonio, R. Coda, C. G. Rizzello, *Foods*, **10**, 316 (2021).
2. S. Hertzler, J. C. Lieblein-Boff , M. Weiler, C. Allgeier, *Nutrients*, **12**, 3704 (2020).

3. O. E. Mäkinen, V. Wanhalinna, E. Zannini, E. K. Arendt, *Crit. Rev. Food Sci. Nutr.*, **56**(3), 339 (2016).
4. M. E. Clegg, A. T. Ribes, R. Reynolds, K. Kliem, S. Stergiadis, *Food Research International*, **148**, 110586 (2021).
5. A. G. A. Sá, Y. M. F. Moreno, B. A. M. Carciofi, *Crit. Rev. Food Sci. Nutr.*, **60**, 3367 (2020).
6. P. Shanthakumar, J. Klepacka, A. Bains, P. Chawla, S. B. Dhull, A. Najda, *Molecules*, **27**, 5354 (2022).
7. K.A. Millar, E. Gallagherb, R. Burkec, S. McCarthyd, C. Barry-Ryan, *J. Food Compos. Anal*., **82**, 103233 (2019).
8. C. Chatterjee, S. Gleddie, C. W. Xiao, *Nutrients*, **10**, 1211 (2018).
9. A. J. Michelfelder, *Am. Fam. Physician*, **79**, 43 (2009).
10. P. Qin, T. Wang, Y. Luo, *J. Agri. Food Research*, **7**, 100265 (2022).
11. C. Raveschot, B. Cudennec, F. Coutte, C. Flahaut, M. Fremont, D. Drider, P. Dhulster, *Frontiers Micro.*, **9**, (2018).
12. M. Kieliszek, K. Pobiega, K. Piwowarek, A. M. Kot, *Molecules*, **26**, 1858 (2021).
13. O. Folin, V. Ciocalteu, *J. Biol. Chemistry*, **73**, 627 (1927).
14. M. Bradford, *Analytical Biochemistry*, **72**(1–2), 248 (1976).
15. M. Sasaki, B. W. Bosman, P. S. Tan, *J. Dairy Research*, **62**, 601 (1995).
16. T. C. Eleman, *Biochem. J*., **141**, 113 (1974).

Bulgarian Chemical Communications, Volume 55, Special Issue C (pp. 65–74) 2023 *DOI: 10.34049/bcc.55.C.0007*

Synthesis, crystallization region and structural peculiarities of the solid solutions in the Li_2MgGeO_4–Li_4GeO_4 system

V. V. Kostov-Kytin*, V. S. Nikolov*, N. V. Kuvandjiev

Institute of Mineralogy and Crystallography, Bulgarian Academy of Sciences, 1113 Sofia, "Akad. G. Bonchev" str., bl. 107

Received: November 2023; Revised: December 2023

Ten compositions of the system Li_2MgGeO_4-Li_4GeO_4 with general formula $Li_{2+2x}Mg_{1-x}GeO_4$ with x = 0–0.9 were studied. The syntheses were carried out by solid state reaction at 1050 °C. The X-ray diffractograms were analyzed with respect to crystallizing phases. It was established that all solid solutions contained an orthorhombic compound isostructural to γ-Li_3PO_4 being the only one or the main phase in all of the synthesized products. Rietveld refinement was applied in order to attain and evaluate certain structural parameters. A linear change of the lattice parameters and a decrease in cell volume were found with increasing Li content. Another clearly outlined dependence is that between the increasing content of lithium, respectively cation charge in the Li3 position and the decrease of approximately 8% in the volume of this cation octahedron. The obtained new results for the concentration region of these γ-type solid solutions as well as for their structural peculiarities can serve as a basis for their synthesis for various applications.

Keywords: oxides, chemical synthesis, phase equilibria, X-ray diffraction, crystal structure.

1. INTRODUCTION

Germanate compounds are widely used for various applications such as ceramics, optics, optoelectronics and lasers. Most of them are isostructural to the corresponding silicate compounds, but compared to the latter, they have lower melting temperatures, which facilitates their synthesis. Among the widely studied germanates are Zn_2GeO_4, Mg_2GeO_4, and Ca_2GeO_4. Mg_2GeO_4 and Zn_2GeO_4 have been tested as dielectric ceramics [1, 2] as well as phosphors after suitable doping by transition ions or rare earth ions for different emission in the visible region [3, 4]. The intermediate compounds of the systems Me_2GeO_4-Li_4GeO_4 (Me = Zn, Mg, Ca) i.e. Li_2ZnGeO_4, Li_2MgGeO_4, and Li_2CaGeO_4 have also been tested as dielectric ceramics [5, 6] and for phosphors [7–11]. Another promising application of these intermediates is as solid-state laser media doped with Cr^{4+} with a wide spectrum of radiation in the near infrared region (1.1–1.6 μm) [12, 13]. In this regard, much has been achieved in research on silicates of the Li_2MgSiO_4 type [14, 15]. Similar results would also be very likely for germanium structural analogues.

A particularly important area of the Me_2GeO_4-Li_4GeO_4 systems are the Li_2MeGeO_4-Li_4GeO_4 subsystems (where Me is Zn or Mg). After replacing of Me by Li in these subsystems, solid solutions with the general formula $Li_{2+2x}Me_{1-x}GeO_4$ crystallize. These solid solutions are isostructural to the orthorhombic γ-Li_3PO_4 and to the high-temperature modifications of Li_2ZnGeO_4 and Li_2MgGeO_4. Due to their specific structure, some of the Li ions are particularly mobile, which predetermines the high ionic conductivity of these solid solutions. The solutions are known as LISICON (lithium superionic conductors). Apart from their high conductivity, some of these solutions (according to the available data) are thermodynamically stable, i.e. unlike Li_2MeGeO_4, they do not show polymorphic transitions, which offers opportunities for single crystal growth (e.g. for solid-state lasers application).

Understanding the mechanism of the $Li_{2+2x}Me_{1-x}GeO_4$ materials ionic conductivity, as well as their potential for use in other applications, requires knowledge of the concentration and temperature regions of crystallization of these solid solutions,

* To whom all correspondence should be sent:
E-mails: vkytin@abv.bg; vnikolov@svr.igic.bas.bg

as well as of their crystal structures behavior upon changes in the Li/Me ratio. In reality, however, only the zinc form (Me = Zn) – $Li_{2+2x}Zn_{1-x}GeO_4$ solid solutions have been studied in detail to date.

The regions of existence of the γ-Li_3PO_4-type $Li_{2+2x}Zn_{1-x}GeO_4$ as well as their crystal structures have been well studied mainly with emphasis on their ionic conductivity. According to the research of Bruce and West [16] $Li_{2+2x}Zn_{1-x}GeO_4$ region is localized from x = 0.20 to x = 0.85 at 1000 °C. At 600 °C the region narrows from x = 0.35 to x = 0.73. Its crystal structure has been determined by H. Hong [17] using single crystal X-ray analysis (Pnma, a = 10.828 Å, b = 6.251 Å, c = 5.140 Å, z = l). The structure has been described as built up by isolated GeO_4 tetrahedra linked to two crystallographic types of mixed (Li, Zn)O_4 tetrahedra in a way to form a rigid three-dimensional network of $Li_{II}Zn(GeO_4)_4$ (Fig. 1a). The three remaining Li^+ ions in $Li_{14}Zn(GeO_4)_4$ have occupancies of 55 and 16%, respectively, at the 4c and 4a interstitial positions (designated Li3 and Li4 in Fig 1a).

In 1979 Plattner &Voellenkle [18] determined by X-ray diffraction the crystal structure of $Li_3Zn_{0.5}GeO_4$ (Pmnb, a = 6.29, b = 10.74, c = 5.17 Å). Although these authors have confirmed its structural identity with Hong's phase (the basic framework of Ge, (Li, Zn), and O atoms is very similar in both refinements) they have failed to identify the existence of one of the eight-fold lithium sites – that one designated as Li4 in Fig 1a (vs. Fig. 1b). The relatively weak X-ray scattering factors for lithium ions puts certain limitations to the X-ray diffraction technique when accurate lithium-ion distributions are required. In 1988 Abrahams *et al*. used powder neutron diffraction patterns obtained at a constant wavelength to solve the crystal structures of two LISICON compounds with formulae $Li_3Zn_{0.5}GeO_4$ and $Li_{3.5}Zn_{0.25}GeO_4$, correspondingly [19]. In 1989 Abrahams *et al*. applied high resolution powder neutron diffraction and re-examined the structure of the former compound [20]. These authors overcome the shortcomings of X-ray diffraction and drew new light on the lithium distribution in the crystal structures of these materials. Thus, the authors: (i) confirmed the location of lithium in the Li4 site; (ii) moved off the Li(3) ion from the special position onto an eightfold general position; (iii) well determined the lithium positions in sites (2) and (2a) (Fig 1c). Abrahams *et al*. [20] also paid attention to the fact that the structures of these lithium ion conductors can be derived from that one of the stoichiometric parent g-Li_2ZnGeO_4 compound, by $Zn^{2+}\rightarrow 2Li^+$ substitution. Thus, while some of the Li atoms substitute for the Zn^{2+} ion in a tetrahedral site – Li1 or Li2 the excess Li atoms occupy any one of the two octahedral interstitial sites – Li3 or Li4 (Fig. 1).

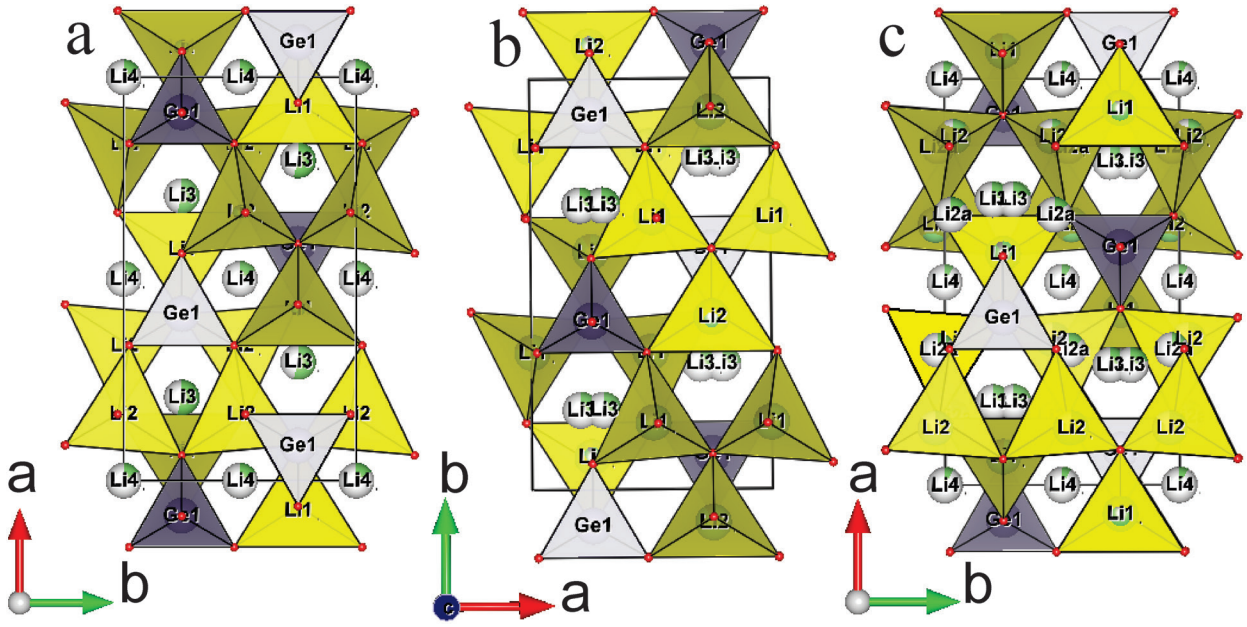

Fig. 1. Crystal structures of $Li_{2+2x}Zn_{1-x}GeO_4$ solid solutions a) $Li_{14}Zn(GeO_4)_4$ (Hong, 1978 – [17]); b) $Li_3Zn_{0.5}GeO_4$ (Plattner &Voellenkle, 1979 – [18]); c) $Li_3Zn_{0.5}GeO_4$ (Abrahams *et al*., 1989 – [20]).

The essential structural feature of the LISICONs is a rigid, three-dimensional network having partially occupied by lithium ions sites linked in a three dimensional interstitial space ensuring fast ion transfer from an occupied interstitial position to a neighboring empty one [21]. For fast Li^+ ion transport, the Li-O polyhedra around adjacent Li^+ positions must share a common face. The smallest diameter of such faces, which act as bottlenecks to ion motion, should be greater than twice the sum of the alkali-ion and oxygen-ion radii. Thus for fast Li^+-ion transport the smallest diameter should exceed 4.32 Å since the radii of the Li^+ and O^{2-} ions are respectively 0.76 and 1.4 Å [22]. In 1977 Hong postulated that in addition to these geometrical constraints, chemical bonding also plays a role in determining alkali ions (A^+) mobility in solid electrolytes [21]. One of the newly noted key features resulting in fast Li-ion conduction for certain lithium super ionic conductors "is the enlarged Li site given by large local space of crystal structures promoting Li disordering." In 2019 He *et al*. established that "the enlarged Li site corresponds to a large local space larger than 2.4 Å in size and can be occupied by Li ion at multiple positions within a very close distance. Li ions move rapidly within the enlarged site, in contrast to thermal vibration centered to the equilibrium positions of a regular site." [23].

The crystal structures of the two most thoroughly researched solid solutions – $Li_3Zn_{0.5}GeO_4$ and $Li_{3.5}Zn_{0.25}GeO_4$, determined by powder neutron diffraction studies as mentioned above provide good evidence for such enlarged sites in which multiple partially-occupied close-neighboring lithium ions with relatively high values of their atomic displacement parameters have been established [19, 20].

In contrast to $Li_{2+2x}Zn_{1-x}GeO_4$ the solid solutions $Li_{2+2x}Mg_{1-x}GeO_4$, have been investigated too insufficiently. In 1971, West et al. established the existence of 4 polymorphic modifications of Li_2MgGeO_4 among which the high-temperature γ-form was found to be isostructural to γ Li_3PO_4 [24]. These modifications were also confirmed by Monnaye et al. and Monnaye [25, 26]. In 2013, Nakayama et al. studied in detail the structural features of the low-temperature modifications and the conditions for transitions between them and to the γ-modification [27]. Only Hong [17] had studied the solid solutions with compositions $Li_{16-2x}D_x(TO_4)_4$, with D = Mg or Zn, T = Si or Ge, and declaring $0<x<4$. The latter formula can also be represented as $Li_{2+2x}D_{1-x}TO_4$ ($0<x<1$) as more suitable for cases where the emphasis of research falls on the substitution of D(Me) elements by lithium. Such an approach is also adopted in the present work. In Hong's work, however, there is no specifics about crystallization regions of the solid solutions, data on the conductivity of only three discrete compositions, namely $Li_{2.5}Mg_{0.75}GeO_4$, $Li_3Mg_{0.5}GeO_4$, and $Li_{3.5}Mg_{0.25}GeO_4$ (x = 0.25; 0.5; 0.75, correspondingly) and the crystal structure of only the zinc analogue of $Li_{3.5}Mg_{0.25}GeO_4$ is presented.

This study presents the results of research on the synthesis conditions, crystallization region and structural characterization of the $Li_{2+2x}Mg_{1-x}GeO_4$ solid solutions from Li_2MgGeO_4 to Li_4GeO_4. Conventional powder X-ray diffraction (CPXRD) was used to characterize the obtained materials. This method does not have the capabilities of other diffraction methods for precise determinations of lithium in terms of its structural positions and occupancy. In this study, however, CPXRD was applied to samples comprising a compositional series. This makes it possible to derive important trends and dependencies related to the crystal-chemical characteristics and behavior of the studied materials, regardless of the noted limitations of the method and the lack of a reliably determined chemical composition.

2. SYNTHESIS AND STRUCTURAL STUDIES

2.1. Synthesis of solid solutions

Due to the lack of data on the region of solid solution crystallization, a study of the entire region of the Li_2MgGeO_4 – Li_4GeO_4 system was planned. A series of $Li_{2+2x}Mg_{1-x}GeO_4$ solid solutions with x = 0, 0.1, 0.2, 0.3, 0.4, 0.5, 0.6, 0.7, 0.8 and 0.9 were synthesized by the solid state method, i.e. the composition of $Li_{2+2x}Mg_{1-x}GeO_4$ was varied from Li_2MgGeO_4 to $Li_{3.8}Mg_{0.1}GeO_4$. Solid phase method was applied as Bruce and West [16] did it. Li_2CO_3 with a purity of 99.9%, MgO with a purity of 99.99% and GeO_2 with a purity of 99.999% were used as starting reagents. Before synthesis, Li_2CO_3 and GeO_2 were dried to a constant weight at 150 °C for 5 hours. MgO was heat treated at 700 °C for 5 hours to convert available amounts of $Mg(OH)_2$ back to MgO. It was found that the starting reagent MgO contains up to 3% $Mg(OH)_2$, which is completely converted into MgO during the treatment. This was confirmed with relevant X-ray and DTA analyses. Weighed with an accuracy of 0.001 g, the starting reagents with a total weight of 4 g were mixed and crushed in an agate

mortar. Synthesis was carried out in a Kanthal resistance furnace with a temperature controller-programmer type Eurotherm 2704. A coated platinum crucible 3×3 cm was used. The samples were decarbonized at 800 °C for 3 hours. The tests showed that under these conditions Li_2CO_3 was completely decarbonized. After a new grinding the samples were heated at 1050 °C for 16 h with double intermediate grinding. Preliminary experiments have shown that this is the optimal temperature for solid-state synthesis to maximally limit the vaporization of components and to obtain as pure as possible final product. The samples were quenched directly from the furnace, i.e. their cooling to 100 °C took 2–3 minutes. The tests after the final synthesis showed that the residual amount corresponds exactly to the theoretical one, i.e. no evaporation losses of components were detected.

2.2. Methods for structural characterization

2.2.1. Powder X-ray diffraction

The diffraction patterns of all samples were collected at room temperature on an Empyrean (MalvernPanalytical) powder X-ray diffractometer, equipped with a multichannel PIXcel3D detector, using HDD Cu Kα (λ = 0.154060 nm) radiation, at 40 kV and 30 mA, in the range 5–80° 2θ and a scan step of 0.013° counting time (s): 23.97 (total time appx. 10 minutes).

2.2.2. Phase identification and choice of starting structural models

The crystal structure of $Li_3Zn_{0.5}GeO_4$ (ICSD #65643; [20]) as determined by Abrahams *et al*., in 1989 was used as an initial structural model for further investigations of the main $Li_{2+2x}Mg_{1-x}GeO_4$ phases (Fig. 1c). Certain replacements and amendments were made in the CIF file in consistency with the compositions of the initial synthesis batches as well as with the limitation of the used X-ray technique for detection of the weak scattering lithium ions as follows:

(i) Zn was replaced by Mg;

(ii) The total occupancy of the mixed tetrahedrally coordinated (Li,Mg) sites was fixed at one;

(iii) The total magnesium content in any of the investigated structures was set to be equal to that one put in the initial synthesis batch and further on it was divided between the two mixed tetrahedrally coordinated (Li/Mg) positions in a ratio of approx. 1:2 (atomic positions Li1 and Li2 in Fig. 1). The occupancies of these positions were subsequently included in the refinement;

(iv) Li(2a) position (Fig. 1c) was omitted from the refinement;

(v) The excess Li atoms in amounts derived from those ones set in the initial batches extracting the lithium from the mixed (Li/Mg) positions were distributed between the two octahedral interstitial sites – Li3 and Li4 randomly but always the occupancy of Li3 at least twice as bigger as that one of Li4. The occupancies of these positions were not included in the refinement procedure;

(vi) Li3 was fixed in the special position x,1/4/,0;

2.2.3. Rietveld Refinements

Ten samples of crystalline samples prepared at 1050 °C from initial batches with various Li/Mg ratios have been studied. The Rietveld refinement procedures were carried out with the GSAS-EXPGUI suite of programs (Larson, Von Dreele, 2004; Toby, 2001) [28, 29]. The Bragg peak profile was modelled using a pseudo-Voigt function; the background curve was fitted using a Chebyshev polynomial with 12 variable coefficients. The scattering curves of neutral atoms, as stored in GSAS, were used. No corrections were made for absorption. All of the atomic thermal displacement parameters were refined isotropically. Expecting similar U_{iso} values for the O atoms, these were refined in a group. The Li and Mg ions in both mixed tetrahedrally coordinated positions of the title compounds were constrained in terms of x, y, z, U_{iso}, and occupancy. Soft constraints (restraints) were imposed on the Ge-O distances. One and the same Restraint Weighting factor (RWf) fixed at 10,000 was used throughout the refinement procedure.

2.2.4. Visualization and geometric parameters calculations

The following programs have been used for graphic presentations:

1. WinPLOTR utilities ver. June 2020 (Thierry Roisnel, Rennes, France) as a Windows tool [30] (powder X-ray diffraction patterns);

2. VESTA ver. 3.3.2 (Koichi Momma, Tsukuba, Japan) [31] for visualization of certain structure and topological motives. The program has also been used for calculation of various geometric parameters such as the average bond lengths between the central atom and its ligands in a coordination polyhedron (abl) and the polyhedral volume (PV) of any cation in the structure.

3. RESULTS

Ten compositions were synthesized in the system Li_2MgGeO_4-Li_4GeO_4 with general formula $Li_{2+2x}Mg_{1-x}GeO_4$ with x = 0–0.9 i.e. from Li_2MgGeO_4 to $Li_{3.8}Mg_{0.1}GeO_4$ and designated hereinafter as Li2Mg, Li2.2Mg0.9, Li2.4Mg0.8, Li2.6Mg0.7, Li2.8Mg0.6, etc.

Initial inspection of the powder X-ray diffraction data as well as the conducted phase identification have revealed that all of the studied samples consist of well crystallized run-products. In all cases the orthorhombic $Li_{2+2x}Mg_{1-x}GeO_4$ is the predominant phase and it is the only one detected in samples $Li_{3.0}Mg_{0.5}GeO_4$, $Li_{3.2}Mg_{0.4}GeO_4$, $Li_{3.4}Mg_{0.3}GeO_4$, and in $Li_{3.8}Mg_{0.1}GeO_4$. Among the concomitant compounds only two have reliably been identified. One of them is the Mg-substituted structural analogue of the monoclinic Li_2ZnGeO_4 (ICSD #34362; [32]). It has occurred in the $Li_{2.0}Mg_{1.0}GeO_4$ (37.0 weight %) and $Li_{2.2}Mg_{0.9}GeO_4$ (26.0 weight %) samples and traces of it could be detected in $Li_{2.4}Mg_{0.8}GeO_4$. The other compound is the monoclinic Li_2GeO_3. (ICSD #100403; [33] which has been detected as a run-product in an amount of about 2 wt% in only one sample – $Li_{2.8}Mg_{0.6}GeO_4$. Other small quantity of unidentified crystalline phases has been detected in the following samples: $Li_{2.0}Mg_{1.0}GeO_4$; $Li_{2.2}Mg_{0.9}GeO_4$; $Li_{2.4}Mg_{0.8}GeO_4$, $Li_{2.6}Mg_{0.7}GeO_4$, and $Li_{3.6}Mg_{0.2}GeO_4$. Subsequently, these have been excluded from the Rietveld refinement procedures which definitely has affected the results of the quantitative analyses but has not impacted determination and evaluation of the main phase crystal chemical peculiarities.

Figure 2 presents PXRD patterns of selected $Li_{2+2x}Mg_{1-x}GeO_4$ with some of the concomitant phases designated therein.

Figure 3 presents Rietveld refinement plot for the $Li_{3.0}Mg_{0.5}GeO_4$ solid solution.

Table 1 presents lattice parameters and refinement details for selected $Li_{2+2x}Mg_{1-x}GeO_4$ solid solutions.

As can be seen from Table 1 with increase of the Li contents into the $Li_{2+2x}Mg_{1-x}GeO_4$ solid solution the lattice parameters *a* and *b* progressively decrease whereas the parameter *c* increases resulting in the lattice volume decrease, after all.

Table 2 presents positional and thermal parameters of atoms in the structure of (sample Li2.8Mg0.6) as obtained from the PXRD studies using Restraint Weighting factor.

Table 3 presents selected geometric parameters measured to characterize the crystal structural peculiarities of $Li_{2+2x}Mg_{1-x}GeO_4$ solid solution.

Figures 4 presents variations of lattice parameters (*a*, *b*, *c*, *V*) and Figure 5 – the relationship be-

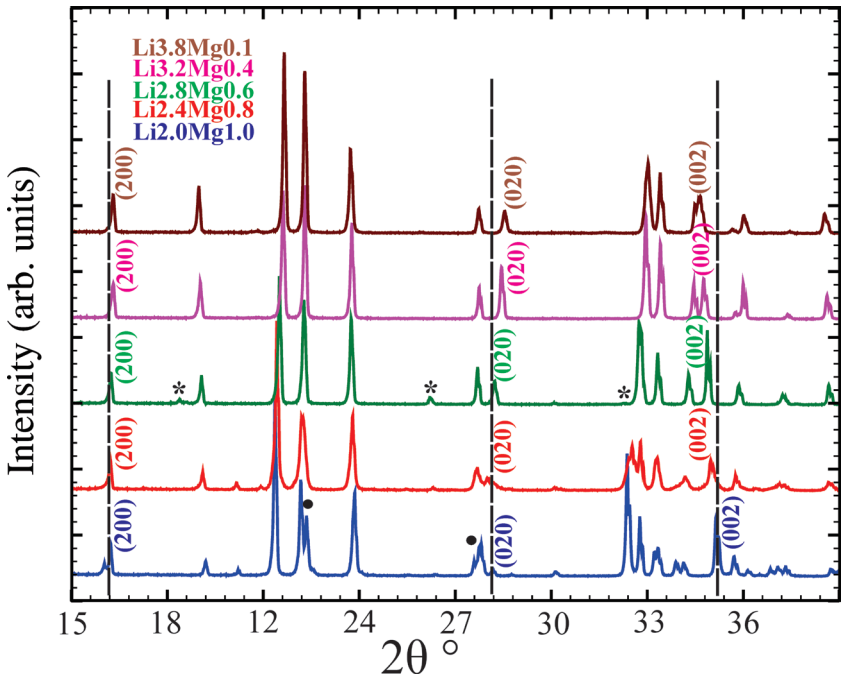

Fig. 2. PXRD patterns of selected $Li_{2+2x}Mg_{1-x}GeO_4$ with some of the concomitant phases designated: • – the monoclinic Li_2MgGeO_4 [32]; ∗ – monoclinic Li_2GeO_3 [33].

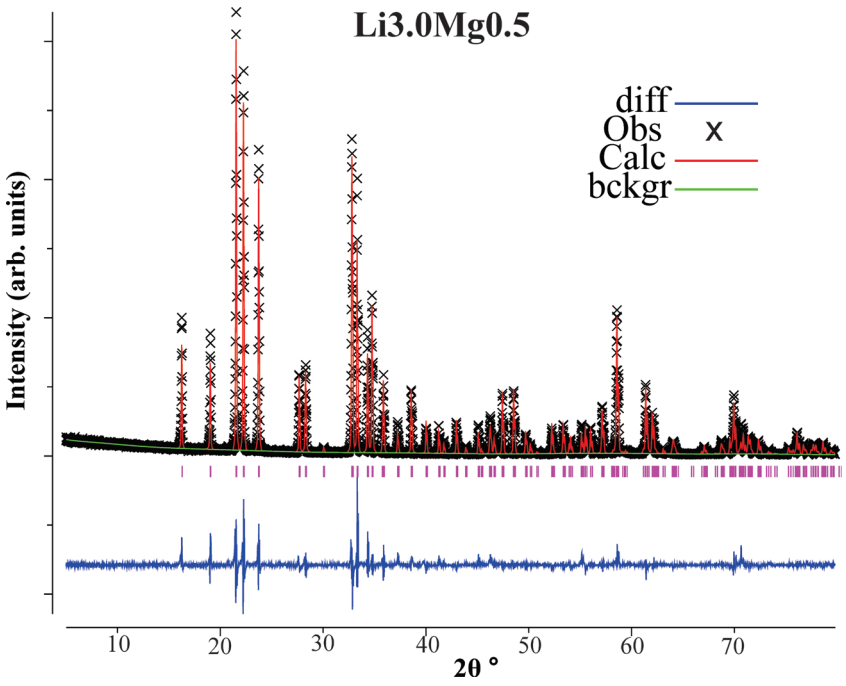

Fig. 3. Rietveld refinement plot for a $Li_{3.0}Mg_{0.5}GeO_4$ solid solution showing experimental data (x), calculated diffraction profile (red curved line), difference curve between experimental and calculated values (solid blue curve at the bottom), background (green line), and calculated Bragg positions of α1 and α2 reflections (small bars above the difference curve).

Table 1. Lattice parameters and refinement details for selected $Li_{2+2x}Mg_{1-x}GeO_4$ solid solution

	Powder X-ray diffraction studies (selected samples):				
	Li2.2Mg0.9 Two phase study	Li2.6Mg0.7 Single phase study	Li3.0Mg0.5 Single phase study	Li3.4Mg0.3 Single phase study	Li3.8Mg0.1 Single phase study
	1	*2*	*3*	*4*	*5*
Space Group, Z	*Pnma, 4*	*Pnma, 4*	*Pnma, 4*	*Pnma, 4*	*Pnma, 4*
a (Å)	10.9475(6)	10.9275(3)	10.9070(2)	10.8968(2)	10.8870(2)
b (Å)	6.4068(4)	6.3540(3)	6.3062(1)	6.2996(1)	6.2611(2)
c (Å)	5.1217(2)	5.1402(2)	5.15990(8)	5.17144(8)	5.1808(1)
V (Å)^3	359.23(4)	356.90(3)	354.9(1)	355.00(1)	353.15(2)
Rwp (%)	18.56	16.34	17.45	16.11	16.48
Rp (%)	13.29	12.38	13.12	11.99	12.32
Red-χ^2	5.966	4.339	5.065	3.553	4.43
N_{obs}	480	252	247	250	249
RF (%)	5.12	4.42	6.29	5.39	6.79
N_{var}	72	48	54	56	57
Number of restraints	4	4	4	4	4
Total restraint χ^2 contribution	40.40	39.30	95.16	4.25	6.15

tween the polyhedral volume of Li3 in its octahedrally coordinated position with the initial lithium content used for the preparation of the studied solid solution compounds. Trend-lines, linear equations and R-squared values are also depicted.

4. DISCUSSION

The presence of the monoclinic Li_2MgGeO_4 among the run products of the syntheses yielding samples with low lithium content (e.g. in $Li_{2.0}Mg_{1.0}$

Table 2. Positional and thermal parameters of atoms in the structure of the Li2.8Mg0.6 sample

Atom	x	y	z	Sof	$100xU_{iso}$,
Ge	0.4142(2)	0.25	0.3297(3)	1	2.56(5)
O1	0.3352(7)	0.0253(7)	0.219(1)	1	3.4(1)
O2	0.0838(9)	0.75	0.167(1)	1	3.4(1)
O3	0.0651(6)	0.25	0.269(1)	1	3.4(1)
Li1	0.426(2)	0.75	0.161(4	0.86	5.4(4)
Mg1	0.426(2)	0.75	0.161(4)	0.14	5.4(4)
Li2	0.168(1)	-0.003(1)	0.307(2)	0.78	2.8(2)
Mg2	0.168(1)	-0.003(1)	0.307(2)	0.22	2.8(2)
Li3	0.204(0)	0.25	0.00	0.16	0.09
Li4	0.00	0.00	0.5	0.08	0.09

Table 3. Selected geometric parameters measured to characterize the crystal structural peculiarities $Li_{2+2x}Mg_{1-x}GeO_4$ solid solution

	GeO tetrahedron		Li1O tetrahedron		Li3O octahedron		Li4O octahedron	
Samples	abl, Å	PV, A^3	abl, Å	PV, A^3	abl, Å	PV, A^3	abl, Å	PV, A^3
Li2.0Mg1.0	1.7317	2.6555	2.0163	3.9768	2.3981	17.0408	2.2344	14.6406
Li2.2Mg0.9	1.7348	2.6618	2.0325	3.8798	2.3987	17.2181	2.2227	14.4034
Li2.4Mg0.8	1.7414	2.7092	2.0317	3.9019	2.3884	16.9592	2.2222	14.3892
Li2.6Mg0.7	1.7434	2.7164	2.0328	4.0223	2.3703	16.6143	2.241	14.7893
Li2.8Mg0.6	1.7439	2.7166	2.0026	4.0218	2.3614	16.4867	2.246	14.9134
Li3.0Mg0.5	1.7411	2.703	2.0091	3.9877	2.3668	16.5384	2.2291	14.5685
Li3.2Mg0.4	1.7623	2.8065	1.9938	3.9358	2.3463	16.2056	2.235	14.7248
Li3.4Mg0.3	1.7561	2.7741	2.0047	3.8534	2.3707	16.6049	2.21	14.3578
Li3.6Mg0.2	1.7436	2.6953	2.0321	4.2327	2.3366	15.9241	2.2739	15.4935
Li3.8Mg0.1	1.7454	2.7271	1.9916	3.9862	2.3517	16.3209	2.2257	14.4926

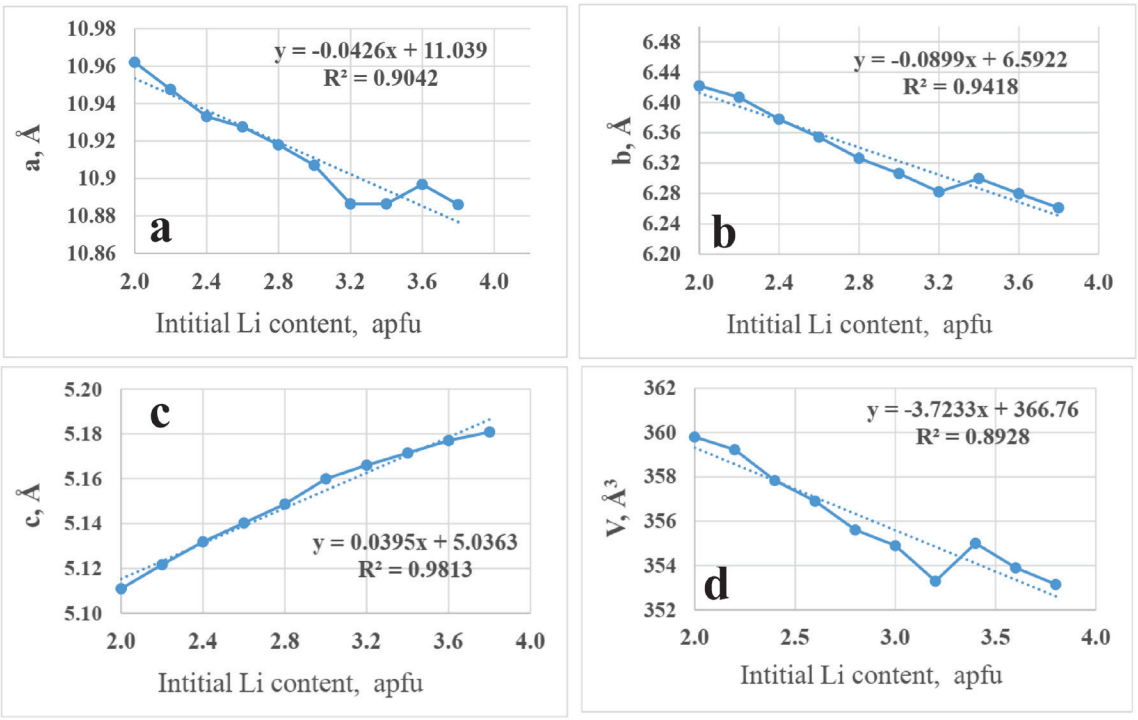

Fig. 4. Variations of lattice parameters (*a*, *b*, *c*, *V*) with initial lithium content for the studied $Li_{2+2x}Mg_{1-x}GeO_4$ solid solutions. The linear trend-lines are depicted as dotted lines.

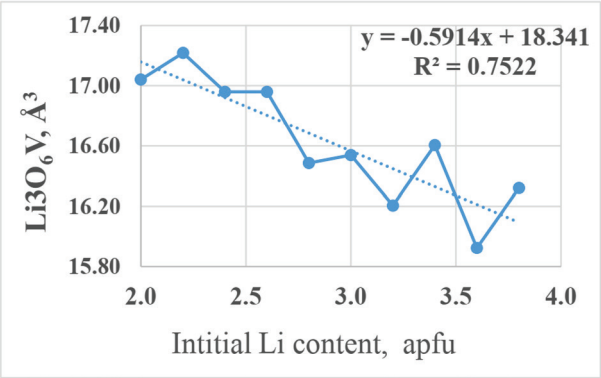

Fig. 5. Relationship between the polyhedral volume of Li3 in its octahedrally coordinated position with the initial lithium content. The linear trend-line is depicted as a dotted line.

– 37 wt %; $Li_{2.2}Mg_{0.9}$ – 26 wt %, and possibly in $Li_{2.4}Mg_{0.8}$; see Supplementary materials) is more or less expected in view of the earlier observations of researchers conducting experiments in a similar system to the one studied here and under similar synthesis conditions. The presence of the monoclinic modification is assumed to be due to the already established polymorphic transitions of Li_2ZnGeO_4 and Li_2MgGeO_4 [16, 34]. The other contaminations do not follow any trends and regularities, both quantitatively and in terms of their structural type. This means that the studied system is very sensitive to any fluctuations in the synthesis conditions and is alternatively also affected by post-synthesis treatment and thermodynamic stability of the end products. In this regard, previous investigation of the $Li_{2+2x}Zn_{1-x}GeO_4$ solid solutions showed that a couple of processes could have occurred at lower temperature such as: polymorph transition, precipitation, transformation of the γ-structure to another γ-substructure as well as the "aging" effect which nature is not entirely clarified, yet [34].

In four out of a total of ten examined $Li_{2+2x}Me_{1-x}GeO_4$ samples the orthorhombic phase is the only registered phase (Table 1, and Figures 2 and 3). In another four cases, the concomitant phases are around and below 4 wt.% of the total amount. Where unidentified phases are present in the final products this inevitably affects the data obtained from the quantitative analysis and the results can only be used as a guide. Additionally, the limitations of the applied diffraction method have led to certain simplification of the initial structural models used to refine the crystal structures of $Li_{2+2x}Me_{1-x}GeO_4$, which subsequently has degraded the values for some of the obtained R-factors (Table 1). In summary, all these shortcomings undoubtedly have affected the reliability of the data concerning the geometric parameters measured in order to characterize the crystal structural peculiarities of $Li_{2+2x}Me_{1-x}GeO_4$ of the studied samples (Table 3; Supplementary materials), especially since there is a lack of specific data on the chemical composition of the main phase.

Regardless of the fluctuations in many of the observed values, some of them exhibit certain trends depending on the initially set amount of lithium in the synthesis batches. It was found in this study that at 1050 °C the range $Li_{2+2x}Mg_{1-x}GeO_4$ exists between x = 0.15 and x = 0.9. In comparison with the solid solutions $Li_{2+2x}Zn_{1-x}GeO_4$ this range is a little wider.

It is worth noting that the volume of the measured unit cells decreases with increasing Li content about 1.7% (Table 1, Figure 4d), accompanied at the same time by a decrease in the values of *a* and *b* lattice parameters, but with an increase in *c*-dimensions (Figure 4 a–c). Moreover, the correlation coefficient between values of the *c*-parameter and initial lithium content is so high that in future investigations this dependence could easily be used for fast chemical composition determination of the studied compounds according to Vegard's rule, for example. The decreases of the unit cells by the increase of the Li content could not be explained taking into account only the ionic differences of Li^{2+} and Mg^{2+} in fourth coordination (0.59 for Li and 0.57 for Mg) [22]. For the zinc form – $Li_{2+2x}Zn_{1-x}Geo_4$ the cell volume decreases slightly too when the Li content increase (atomic radius of 0.6 for Zn). [16, 22]. It seems likely that inner electrostatic interactions predetermine such shrinkage.

Another clearly outlined dependence is that one between the increasing content of lithium in the Li3 position and the decrease in the volume of the octahedrally coordinated polyhedron it occupies there (approx. 8% within the studied compositional range). A plausible reason for this is the ever-increasing electrostatic attraction between the increasing in number lithium cations populating the central part of the octahedral-shaped interstitium in this part of the structure (increase in positive charge) and the surrounding ligands (oxygens). The average bond length in the polyhedron changes from 2.40 Å to 2.34 Å or about 2.5% in the studied compositional range (Table 3, column 9). The dimensions are comparable to those reported by He et al. in 2019 [24] to ensure concerted migration of the Li ions. Along with this, however, it is quite possible that such volume shrinkage

may lead to reduction of the number of multiple partially-occupied close-neighboring lithium sites and further to cause their unification in common positions, which will inevitably affect the values of the activation energy needed to facilitate Li-ion diffusion through the structure. To the best of our knowledge this is the first experimentally supported evidence for such structural shrinkage and the possible consequences.

5. CONCLUSION

This study establishes for the first time that the $Li_{2+2x}Mg_{1-x}GeO_4$ solid solutions exist within wide limits, just like the corresponding $Li_{2+2x}Zn_{1-x}GeO_4$ solid solutions. The presence of small amounts of concomitant phases among the run-products could be due to polymorphic transitions for compositions of x from 0 to 0.2 or occur probably due to interactions with the atmosphere or as a result of small transformations of the γ-phase to other γ-modifications at lower temperatures for the rest of the compositions. Similar transformations at low temperatures, resulting in a sharp reduce in the ionic conductivity, have previously been described for some $Li_{2+2x}Zn_{1-x}GeO_4$ solid solutions and undoubtedly necessitate further research. Regardless of the presence of by-phases, certain trends were found in some of the structural parameters of the synthesized $Li_{2+2x}Mg_{1-x}GeO_4$ with a change in the Li/Mg ratio. The volume of the measured unit cells decreases with increasing Li content accompanied at the same time by a decrease in the values of *a* and *b* lattice parameters, but with an increase in *c*-dimensions. Moreover, the correlation coefficient between values of the *c*-parameter and initial lithium content is very high (Vegard's low).

Another clearly outlined dependence is that, between the increasing content of lithium in the Li3 position and the decrease in the volume of the octahedrally coordinated polyhedron Li occupies there (approx. 8%). Undoubtedly, changes in the structural parameters of $Li_{2+2x}Mg_{1-x}GeO_4$ solid solutions with a change in the Li/Mg ratio will have an impact on the properties of solid solutions ceramics as ion conductivity, dielectric permittivity, and phosphor or laser emission after doping.

Acknowledgements: *The authors acknowledge the technical support from the project PERIMED BG- 05M2OP001-1.002-0005 /29.03.2018 (2018–2023).*

REFERENCES

1. J. Chen, Y. Tang, C. Yin, M. Yu, H. Xiang, C. Li, X. Xing, L. Fang, *JACerS*, **103**(3), 1789 (2020). https://doi.org/10.1111/jace.16855.
2. S. Wu, Q. Ma, *J. Alloys Compd*., **567**, 40 (2013). https://doi.org/10.1016/j.jallcom.2013.03.052.
3. H. M. Yang, J. Shi, M. L. Gong, H. Liang, *Mater. Lett.*, **64**, 1034 (2010). https://doi.org/:10.1016/j.matlet.2010.02.001.
4. H. M. Yang, Z. Wang, M. L. Gong, H. Liang, *J. Alloys Compd.*, **488**(1), 331 (2009). https://doi.org/10.1016/j.jallcom.2009.08.123.
5. C. Li, H. Xiang, M. Xu, Y. Tang, L. Fang, *J. Eur. Ceram. Soc.*, **38**(4), 1524 (2018). https://doi.org/10.1016/j.jeurceramsoc.2017.12.038.
6. J. I. Viegasa, R. L. Moreira, A. Diasa, *Vib. Spectrosc.*, **110**, 103 (2020). https://doi.org/10.1016/j.vibspec.2020.103130.
7. Y. Jin, Y. Hu,. *Mater. Res. Bull.*, **61**, 16 (2014). http://dx.doi.org/10.1016/j.materresbull.2014.09.085.
8. V. Berezovskaya, N. P. Efryushin, I. I. Seifullin, E. E. Martsinko, B. I. Zadneprovski ,G. B. Stryganyuk, A. S. Voloshinovskii, S. M. Levshov, V. P. Dotsenko, *Ceram. Int.*, **39**, 6835 (2013). https://doi.org/10.1016/j.ceramint.2013.02.015.
9. R. Cao, D. Ceng, X. Yu, S. Guo, Y. Wen, G. Zheng, *Funct. Mater. Lett.*, **8**(5), 1550046 (2015). https://doi.org/10.1142/S1793604715500460.
10. N. Bednarska-Adam, M. Kuwik, E. Pietrasik, W. A. Pisarski, T. Goryczka, B. Macalik, J. Pisarska, *Materials*, **15**, 5263 (2023). https://doi.org/10.3390/ma15155263.
11. Y. Jin, Y. Hu, H. Duan, L. Chen, X. Wang, *RSC Adv.*, **4**(22), 11360 (2014). https://doi.org/10.1039/C3RA47760F.
12. C. Li, J. Xu, W. Liu, D. Zheng, S. Zhang, Y. Zhang, H. Lin, L. Liu, J. Liu, F. Zeng, *J. Alloys Compd.*, **636**, 211 (2015). http://dx.doi.org/10.1016/j.jallcom.2015.02.121.
13. D. Wang, X. Zhang, X. Wang, Z. Leng, Q. Yang, W. Ji, H. Lin, F. Zeng, C. Li, Z. Su, *Crystals*, **10**(11), 1019 (2020). https://doi.org/10.3390/cryst10111019.
14. C. Jousseaume, A. Kahn-Harari, J. Derouet, D. Vivien, in: Advanced Solid-State Lasers, (M. Fermann and L. Marshall, eds.), 68 of Trends in Optics and Photonics Series (Optica Publishing Group, 2002), paper TuB 12. https://doi.org/10.1364/ASSL.2002.TuB12.
15. C. Anino, J. Thery, D. Vivien, in: Advanced Solid State Lasers (ASSL) p. SC6). Optica Publishing Group (1997). https://doi.org/10.1364/ASSL.1997.SC6.
16. P. G. Bruce, A. R. West, *Mater. Res. Bull.*, **15**(3), 379 (1980). https://doi.org/10.1016/0025-5408(80)90182-8.
17. H. P. Hong, 1978. *Mater. Res. Bull.*, **13**(2), 117 (1978). https://doi.org/10.1016/0025-5408(78)90075-2.
18. E. Plattner, H. Völlenkle, *Monatsh. Chem.*, **110**, 693 (1979). https://doi.org/10.1007/BF00938373.
19. I. Abrahams, P. G. Bruce, A. R. West, W. I. F. David, *J. Solid State Chem.*, **75**(2), 390 (1988). https://doi.org/10.1016/0022-4596(88)90179-X.

20. I. Abrahams, P. G. Bruce, W. I. F. David, A. R. West, *Acta Crystallogr. B*, **45**(5), 457 (1989). https://doi.org/10.1107/S0108768189006245.
21. H. Y-P. Hong, Chapter 10. New Solid Electrolytes, in: Solid State Chemistry of Energy Conversion and Storage, June 1, 179 (1977). https://doi.org/10.1021/ba-1977-0163.ch010.
22. R. D. Shannon, *Acta Crystallogr. A*. **32** (5), 751 (1976). https://doi.org/10.1107/S0567739476001551.
23. X. He, Q. Bai, Y. Liu, A. M. Nolan, C. Ling, Y. Mo, *Adv Energy Mater.*, **9**(43), 1902078 (2019). https://doi.org/10.1002/aenm.201902078.
24. A. R. West, F. P. Glasser, *J. Mater. Sci.*, **6**, 1100 (1971). https://doi.org/10.1007/BF00980609.
25. B. Monnaye, C. Garrault, G. Perez, R. Bouaziz, *C. r. hebd. séances Acad. sci. serie C*. **278**(4), 251 (1974).
26. B. Monnaye, Li_2MGeO_4 series (M = Mg Ca, Fe, Co, Ni Zn, Cd) – structural relationship between mixed germinate, *Rev. Chim. Miner.,* **13**(5), 422 (1976).
27. N. K. Nakayama, K. Takahashi, K. Fujiwara, A. Nakatsuka, M. Isobe, Y. Ueda, *TMRS-J*, **38**(3), 419 (2013). https://doi.org/10.14723/tmrsj.38.419.
28. A. C. Larson, R. B. Von Dreele, General Structure Analysis System (GSAS), Report LAUR, Los Alamos National Laboratory. 86 (2000). https://www.ncnr.nist.gov/xtal/software/gsas.html.
29. B. H. Toby, EXPGUI, a graphical user interface for GSAS, *J. Appl. Crystallogr.*, **34**, 210 (2001). https://doi.org/10.1107/S0021889801002242.
30. T. Roisnel, J. Rodriguez-Carvajal, WinPLOTR, version May 2000: Materials Science Forum, in: Proceedings of the 7th European Powder Diffraction Conference, Barcelona, Spain, 20–23 May 2000, R. Delhez, E. J. Mittenmeijer (eds.), Scitec Publications, Ltd., Baech, Switzerland, 2000, p. 118.
31. K. Momma, F. Izumi, VESTA 3 for three-dimensional visualization of crystal, volumetric and morphology data, *J. Appl. Crystallogr.*, **44**, 1272 (2011). https://doi.org/10.1107/S0021889811038970.
32. E. Plattner, H. Völlenke, A. Wittmann, *Monatsh. Chem.*, **107**(4), 921 (1976). https://doi.org/10.1007/BF00904478.
33. H. Völlenkle, *Z. Kristallogr. – Cryst. Mater.*, **154**(1–4), 77 (1981). https://doi.org/10.1524/zkri.1981.154.14.77.
34. P. G. Bruce, A. R. West, *J. Solid State Chem.*, **44**(3), 354 (1982). https://doi.org/10.1016/0022-4596(82)90383-8.

Bulgarian Chemical Communications, Volume 55, Special Issue C (pp. 75–79) 2023 *DOI: 10.34049/bcc.55.C.0008*

Personalized approach in defining the level of interest during lung electrical impedance tomography

I. Minev[1,2*], V. Jukic[3], T. Gogova[2], N. Traykova[1,2]

[1] *Department of Anesthesiology, Emergency, and Intensive care medicine; Medical University of Plovdiv, Bulgaria 15A, Vasil Aprilov, Blvd., Plovdiv 4000*
[2] *University Hospital "St. George", Plovdiv, Bulgaria*
[3] *ServerNet Srl., Trieste, Italy*

Received: November 2023; Revised: December 2023

Electrical impedance tomography (EIT) is a non-invasive method for personalized monitoring of lung ventilation at the bedside. Although for years in clinical practice there are no clear recommendations for optimal placement of the electrodes. The objective is to develop a protocol for defining the level of interest, electrode belt positioning and individualized reconstruction of the EIT images. A computed tomography (CT) scan analysis is used for defining the level of interest and providing reference points for belt positioning. The margins of the patient's thorax are determined by applying a fem mesh to the CT image. Subsequently the raw data from the EIT is reconstructed within the individualized contour of the thorax reflecting the body structure of the patient. Applying the protocol for defining a level of interest, belt positioning and individualized reconstruction of the EIT images resulted in significant conformity between the lung areas on the CT image and the reconstructed EIT image taken at the corresponding thoracic level. Thus, the limitations for placing the EIT belt at different, than initially recommended positions are surmounted and indications for potential clinical application of EIT in conditions which are characterized by heterogeneously disseminated or solitary lesions. The personalized approach in EIT application reveals its potential to support the optimization of mechanical ventilation according to the individual condition and disease, especially in case of heterogeneously disseminated or solitary lesions.

Keywords: EIT, electrode belt positioning, personalized monitoring, mechanical ventilation.

INTRODUCTION

Electrical impedance tomography (EIT) is designed and promoted as a noninvasive method [1] for personalized monitoring [2, 3] of lung ventilation at the bedside. The EIT devices are significantly informative [4] about the heterogeneous characteristics [5] of lung function, caused by different pathological conditions [6–9]. Although four decades in clinical practice [10], its potential is not fully revealed. The informational value of the method is significantly reduced [11] due to the fact that there are no guidelines for sufficient personalization of the acquired data. There are several reasons that limit EIT application in the intensive care units, narrowing its use. The first is the lack of clear recommendations for optimal placement [12] of the EIT electrodes. It is caused by the absence of instructions on determining the level of interest. Thus, there is no possibility to correct the data of the raw EIT images in accordance with the patient's anatomic characteristics and create reliable images with high resolution. Nevertheless, the application of the EIT at certain levels [13] of the thorax restricts its ability to assess the pathological process development if it is located elsewhere. Therefore, our goal is to develop a protocol for defining the level of interest, electrode belt positioning and individualized reconstruction of the EIT images.

MATERIALS AND METHODS

A retrospective analysis of anonymized raw data from the EIT monitor (Swisstom BB2 EIT Monitor) in comparison with thoracic CT scans (Siemens

* To whom all correspondence should be sent:
E-mail: ivaylo.minev@mu-plovdiv.bg

Somatom Definition AS) was performed. There was used data of patients with lung contusion, admitted in the ICU of the Department of Anesthesiology and Intensive care, University hospital "St. George" – Plovdiv, Bulgaria. Based on analysis of thoracic CT scans the level of interest was defined as the most significant intersection between the injured lung zones and the plane where the electrodes for EIT should be placed. According to the study protocol a radiologist proposed appropriate anatomical markers on the patient's skin. These reference points were used to guide the placement of the belt with EIT electrodes. A two-dimensional fem mesh was created. The spatial determination of the thoracic borders was made by placing the fem mesh onto the CT scan image taken at the level of interest and adjusting the mesh to the contour of the patient's thorax. The raw EIT data was processed within this personalized contour, followed by a reconstruction of the raw EIT image, reflecting patient anatomical characteristics.

RESULTS AND DISCUSSION

Some pathological processes cause heterogeneous lung tissue [14] alteration, which does not correspond to the recommended levels [12] for positioning of the EIT belt thus compromising the conclusions [15] of the EIT results. The areas affected by these conditions could be identified by more comprehensive image diagnostic methods like CT and MRI. We provide researchers with methodology for reasonable definition of unconventional levels of interest determined by the location of the lesion and how to define the EIT belt positioning. In our protocol we have chosen the CT image as a reference method.

Process description

Based on the CT scan analysis we define the level of interest (topographically described with skin markers and angle) as the slice containing the largest area of the investigated pathological process (Fig. 1).

This determines the level of the EIT belt positioning. Such positioning ensures that the raw EIT image will contain the required information for description of the injured zones.

According to the study protocol a radiologist proposed appropriate anatomical markers on the patient's skin. These reference points were used to guide the placement of the belt with EIT electrodes (Fig. 2).

The initial EIT image by default has a circular shape (Fig. 3) that does not correspond to the contour of the patient's thorax. Therefore, the primary signal in every pixel of the raw image will not correctly represent the impedance values generated in the patient thorax.

To overcome this discrepancy, the initial image should be reshaped in order to match the real contour of the patient thorax. To support the EIT image reconstruction optimization, we provide a rationale on how to use a fem mesh for precise matching of the intersection of the patient thorax obtained by CT with the EIT image and increase the informational

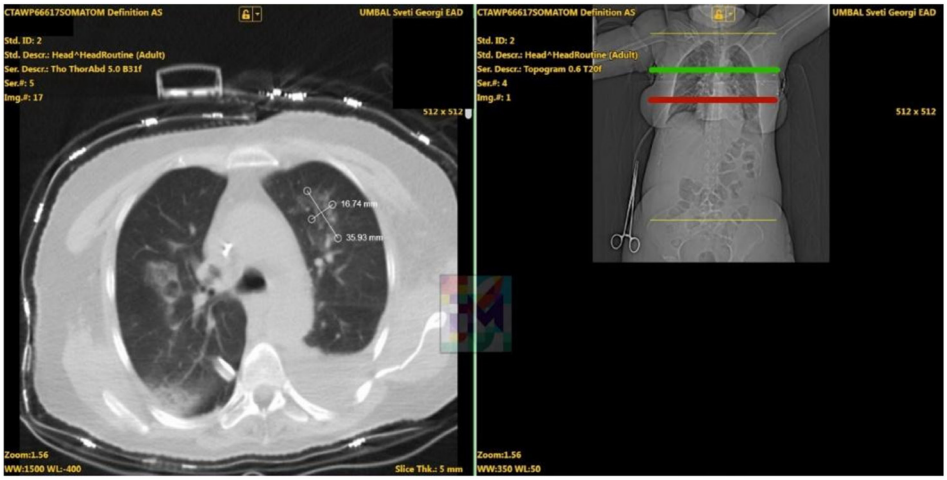

Fig. 1. A CT scan of a patient with chest trauma.

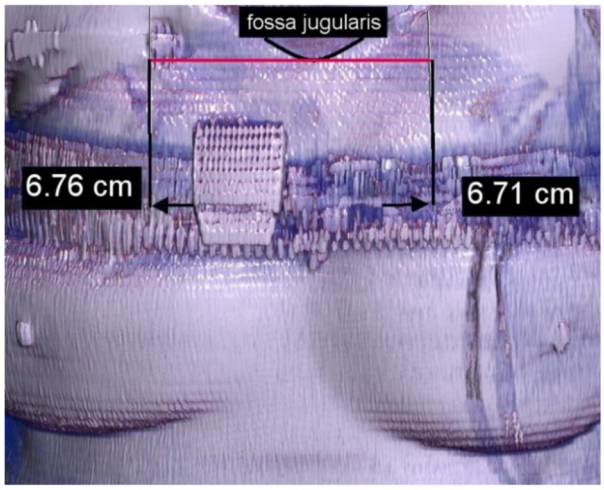

Fig. 2. CT reconstruction of the body with distance to the skin markers.

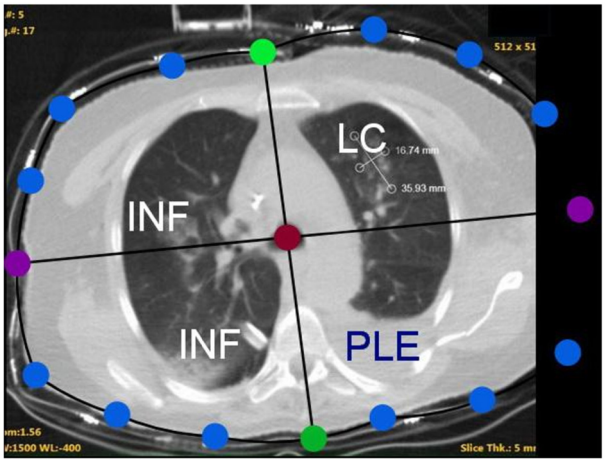

Fig. 4. The fem-mesh over imposing on to the CT scan.

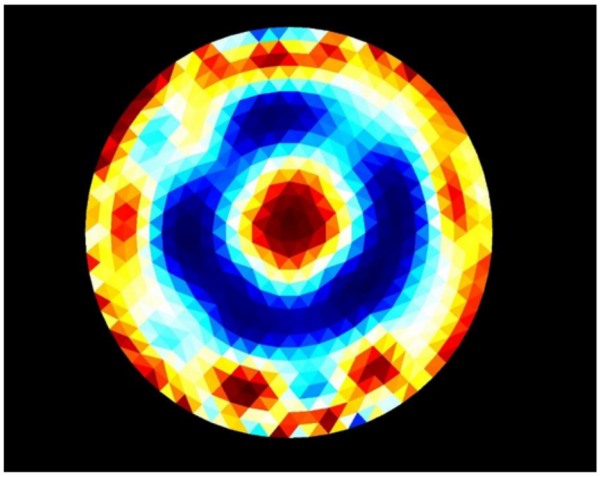

Fig. 3. Initial non-personalized EIT image.

value of the functional EIT images taken at unconventional levels of interest.

We created a two-dimensional fem mesh of 16 cartesian points - 4 pivotal points defining the anteroposterior and transverse diameters of the patient's thorax, one constrained center, 3 points on each quadrant (Fig. 4).

There are some constraints. The points of the mesh could not be too close or too distant or overlap the rule of the mesh, the topology could not be folded, because it will create null value [16]. The CT scan image is used for measuring 4 points defining antero-posterior and transverse diameters of the thorax. Following that a reference image of the CT scan at the level of interest (angle, points) is generated. The reference image size must be at least 512×512 pixels with resolution of minimum 20 pixels per cm^2. Placing the points of the mesh on the contour of the patient's thorax (Fig. 4) on the reference image results in spatial definition of the thoracic borders.

The primary use of the mesh is to calculate data. We start with normalized condition and create a reconstruction of the image. We do the image reconstruction with a fem model of more than 20000 elements which describes a standard thorax with a resolution better than around 5×5 mm.

Following algorithm optimization and fine tuning, higher resolution of the EIT image is achieved. After the EIT scan is obtained the raw file of numerical data from the EIT device is imported into the fem model and a new personalized static EIT image is generated. The data is processed by input filter – the voltage is being calculated out of current and impedance pairs and oversaturated and poorly saturated leads are taken out. The result is 32×32(1024) voltage measurement used by inverse solver [17] to create the static image on the fem model created by a specific mesh matching the CT image.

The result is a color-coded two-dimensional fem diagram representing the body composition of the patient in that specific slice. It contains no patient identification or protected data information. This personalized static EIT image should "perfectly" fit over an imposed CT scan taken at the same level of interest. The degree of match between the EIT static image and the CT scan is assessed by calculating the % of overlapping conformity.

Protocol application

On Figure 1 a thoracic CT scan of a patient with lung contusion is presented. The level and the angle of positioning of the electrodes is defined by the plane with the largest intersection with the injured zones (the lung contusion – LC, the infiltrative changes – INF and the pleural effusion – PLE). This level (indicated in green) is significantly higher than the recommended by the vendor V intercostal space (indicated in red). Therefore, in patients with lung contusion at a level different than the recommended level of belt positioning, following the vendor's instructions would not result in reliable information about the distribution of lung ventilation in the injured zones.

Figure 3 displays a non-personalized EIT image of the same patient. By definition it is constructed within the contour of a circle. The resolution is low and the correspondence to the real patient's thorax anatomy is weak. Furthermore, the initial reconstruction is made according to a shape of a thorax transection at level of fifth-sixth intercostal space of an ideal patient and a blend covering the thoracic wall and mediastinum is used (Fig. 5).

The application of the protocol for defining the level of interest, electrode belt positioning and individualized reconstruction of the EIT images, resulted in significant conformity between the CT scan and the EIT image taken at the same thoracic level (Fig. 6).

The impedance was not equally distributed. Several abnormality zones were marked and compared with the corresponding zones of the CT image. The

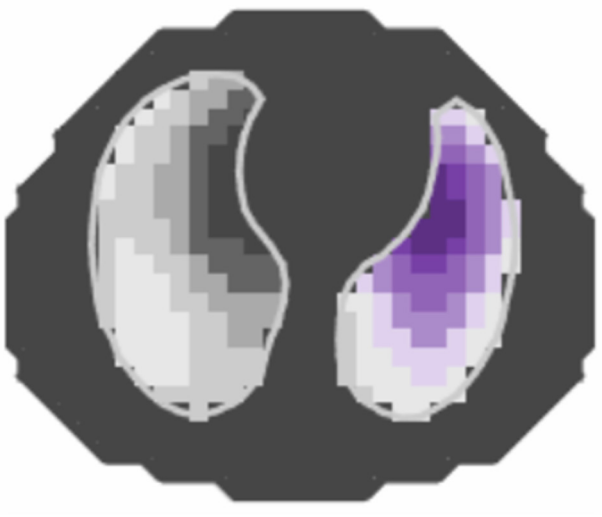

Fig. 5. EIT image with over-imposed blend.

visual analysis revealed considerable sensitivity of the EIT to gas and water distribution [18, 19].

Dorsally and bilaterally on the EIT image an impedance abnormality with horizontal ventral border was observed. On both sides of the CT scan signs related to water accumulation were visible. On the left there was pleural effusion – PLE and on the right infiltrative process – INF. It is important to point out that the ventral margin of the pleural effusion on the CT scan matched the change in the impedance distribution on the EIT image. In contrast, the ventral margin of the infiltrative process was lower than the corresponding change in the impedance, suggesting that the electrical impedance tomography provides higher

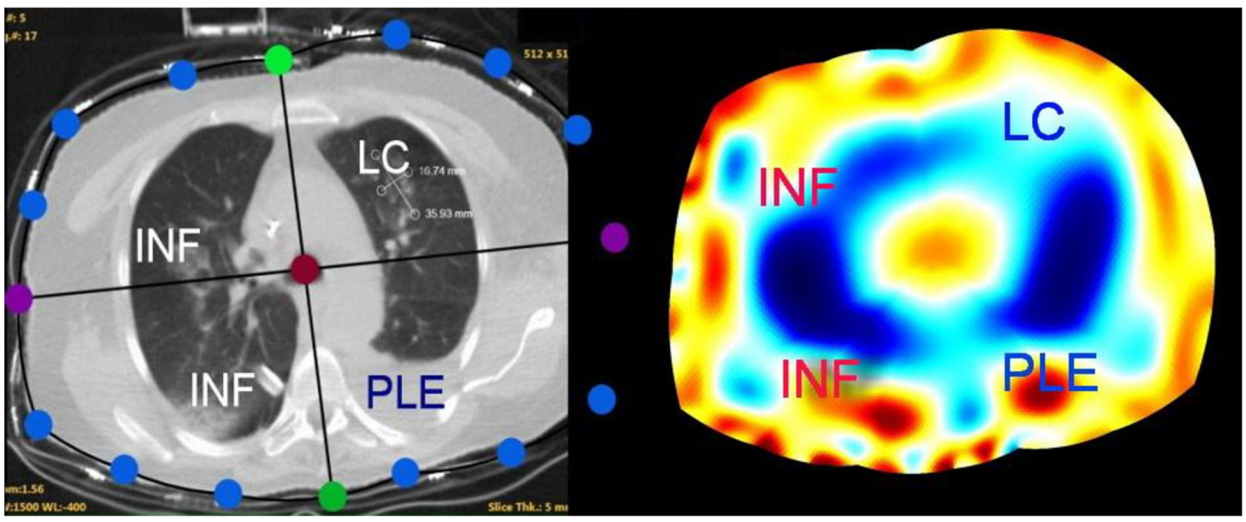

Fig. 6. The personalized EIT static image in comparison to the CT scan.

sensitivity to the changes in water distribution than the CT scan but lower resolution. EIT abnormalities reflect the tissue function alteration and visualize prospective changes prior organizational structural changes [20]. Different factors affect the water accumulation and the impedance changes in these two pathological focuses. Pleural effusions are poor of biological membranes in the liquid [21–23] and gravity is a major factor. The infiltration is related to inflammation that results in water accumulation in the lung tissue due to changes in biological membrane permeability and is dependent on gravity and lung tissue architecture (vascularization and ventilation in the segments). In these regions restricted distribution of ventilation [24, 25] is observed on dynamic images. Considering the differences in the pathophysiology further investigation should be performed.

CONCLUSIONS

The protocol for defining the level of interest, electrode belt positioning and individualized reconstruction of the EIT images overcomes the limitations for placement of the electrode belt at levels different than the initially recommended. In addition, it improves EIT clinical application for optimization of lung ventilation monitoring. Furthermore, the protocol reveals the potential of the EIT to be used for monitoring the dynamics of the lung injury in conditions, characterized by heterogeneous dissemination or solitary lesions.

Acknowledgments: *Project BG05M2OP001-1. 002-0005 – Competence Center "Personalized Innovative Medicine (PERIMED)", financed by Operational Program "Science and Education for Smart Growth", EU, ESIF; Project NO-08/2021 "Investigating the capabilities of EIT as a clinical method for monitoring lung injury dynamics in patients with thoracic trauma", MU-Plovdiv.*

REFERENCES

1. S. Leonhardt, B. Lachmann, *Intensive Care Med*., **38**, 1917 (2012).
2. T. Muders, H. Luepschen, C. Putensen, *Curr. Opin. Crit. Care*, **16**, 269 (2010).
3. J. M. Constantin, S. Perbet, J. Delmas, E. Futier, *Crit. Care*, **18**, 164 (2014).
4. B. Vogt, S. Pulletz, G. Elke, Z. Zhao, P. Zabel, N. Weiler, I. Frerichs, *J. Appl. Physiol.*, **113**, 1154 (2012).
5. R. Bhatia, G. M. Schmölzer, P. G. Davis, D. Tingay, *Intensive Care Med*., **38**, 308 (2012).
6. S. Pulletz, M. Kott, G. Elke, D. Schädler, B. Vogt, N. Weiler, I. Frerichs, *Multidiscip. Respir. Med*., **7**, 44 (2012).
7. B. Vogt, Z. Zhao, P. Zabel, N. Weiler, I. Frerichs, *Am. J. Physiol. Lung Cell. Mol. Physiol.*, **311**, L8 (2016).
8. R. E. Serrano, L. B. de, O. Casas, T. Feixas, N. Calaf, V. Camacho, I. Carrió, P. Casan, *J. Sanchis, P. Riu, Physiol. Meas*., **23**, 211 (2002).
9. Z. Zhao, U. Müller-Lisse, I. Frerichs, R. Fischer, K. Möller, *Physiol. Meas*., **34**, N107 (2013).
10. A. Adler, D. Holder, Electrical Impedance Tomography: Methods, History and Applications, ISBN: 978-0-429-39988-6, DOI: 10.1201/9780429 399886, 2022.
11. W. R. Lionheart, *Physiol. Meas*., **25**, 125 (2004).
12. J. Karsten, T. Stueber, N. Voigt, E. Teschner, H. Heinze, *Crit. Care*, **20**, 3 (2016).
13. S. Krueger-Ziolek, B. Schullcke, J. Kretschmer, U. Müller-Lisse, K. Möller, Z. Zhao, *Physiol. Meas*., **36**, 1109 (2015).
14. J. Gao, S. Yue, J. Chen, H. Wang, *Bio-Med. Mater. Eng*., **24**, 2229 (2014).
15. F. Reifferscheid, G. Elke, S. Pulletz, B. Gawelczyk, I. Lautenschläger, M. Steinfath, N. Weiler, I. Frerichs, *Respirology*, **16**, 523 (2011).
16. J. T. Schwartz, Differential Geometry and Topology, G&B Science Pub, ISBN-13: 978-9990196689, 1968.
17. H. Wang, E. Zimmermann, M. Weigand, H. Vereecken, J. A. Huisman, Geophys. *J. Int.*, **235**, 2888 (2023).
18. C. Trepte, C. Phillips, J. Solà, A. Adler, S. Haas, M. Rapin, S. Böhm, D. Reuter, *Crit. Care*, **20**, 18 (2016).
19. F. Fu, B. Li, M. Dai, S. J. Hu, X. Li, C. H. Xu, B. Wang, B. Yang, M. X. Tang, X. Z. Dong, Z. Fei, X. T. Shi, *PLoS One*, **9**(12), e113202 (2014).
20. S. Hannan, M. Faulkner, K. Aristovich, J. Avery, M. Walker, D. Holder. *NeuroImage*, **209**, 116525 (2020).
21. J. M. Porcel, M. Azzopardi, C. F. Koegelenberg, F. Maldonado, N. M. Rahman, Y. C. Lee, *Expert Rev. Respir. Med*., **9**, 801 (2015).
22. S. P. Chubb, R. A. Williams, *Clin. Biochem. Rev*., **39**(2), 39 (2018).
23. P. Kunst, A. Vonk Noordegraaf, E. Raaijmakers, J. Bakker, A. Groeneveld, P. Postmus, P. de Vries, *Chest*, **116**, 1695 (1999).
24. J. Spaeth, K. Daume, U. Goebel, S. Wirth, S. Schumann, *Br. J. Anaesth*., **116**, 838 (2016).
25. T. Becher, B. Vogt, M. Kott, D. Schädler, N. Weiler, I. Frerichs, *PLoS One*, 11, e0152267 (2016).

Bulgarian Chemical Communications, Volume 55, Special Issue C (pp. 81–86) 2023 *DOI: 10.34049/bcc.55.C.0009*

Cervical cancer: a review of economic evidence for different prevention and treatment strategies

E. Z. Gavazova[1], R. A. Staynova[1*], D. D. Grekova-Kafalova[1], Y. Zh. Gvozdeva[1,2], M. I. Kassarova[2]

[1] *Department of Pharmaceutical Sciences, Faculty of Pharmacy, Medical University of Plovdiv, 15A Vassil Aprilov Blvd., 4002 Plovdiv, Bulgaria*
[2] *Research Institute at Medical University of Plovdiv, Plovdiv, Bulgaria*

Received: November 2023; Revised: December 2023

Cervical cancer remains a significant global health concern, affecting thousands of women annually. It is the fourth most common cancer in women. Almost all cases of cervical cancer are caused by human papillomavirus (HPV). Prophylactic strategies such as HPV vaccination and screening are proven effective approaches to prevent cervical cancer and are also cost-effective. This article presents a scoping review of current economic evidence for cervical cancer prevention and treatment.

Keywords: cervical cancer; treatment; HPV vaccination; costs; cost-effectiveness; cost-utility; pharmacoeconomic evaluation.

INTRODUCTION

Cervical cancer remains a significant global health concern, affecting thousands of women annually [1]. The prevalence of cervical cancer varies worldwide, with higher rates reported in specific regions [2]. It is important to note that prevalence figures can change over time due to factors such as alterations in risk factors, screening practices, and healthcare access. Prevalence is often expressed as the number of cases per 100,000 women. In 2020, the World Health Organization (WHO) estimated 604,000 new cases of cervical cancer worldwide, resulting in approximately 342,000 deaths [3]. Cervical cancer is more common in less developed regions, where access to screening and preventive measures may be limited. Sub-Saharan Africa, South-Central Asia, and parts of Latin America have been identified as regions with higher cervical cancer incidence and mortality rates [4].

As advances in medical science continue to enhance treatment options for this malignancy, the economic implications of these interventions come under increased scrutiny [5]. Pharmacoeconomic evaluation, a critical component of health economics, provides a systematic framework to assess the financial impact of healthcare interventions [6]. In the context of cervical cancer treatment, understanding the cost-effectiveness, cost-benefit, and cost-utility of various therapeutic approaches becomes essential for healthcare decision-makers, clinicians, and patients [7].

The importance of pharmacoeconomic evaluations in cervical cancer treatment lies in their potential to inform healthcare policies, resource allocation, and treatment decisions. As healthcare systems strive for optimal allocation of limited resources, understanding the economic outcomes associated with cervical cancer interventions becomes imperative [8].

Through this review, we aim to contribute to the body of knowledge that guides evidence-based decision-making, ultimately fostering improved patient outcomes and resource utilization in the realm of cervical cancer care.

METHODS

The following electronic databases were searched for relevant publications: PubMed, Google Scholar, and Scopus. Key terms used in the search

* To whom all correspondence should be sent:
E-mail: radiana.staynova@mu-plovdiv.bg

were *cervical cancer*, *treatment*, *HPV vaccination*, *costs*, *cost-effectiveness*, *cost-utility*, and *pharmacoeconomic evaluation*. Only publications in English were considered. Full-text articles using different economic methodologies were included in the analysis. Review articles and those not written in English were excluded.

RESULTS AND DISCUSSION

Cervical cancer treatment

The treatment options for cervical cancer depend on several factors, including the stage of the cancer, the patient's overall health, and individual preferences. Treatment may involve a combination of surgery, radiation therapy, and chemotherapy [9] (Fig. 1). Removal of the uterus is a common surgical procedure for cervical cancer. Depending on the extent of the cancer, the surgeon may also remove surrounding tissues, such as the ovaries and fallopian tubes [10]. If cancer has spread, the surgeon may remove nearby lymph nodes to assess the extent of the disease [11].

During external beam radiation, high-energy rays are directed at the cancer from outside the body [12]. This is often used after surgery to eliminate any remaining cancer cells. In brachytherapy, radioactive sources are placed directly into or near the tumor. This type of radiation therapy is often used to treat small tumors or as part of the overall treatment [13].

Medicines are administered intravenously or orally to destroy cancer cells throughout the body. Chemotherapy is often used in conjunction with radiation therapy [14]. Neoadjuvant chemotherapy is given before surgery or radiation therapy to shrink the tumor and make other treatments more effective. Adjuvant chemotherapy is administered after surgery or radiation to eliminate any remaining cancer cells [15]. Bevacizumab, an available targeted therapy that targets blood vessel formation in tumors, may be used in combination with chemotherapy for advanced or recurrent cervical cancer [16]. Pembrolizumab is an immune checkpoint inhibitor that may be used for advanced cervical cancer that has not responded to other treatments.

HPV vaccination

There are several HPV (human papillomavirus) vaccines that have been developed and are used globally. *Gardasil 9* is a vaccine that protects against nine types of HPV. It is approved for use in both males and females. In addition to preventing cervical cancer, it also provides protection against other HPV-related cancers and genital warts [17]. There is also 4-valent *Gardasil*. *Cervarix* is a bivalent vaccine that protects against two types of HPV: HPV types 16 and 18. It is primarily designed to prevent cervical cancer and is approved for use in females [18].

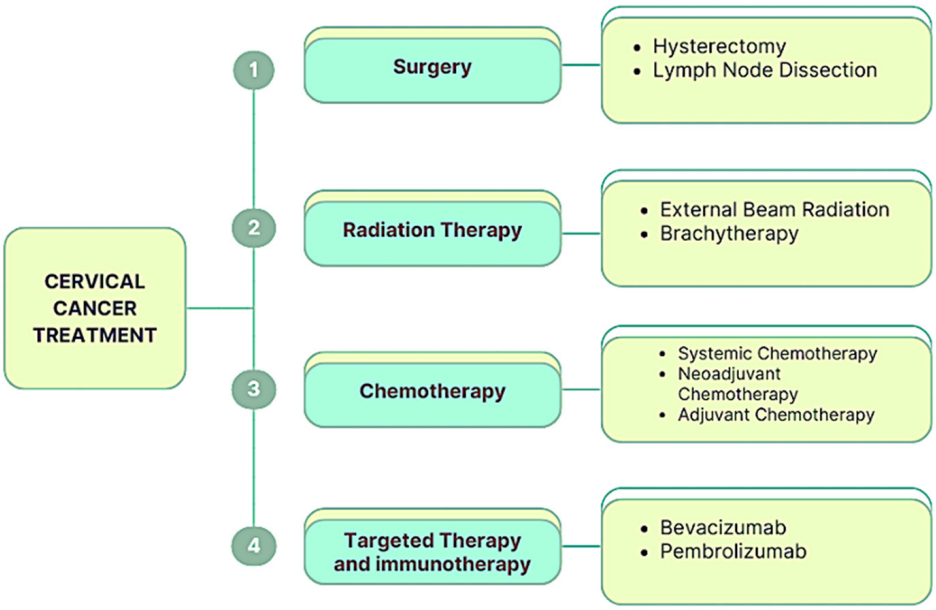

Fig. 1. Cervical cancer treatment options.

These vaccines are designed to prevent infection with certain types of HPV, including those that are associated with cervical cancer and other HPV-related cancers. HPV vaccination has been proven to significantly reduce the incidence of cervical cancer by preventing infections with high-risk HPV types. This prevention has a substantial impact on the overall cost of treating and managing cervical cancer [19]. In addition to preventing cervical cancer, HPV vaccination also reduces the incidence of other HPV-related cancers, such as anal, vulvar, vaginal, penile, and oropharyngeal cancers.

Economic evidence for cervical cancer prevention and treatment

Overall, 114 studies were identified through electronic databases. We analyzed 20 studies that met our inclusion criteria (Table 1). Most of the studies (n = 9) used the cost-effectiveness pharmacoeconomic method [20–28]. The studies vary in settings; many of them are conducted in middle and low-income countries. The objective of these studies was to assess the cost-effectiveness of HPV vaccination. A pharmacoeconomic evaluation using cost-utility analysis was performed to compare HPV vaccination and screening in Indonesia [29]. A systematic review conducted in 2017 summarizes the health-economic studies of HPV vaccination in Southeast Asian countries. The studies included in this review consider factors such as vaccine costs, disease prevention, and the long-term economic impact of vaccination programs [30]. Other therapeutic approaches are analyzed using the cost-benefit [31] and cost-utility methods [32, 33]. Three studies evaluate the budget impact and economic burden of cervical cancer [34–36]. Four of the analyzed studies use cost of illness methodology [7, 37–39].

Increnental Cost Effectiveness Ratios (ICERs) for HPV screening methods, such as HPV testing as a primary screening tool for cervical cancer, have generally been found to be cost-effective. HPV testing has demonstrated improved sensitivity for detecting high-grade cervical intraepithelial neoplasia

Table 1. Pharmacoeconomic studies related to prevention and treatment of cervical cancer

Author, Year of publication	Country	Type of pharmacoeconomic evaluation	Compared alternatives
Usher *et al*., 2008 [20]	Ireland	Cost- effectiveness	HPV vaccination
Annemans *et al*., 2009 [21]	Belgium	Cost-effectiveness	Quadrivalent vaccine
Ezat and Aljunid, 2010 [22]	Malaysia	Cost-effectiveness	HPV vaccination
Praditsitthikorn *et al*., 2011 [31]	Thailand	Cost-benefit	Policy implementation and prevention and control of cervical cancer
Kostinov and Zverev, 2012 [23]	Russia	Cost-effectiveness	HPV vaccination
Setiawan *et al.,* 2015 [24]	Indonesia	Cost-effectiveness	HPV vaccination
Agapova *et al.,* 2015 [34]	Ireland	Cost analysis, Markov modelling	Cytology and co-testing
Guerrero *et al*., 2015 [32]	Philippines	Cost-utility	Screening and vaccination
Liu *et a*l., 2016 [7]	Canada	Cost of illness	–
Setiawan *et al*., 2016 [29]	Indonesia	Cost-utility, Markov modelling	Vaccination and screening for HPV
Cheikh *et al*., 2016 [37]	Morocco	Cost of illness	–
Tay *et al.,* 2018 [25]	Singapore	Cost-effectiveness	School – based HPV vaccination campaign
Jiang *et al*., 2019 [26]	China	Cost-effectiveness	9-valent HPV vaccine
Castañon *et al*., 2019 [33]	UK	Cost -utility	HPV testing
Setiawan *et al*., 2020 [35]	Indonesia	Budget impact analysis and Markov modelling	HPV vaccination
Wu *et al.,* 2020 [38]	China	Cost of illness	–
Vale *et al*., 2021 [27]	Brazil	Cost-effectiveness	Cytology against HPV screening
Ibáñez *et al.,* 2021 [36]	Spain	Cost analysis	Cervical cancer screening
Wondimu *et al*., 2022 [28]	Ethiopia	Cost-effectiveness	quadrivalent and nonavalent human papillomavirus vaccines
Lebanova *et al*., 2023 [39]	Bulgaria	Cost of illness	–

(CIN) compared to traditional Pap smears, leading to earlier detection and prevention of cervical cancer [40].

Costs associated with cervical cancer

Cervical cancer imposes both direct medical and non-medical costs, contributing to the economic burden on individuals, healthcare systems, and society as a whole (Fig. 2). Understanding these direct medical and non-medical costs is crucial for conducting comprehensive pharmacoeconomic analyses. Evaluations aim to assess the cost-effectiveness of interventions, considering both the economic impact on healthcare systems and the financial burden on patients and their families. Reducing the overall burden of cervical cancer includes not only improving treatment outcomes but also addressing the economic challenges associated with the disease [41].

Direct Medical Costs

- *Treatment Costs*: This includes expenses related to medical procedures, surgery, chemotherapy, radiation therapy, targeted therapy, immunotherapy, and other interventions used in the treatment of cervical cancer.
- *Hospitalization Costs*: Expenses related to hospital stays, which may be necessary for surgeries, recovery, or intensive treatments.
- *Diagnostic Costs*: Costs associated with diagnostic procedures such as biopsies, imaging (MRI, CT scans), and laboratory tests.
- *Medication Costs*: The cost of pharmaceuticals used in treatment, including chemotherapy drugs, targeted therapies, and supportive medications.
- *Follow-up Care Costs*: Regular follow-up visits, imaging, and tests to monitor the patient's condition and detect any potential recurrence.
- *Palliative Care Costs*: If required, the costs associated with palliative care and pain management.

Direct Non-Medical Costs

- *Travel Expenses*: Costs related to transportation to and from medical appointments, including fuel, public transportation, or lodging for patients who need to travel for treatment.
- *Accommodation Costs*: For patients who require treatment away from their home, accommodation expenses may be incurred.
- *Caregiver Costs*: The economic impact on caregivers, including potential lost income due to time spent caring for the patient.
- *Productivity Loss*: Direct non-medical costs also encompass the economic impact of reduced productivity or absence from work for both patients and their caregivers.

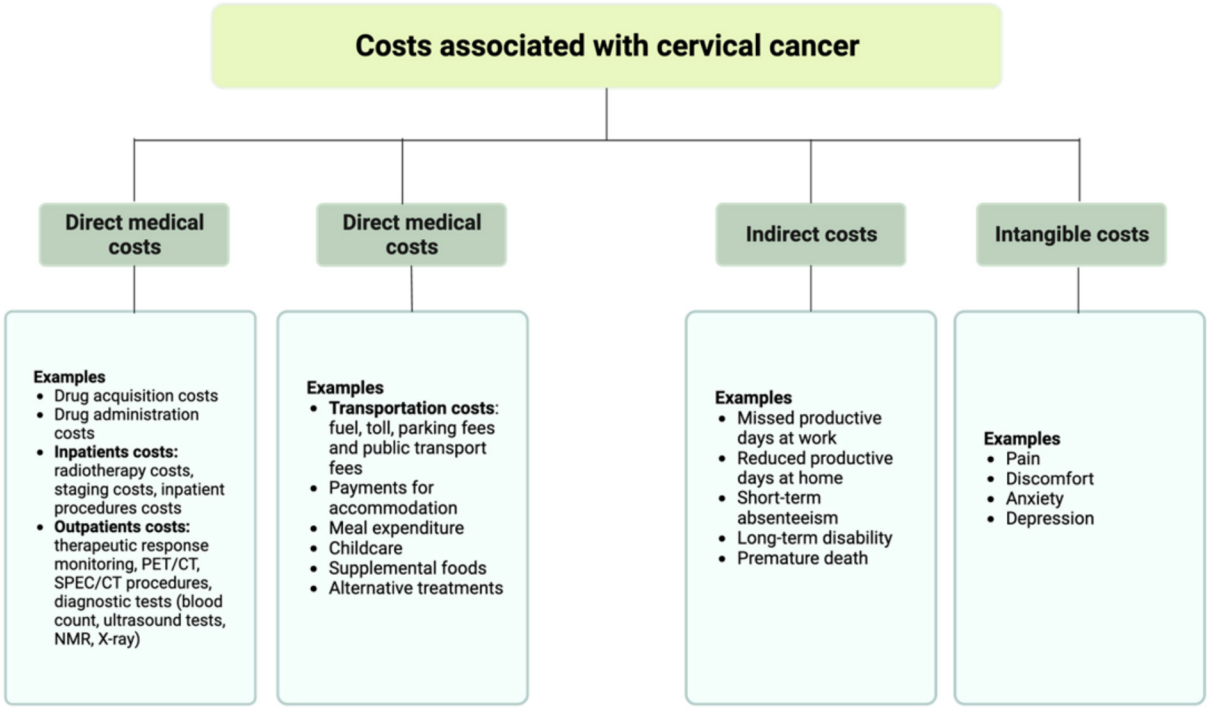

Fig. 2. Costs associated with cervical cancer treatment.

- *Counseling and Support Services*: Costs associated with psychological support services, counseling, and other support mechanisms.

Indirect costs

Indirect costs refer to the economic impact of the disease that extends beyond direct medical expenses. These costs encompass various factors that can affect individuals, families, and society as a whole. Here are some key components of the indirect costs associated with cervical cancer:

- *Productivity Loss*: Cervical cancer may lead to absenteeism and reduced productivity in the workplace due to treatment-related side effects, recovery periods, and medical appointments. Caregivers, often family members or friends, may also experience productivity loss as they may need to take time off work to provide support and care.
- *Premature Mortality and Disability*: Premature mortality resulting from cervical cancer deprives the workforce of potentially productive individuals, leading to lost economic contributions. Disability caused by the disease, or its treatment can result in long-term or permanent work limitations, impacting a person's ability to earn a living.
- *Impact on Caregivers*: Family members or friends who take on the role of caregivers may experience economic strain due to reduced work hours, career interruptions, or the need to hire additional help.

It is important for individuals diagnosed with cervical cancer to consult with a multidisciplinary healthcare team, including gynecologic oncologists, radiation oncologists, medical oncologists, and other specialists. The treatment plan should be tailored to the specific characteristics of the cancer and the patient's overall health [42]. Additionally, prevention through HPV vaccination and regular screenings such as Pap smears and HPV tests is crucial for early detection and treatment. Patients should discuss potential side effects, long-term effects, and the overall prognosis with their healthcare team to make informed decisions about their treatment.

Bulgaria has witnessed a significant incidence of illness and death resulting from cervical cancer, coupled with low coverage in immunization. During the years 2018–2020 in Bulgaria, the cumulative loss of life amounted to an estimated total of 20,446 years, attributed to cervical cancer [39]. There is a necessity to reconsider the approach to disease prevention, emphasizing a reassessment of strategies involving compulsory screening and immunizations [43]. Healthcare professionals in Bulgaria are cognizant of the concerning levels of cervical cancer occurrence and mortality within the nation. Nonetheless, a lack of robust communication and collaboration between policymakers and frontline healthcare personnel has resulted in an insufficient flow of information about existing programs. The absence of a clear health policy about screening is identified as a primary barrier to the effective implementation of a comprehensive screening initiative [44].

CONCLUSIONS

Cervical cancer management is an ongoing research area. There is a need for improvement of the prevention and information campaigns for cervical cancer awareness, especially in the developing countries. Pharmacoeconomic studies utilize various methods and study perspectives. They show the economic impact of the disease and the cost effectiveness of novel therapies. HPV vaccination has a broader public health impact by reducing the transmission of the virus within the population. This, in turn, helps to decrease the overall burden of HPV-related diseases, leading to improved public health outcomes. Studies have shown that the economic benefits of HPV vaccination extend beyond healthcare cost savings. Preventing HPV-related diseases contributes to increased productivity and improved quality of life for individuals and their families. It's important to note that the cost-effectiveness of HPV vaccination may vary by region and healthcare system. Additionally, ongoing research and public health efforts aim to improve vaccination coverage rates and address challenges related to access, equity, and awareness.

Acknowledgements: *This article is published with the support of the Project № BG05M2OP001-1.002-0005-C 03, Center for Competence "Personalized Innovative Medicine (PERIMED)", work package – 8; funded by the Operational Program "Science and Education for Intelligent Growth" 2014–2020, co-financed by the European Union through the European Regional Development Fund.*

REFERENCES

1. https://gco.iarc.fr/today/home.
2. S. Zhang, H. Xu, L. Zhang, Y. Qiao, *Chin J. Cancer Res*., **32**, 720 (2020).

3. D. Singh, J. Vignat, V. Lorenzoni, M. Eslahi, O. Ginsburg, B. Lauby-Secretan, M. Arbyn, P. Basu, F. Bray, S. Vaccarella, *Lancet Glob. Health*, **11**, 197 (2022).
4. S. Pimple, G. Mishra, *CytoJournal,* **19**, 21 (2022).
5. H. Dau, J. Trawin, C. Nakisige, B. A. Payne, M. Vidler, J. Singer, J. Orem, L. Smith, G. Ogilvie, *Int. J. Gynaecol. Obstet.*, **160**, 751 (2022).
6. J. Bodrogi, Z. Kaló, *Br. J. Pharmacol.*, **159**, 1367 (2010).
7. N. Liu, N. Mittmann, P. C. Coyte, R. Hancock-Howard, S. J. Seung, C. C. Earle, *Am. J. Obstet. Gynecol.*, **214**, 615 (2016).
8. D. B. Vale, J. C. Teixeira, *Nat. Med.*, **29**, 3004 (2023).
9. B. A. Wuerthner, M. Avila-Wallace, *Nurse Pract. Am. J. Prim. Health Care*, **41**, 18 (2016).
10. C. A. Burmeister, S. F. Khan, G. Schäfer, N. Mbatani, T. Adams, J. Moodley, S. Prince, *Tumour Virus Res.*, **13**, 200238 (2022).
11. C. A. Johnson, D. James, A. Marzan, M. Armaos, *Semin. Oncol. Nurs*., **35**, 166 (2019).
12. C. Marth, F. Landoni, S. Mahner, M. McCormack, A. Gonzalez-Martin, N. Colombo, *Ann. Oncol.*, **28**, 72 (2017).
13. Y. Himoto, Koji Yamanoi, Y. Kurata, *Eur. Radiol.*, **13**, 1 (2023).
14. K. S. Rallis, T. H. L. Yau, M. Sideris, *Anticancer Res.*, **41**, 1 (2021).
15. A. Gadducci, S. Cosio, *Anticancer Res.*, **40**, 4819 (2020).
16. E. Zsiros, S. Lynam, K. M. Attwood, C. Wang, S. Chilakapati, E. C. Gomez, S. Liu, S. Akers, S. Lele, P. J. Frederick, K. Odunsi, *JAMA Oncol.*, **7**, 78 (2021).
17. T. C. Pomfret, J. M. Gagnon Jr, A. T. Gilchrist, *J. Clin. Pharm. Ther.*, **36**, 1 (2011).
18. M. R. Schmiedeskamp, D. R. Kockler, *Ann. Pharmacother.*, **40**, 1344 (2006).
19. E. P. Armstrong, *J. Manag. Care Pharm.*, **16**, 217 (2010).
20. C. Usher, L. Tilson, J. Olsen, M. Jepsen, C. Walsh, M. Barry, *Vaccine*, **26**, 5654 (2008).
21. L. Annemans, V. Rémy, J. Oyee, N. Largeron, *PharmacoEconomics*, **27**, 231 (2009).
22. W. Puteh, SM Aljunid, *Asian Pac. J. Cancer. Prev.*, **11**, 79 (2010).
23. M. P. Kostinov, V. V. Zverev, *J. Microbiol. Epidemiol. Immunobiol*., **43**, (2012).
24. D. Setiawan, J. Luttjeboer, T. A. Westra, J. C. Wilschut, A. A. Suwantika, T. Daemen, J. Atthobari, B. Wilffert, M. J. Postma, *Expert Rev. of Vaccines*, **14**, 589 (2015).
25. S. Tay, T-Y. Hsu, A. Pavelyev, A. Walia, A. Kulkarni, *BJOG*, **125**, 478 (2018).
26. Y. Jiang, W. Ni, J. Wu, *BMJ Open,* **9**, e031186 (2019).
27. D. B. Vale, M. T. Silva, M. G. Discacciati, I. Polegatto, J. C. Teixeira, L. C. Zeferino, *PloSOne*, **16**, e0251688 (2021).
28. A. Wondimu, M. J. Postma, M. van Hulst, *Vaccine*, **40**, 2161 (2022).
29. D. Setiawan, F. C. Dolk, A. A. Suwantika, T. A. Westra, J. C. WIlschut, M. J. Postma, *Value in Health Reg. Issues, VHRI*, **9**, 84 (2016).
30. D. Setiawan, M. P. Oktora, R. Hutubessy, Arthorn Riewpaiboon, M. J. Postma, *Expert Rev. Vaccines*, **16**, 933 (2017).
31. N. Praditsitthikorn, Y. Teerawattananon, S. Tantivess, S. Limwattananon, A. Riewpaiboon, S. Chichareon, N. Ieumwananonthachai, V. Tangcharoensathien, *PharmacoEconomics*, **29**, 781 (2011).
32. A. M. Guerrero, A. J. Genuino, M. Santillan, N. Praditsitthikorn, V. Chantarastapornchit, Y. Teerawattananon, M. Alejandria, J. A. Toral, *BMC Public Health*, **15**, 730 (2015).
33. A. Castañon, M. Rebolj, P. Sasieni, *J. Med. Screen.*, **26**, 44 (2018).
34. M. Agapova, A. Duignan, A. Smith, C. O'Neill, A. Basu, *Expert Rev. Pharmacoeconom. Outcomes Res*., **15**, 999 (2015).
35. D. Setiawan, Andrijono, S. R. Hadinegoro, H. Meyta, R. V. Sitohang, G. Tandy, D. A. Perwitasari, M. J. Postma, *PloSOne*, **15**, e0230359 (2020).
36. R. Ibáñez, M. Mareque, R. Granados, D. Andía, M. García-Rojo, J. C. Quílez, I. Oyagüez, *BMC Women's Health*, **21**, 178 (2021).
37. A. Cheikh, S. El Majjaoui, N. Ismaili, Z. Cheikh, J. Bouajaj, C. Nejjari, A. El Hassani, Y. Cherrah, N. Benjaafar, *Pan. Afr. Med. J.*, **23**, 209 (2016).
38. Q. Wu, M. Jia, H. Chen, S. Zhang, Y. Liu, K. Prem, M. Qian, H. Yu, *PloSOne*, **15**, e0232129 (2020).
39. H. Lebanova, S. Stoev, E. Naseva, V. Getova, W. Wang, U. Sabale, E. Petrova, *Int. J. Environ. Res. Public Health*, **20**, 2746 (2023).
40. A. W. M. Suijkerbuijk, R. Donken, A. K. Lugnér, G. A. de Wit, C. J. L. M. Meijer, H. E. de Melker, J. A. Bogaards, *Expert Rev. Vaccines*, **16**, 361 (2016).
41. A. Pista, C. Costa, C. Saldanha, J. A. F. Moutinho, J. M. Moutinho, F. Arrobas, C. Catalão, J. Kempers, *BMC Public Health*, **19**, 235 (2019).
42. A. R. Teixeira, M. Abreu, *Cureus*, **15**, e48626 (2023).
43. M. Karcheva, A. Yordanov, S. Kostadinov, *Germs*, **10**, 322 (2020).
44. Z. Valerianova, Y. Panayotova, C. Amati, P. Baili, *Tumori*, **96**, 538 (2010).

Bulgarian Chemical Communications, Volume 55, Special Issue C (pp. 87–93) 2023 *DOI: 10.34049/bcc.55.C.0010*

Application of liquid biopsy in patients with breast cancer

G. Raycheva*[1], V. Popov[1], H. Ivanov[2], N. Miteva-Marcheva[2], M. Topalov[2], A. Linev[2], V. Stoyanova[2], Z. Grudeva-Popova[1]

[1] *Department of Clinical Oncology, Medical University Plovdiv*
[2] *Department of Pediatrics and Medical Genetics, Medical University Plovdiv*

Received: November 2023; Revised: December 2023

Breast cancer in women is the leading cause of global malignancy incidence for 2020 with an estimated 2.3 million new cases. Among women, breast carcinoma accounts for 1 in 4 cancer cases and 1 in 6 deaths. Projections indicate that the incidence of breast cancer will reach approximately 3.2 million per year by 2050.

The aim of our investigation is to develop and implement a modern algorithm for non-invasive monitoring of therapeutic response and minimal residual disease by liquid biopsy in patients with breast cancer. Liquid biopsy was studied in 50 breast cancer patients (26 in adjuvant and 24 in metastatic stage). ddPCR was performed to detect and quantify PIK3CA mutations. Patients testing positive for PIK3CA mutations underwent serial monitoring of their ctDNA.

PIK3CA mutations were identified in 8 (16%) of patients. On serial follow-up, five of the patients showed an increase in the amount of the mutation, which corresponded with poor response to treatment and fatal outcome. Conversely, three patients showed a decrease in the amount of the mutation, which was associated with a good response to treatment.

Liquid biopsy is an alternative for making a diagnosis for tumors in which it is difficult to conduct repeated invasive examinations. ctDNA is a non-invasive method to monitor tumor evolution, treatment response and assess patient prognosis. Serial ctDNA monitoring can help to predict relapse and to personalize therapy.

Keywords: breast cancer, liquid biopsy, ctDNA.

INTRODUCTION

The incidence of new cancer patients is increasing every year. Statistics show that by 2030, carcinomas will be the leading cause of death and the main barrier to increasing life expectancy in every country of the world in the 21st century. The reasons are diverse and include both population aging and population growth [1]. The main risk factors are associated with socio-economic development [2]. Breast cancer is the most commonly diagnosed cancer. Breast cancer is the fifth leading cause of cancer death in the world with 685,000 deaths. In countries with an average life expectancy of over 70 years, approximately 1 in 8 women will be diagnosed with breast cancer, 70% of cases occurring after the age of 60 [3].

The increased incidence rates in countries with a higher HDI (Human Development Index) index can be explained by some reproductive and hormonal risk factors (early age of menarche, later onset of menopause, advanced age at first birth, younger number of children, less breastfeeding, menopausal hormone replacement therapy, oral contraceptive use), lifestyle risk factors (alcohol intake, overweight, lack of physical activity) as well as better diagnosis thanks to of mammographic screening [4].

Estimates indicate that the incidence of breast cancer will reach approximately 3.2 million annually by 2050. These figures reflect the impact on society worldwide and emphasize the need for timely preventive measures. Breast cancer screening programs aim to reduce mortality through early detection and effective treatment [5].

Breast cancer is a heterogeneous disease in terms of its etiology and pathological characteristics, in some cases it progresses slowly and has an excellent prognosis, and in others it has an aggressive course

* To whom all correspondence should be sent:
E-mail: dr.graycheva@gmail.com

and an unfavorable outcome. In 63% of cases, the diagnosis is made in a localized stage, 28% in locally advanced, only in 5–6% in metastatic [6]. The overall five-year survival rate for breast cancer in the USA is 89.9%, for Europe – 86.6%, and in Bulgaria – 72.8%.

The different variants of this neoplasm are distinguished by variable histopathological and biological characteristics, varied response to the applied systemic therapies and different outcome of the disease.

The long-term prognosis for early-stage patients is good, but some tumors recur years after initial therapy is completed. Tumor heterogeneity and clonal evolution can be the reason for the development of distant metastases and resistance to the current treatment. These are also the leading causes of death.

Imaging studies and pathological analysis are leading in making the initial diagnosis, but they have their limitations in monitoring the effect of treatment, detection of residual disease and disease progression. Liquid biopsy is increasingly used as a non-invasive method for monitoring patients with oncological diseases. Detection of ctDNA in plasma can be used to non-invasively scan tumor genomes and determine tumor burden. Liquid biopsy allows detection of genomic alterations, therapeutic monitoring with early detection of resistance, and potential detection of disease progression prior to clinical and radiological confirmation.

MATERIALS AND METHODS

For the period 2020–2022 are tested patients with newly diagnosed carcinoma of the mammary gland treated at the Medical Oncology Clinic of UMHAT "Sv. Georgi", Plovdiv. 50 patients with breast cancer were monitored – 26 in the adjuvant stage and 24 in the metastatic stage. Patients were followed up before starting systemic treatment (baseline), at 1, 3 and 6 months by liquid biopsy for quantification of cfDNA. Genome sequencing was performed and somatic mutations were monitored by ddPCR.

Sequencing libraries were generated according to the instructions in the TruSight Tumor 15 Reference Guide. The assay requires a minimum of 10 ng of input DNA for each of 2 oligo pools (pool A and pool B), which are pooled and sequenced together after a library amplification step.

Libraries from plasma cfDNA were sequenced on a MiSeq® sequencing system with paired-end configuration (2×151 bp).

Illumina® TruSight® Tumor Protocol 15 describes a PCR-based multiplex method for preparing sequencing libraries from DNA extracted from formalin-fixed, paraffin-embedded (FFPE) tissue samples. The reagents in the TruSight Tumor 15 kit allow the preparation of up to 48 indexed libraries paired from 24 DNA samples. The kit is optimized to provide amplicon coverage of 15 genes for high-sensitivity analysis of low-frequency somatic variants from FFPE samples of solid tumors. These genes and gene regions include single nucleotide variants (SNVs), insertions, deletions (indels) and amplifications that are associated with cancer.

The assay contains two separate sets of labeled oligonucleotide primers. These pools are used in multiplex PCR to amplify regions of DNA extracted from FFPE samples for specific purposes. Using adapters provided in the kit, libraries are indexed, further amplified, and then mixed in one tube in preparation for a paired-end sequencing run. After sequencing is complete, the analysis report provides a specific set of single nucleotide variants (SNVs) and small insertions, deletions, and amplifications associated with solid tumors.

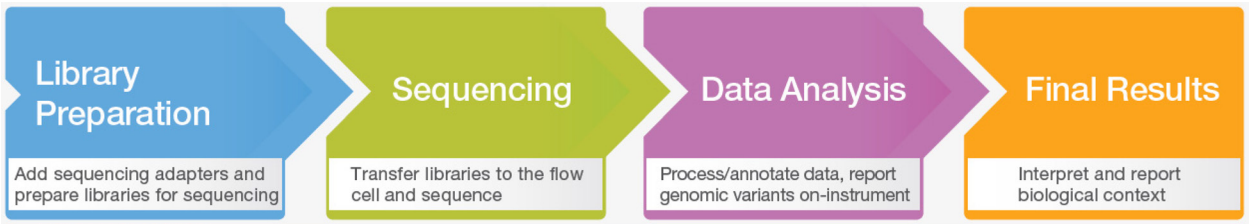

Fig. 1. MiSeq System Workflow – The MiSeq System's simplified workflow enables rapid NGS performance. Libraries can be prepared with any compatible library preparation kit. The sequencing time of five and a half hours included cluster generation, sequencing, and base counting with dual surface scan quality assessment for 2×25 base pairs running on a MiSeq system with MiSeq management software.

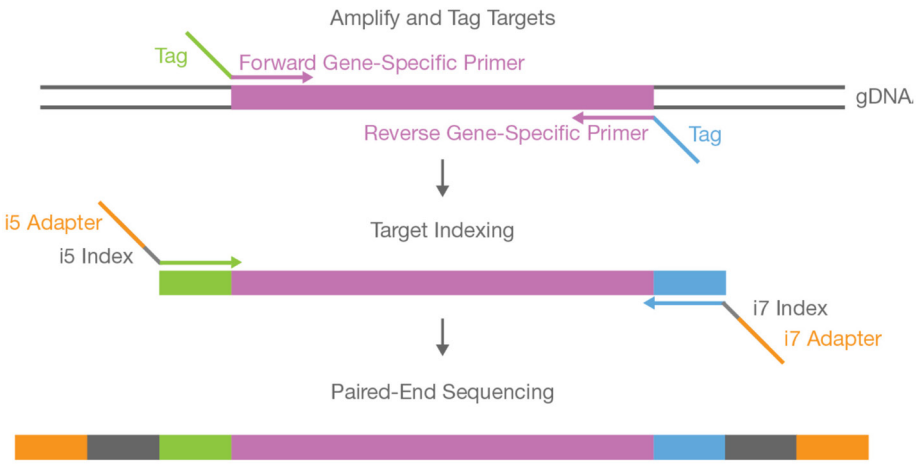

Fig. 2. How the analysis works.

DNA sequencing is the first and most basic information that can be obtained about a gene. This requires an automated and rapid system with a wide variety of applications, capable of de novo sequencing, resequencing (mutational profiling), microsatellite analyses, MLPA, AFLP, LOH, MLST, and SNP validation. (3500DX Series Genetic Analyzers (8-capillary sequencer/ GenomeLab™ GeXP Genetic Analysis System) with in vitro diagnostic capability)

Sequencing the genes responsible for the disease provides information in several directions:

1. Creating a personalized treatment plan for the disease based on the mutant gene and/or genes causing the disease, for example, sequencing the coding sequences of genes associated with breast cancer. The method is recommended when the patient has an unknown mutational status and does not belong to an ethnic group with characteristic mutations. Sequencing analysis revealed small deletions, insertions, missense, nonsense and splice site mutations.

2. The collected information from the group of patients with proven disease allows mapping of the most frequent mutations for the Bulgarian population, which allows the development of a faster and cheaper screening method based on DNA (free-cell DNA in tumors) and digital multiplex PCR, with specific primers. In this way, the patient will be diagnosed more quickly with the subsequent appointment of treatment, without the need to sequence the gene or genes. If a stretch of DNA containing a mutation has a known sequence, this can be used for clinical research. For this purpose, an oligonucleotide sample complementary to the region of interest with a mutation is synthesized. The sample will only bind complementary to DNA obtained from an individual with this mutation. The sample can be used as a PCR primer. If the DNA is amplified by PCR, the primer will not bind to normal DNA and there will be no amplification. Binding the primer to DNA from a patient and amplifying their DNA will indicate that the template DNA from that individual contains the mutation.

3. Isolation of cfDNA and monitoring of patients with proven somatic mutations by quantitative measurement of cfDNA by ddPCR.

MRD monitoring was performed by absolute quantitative (number of molecules per microliter) measurement of the established somatic mutation by means of digital real time PCR. Digital droplet PCR is a PCR technology that enables accurate absolute quantification of target molecules with a very high degree of sensitivity. In essence, the method combines the simplicity of traditional PCR and the functions of quantitative real time quantitative PCR (qRT-PCR). Unlike qRT-PCR, quantification is absolute and no calibration standards are used, making the process faster, more accurate and reproducible. The basic principle involves extreme dilution and separation of the sample into millions of individual units/droplets that ideally contain or do not contain the desired molecule. Each droplet contains all the reagents required for a PCR reaction and basically functions as a micro-PCR reactor. If the droplet contains the molecule of interest, PCR amplification gives a positive signal. If not - no signal. If the number of individual droplets is known, the initial amount of target molecules can be estimated from knowing the total number of positive and negative signals.

Because each droplet encapsulates a single molecule, researchers can quickly determine the absolute number of droplets containing a specific target DNA and compare the number to that of droplets with wild-type DNA. The Raindrop Digital Droplet PCR System shifts the current paradigm in digital droplet PCR (ddPCR) reaction from one marker-one color to two colors of different intensities per marker allowing multiplexing of targets up to 10 markers in one reaction.

Digital genomic technologies (Digital PCR (droplet)) offer higher sensitivity than massively parallel sequencing technologies and have been used as a method to validate results and quantify ctDNA. It is more cost-effective and faster methods in which a plasma ctDNA sample of patients can be used to non-invasively scan for tumor genes for breast cancer.

A droplet generator was used to divide the reaction mixture into about 20,000 nanoliter-sized droplets. Samples were subjected to polymerase chain reaction on a thermal cycler, droplets from each sample were analyzed on a dedicated QX200 droplet reader. The droplets pass sequentially through a two-color optical detection system. PCR-positive and PCR-negative droplets are counted, providing absolute quantification of the DNA of interest.

In our patients it was done ddPCR to detect and quantify PIK3CA mutations. Patients testing positive for PIK3CA mutations underwent serial monitoring of their ctDNA.

RESULTS

Patient characteristics

The clinico-pathological characteristics of the tumors of the 50 patients examined are presented in Figure 3: with luminal type A there are 29 patients (58%), with luminal type B there are 6 patients (12%), with HER2-positive BC there are 11 patients (22%) and with TNBC were 4 patients (8%).

Table 1. Clinical and laboratory characteristics of the patients

Parameters	Patients n (%)
Family history	20 (40%)
BMI ≥ 35, n (%)	24 (48%)
Hgb < 100 g/l, n (%)	17 (34%)
WBC ≥ 10.5 G/l, n (%)	11 (22%)
PLT ≥ 350 G/l, n (%)	14 (28%)
Ca 15-3 ≥ 25 U/l, n (%)	26 (52%)
CEA ≥ 3 ng/mL, n (%)	18 (36%)

Table 2. Gene list in TruSight Tumor 15 kit

TruSight Tumor 15 Gene List		
AKT1	GNA11	NRAS
BRAF	GNAQ	PDGFRA
EGFR	KIT	PIK3CA
ERBB2	KRAS	RET
FOXL2	MET	TP53

All patients underwent genomic sequencing after surgery and before starting chemotherapy (Table 2).

The frequency of the studied genes corresponds to that described in the literature. A total of 8 (16%) patients had a PIK3CA mutation in their primary tumor (Fig. 4).

PIK3CA mutations (H1047R, E545K, E542K, N345K, and H1047L) were analyzed with the QX200 Droplet Digital PCR System (Bio-Rad Laboratories) (Fig. 5). 5 patients had mutations in exon

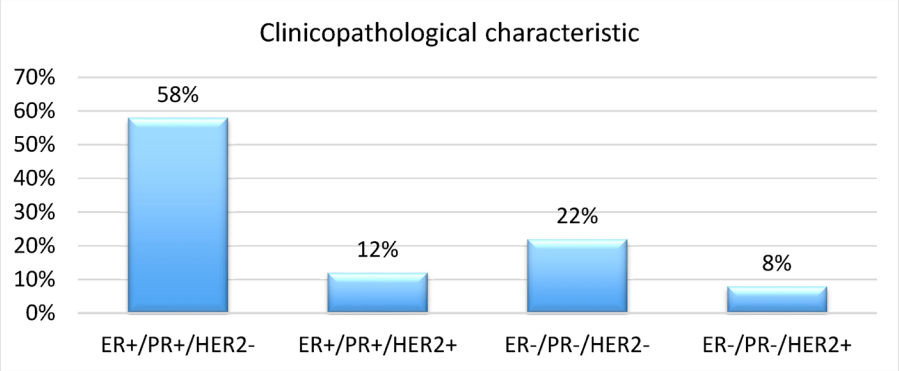

Fig. 3. Distribution of patients with breast cancer according to IHC.

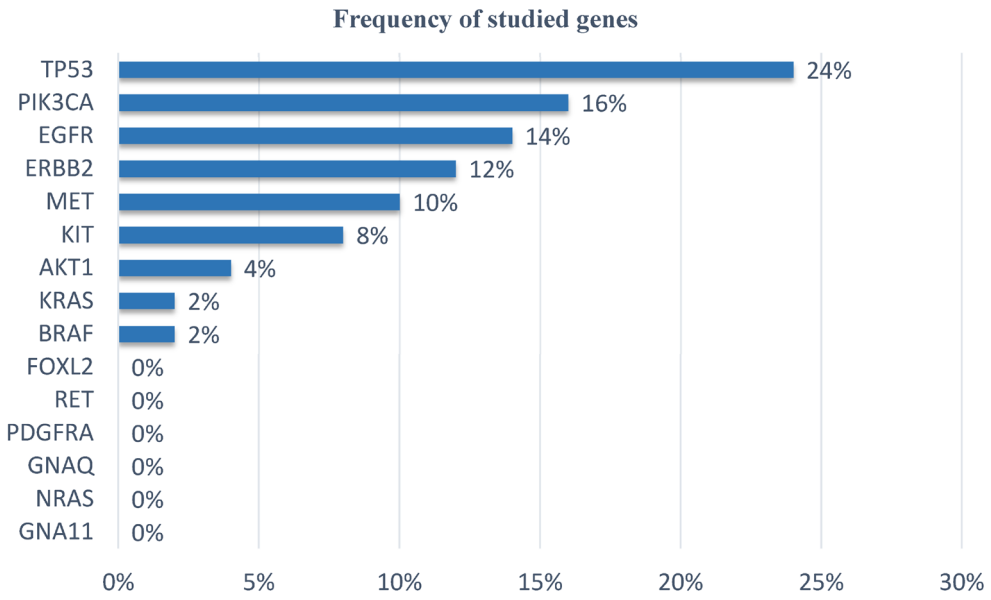

Fig. 4. Frequency of studied genes in breast cancer patients.

9 (E542K and E545K) and 2 had mutations in exon 20 (H1047L and H1047R). In 1 patient was found a mutation in N345K.

Of these 8 patients with PIK3CA mutations, 3 had luminal type A tumor, 2 had luminal type B, 2 had HER2-positive tumors, and 1 had TNBC. 5 of the patients received 6 courses of chemotherapy, and 3 of them received endocrine therapy. In serial follow-up, five of the patients showed an increase in the amount of the mutation, which corresponded with a poor response to the ongoing treatment and a fatal outcome. In contrast, 3 patients showed a decrease in the amount of the mutation, which was associated with a good response to treatment.

DISCUSSION

Clinicopathological characterization of breast cancer was determined by estrogen receptor (ER),

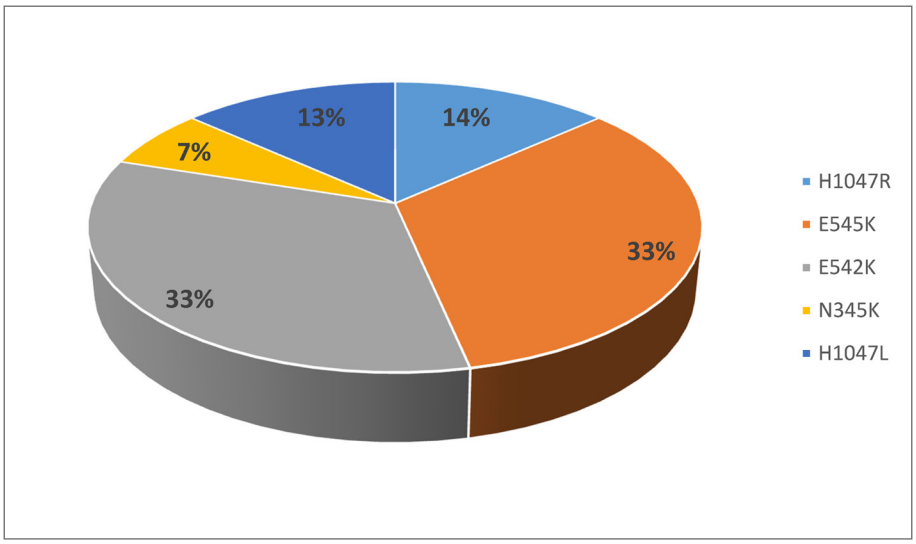

Fig. 5. Frequency of the most common mutations in PIK3CA examined by ddPCR.

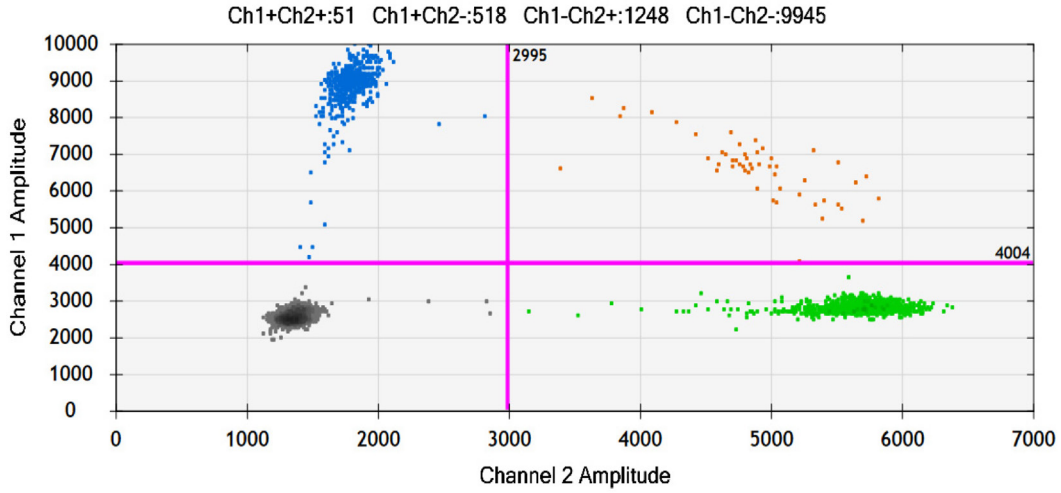

Fig. 6. Results from ddPCR- black droplets are empty droplets, green droplets are with wild type mutations, orange droplets are droplets having signals for both wild type and mutant type mutations, and blue droplets are for mutant alleles only.

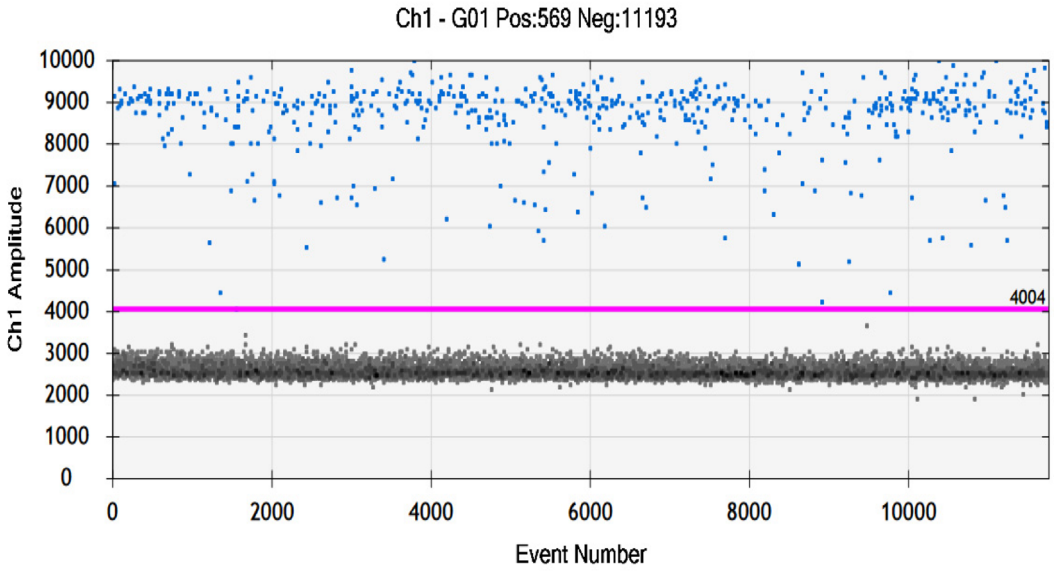

Fig. 7. Results from ddPCR-mutant alleles.

progesterone receptor (PgR), human epidermal growth factor receptor type 2 (HER2) and Ki67 status. Depending on this, we distinguish 4 immunohistochemical (IHC) tumor subtypes: luminal A, luminal B, HER2-positive type and triple negative (TN) type. Therapeutic behavior is determined depending on the specific subtype. However, genetic aberrations occurring in the tumor can significantly alter the effect of the treatment being administered [7].

PIK3CA (phosphatidylinositol-4,5-bisphosphate 3-kinase catalytic subunit alpha) the gene encoding phosphatidylinositol-3-kinase (PI3K) catalytic subunit p110-alpha is commonly mutated in breast cancer (21–35%) and is associated with progression of the tumor. This leads to hyperactivation of the PI3K/AKT/mTOR pathway, which plays a key role in several cellular processes related to oncogenesis—migration, metabolism, cell growth, and proliferation [8].

The most frequently encountered point mutations are E545K, E542K and H1047R/L, they are responsible for 70–80% of all PIK3CA mutations. The frequency is highest in luminal type and HER2-

positive breast cancer, lower in triple-negative breast cancer [9]. The presence of the PIK3CA mutation is also associated with resistance to targeted therapy with trastuzumab [10]. ER-positive patients who have PIK3CA mutations show better results from treatment with aromatase inhibitors. PIK3CA mutations are potential targets and predictive markers for the efficacy of novel molecularly targeted agents [11]. Alpelisib is a PI3Kα tyrosine kinase inhibitor that was tested in the SOLAR-1 study. Patients in this trial who had received prior endocrine therapy received either a combination of alpelisib/fulvestrant (a synthetic estrogen receptor antagonist) or placebo/fulvestrant. Mutational status was found to be a predictive response factor for progression-free survival (PFS). Final results for overall survival (OS) demonstrated a 7.9 month numerical improvement for this group of patients [12]. Based on data from this clinical trial, the FDA approved in May 2019 the combination of alpelisib with fulvestrant in postmenopausal women and men with HR+/HER2−, PIK3CA-mutated, advanced, or metastatic breast cancer after progression during or after treatment with endocrine-based regimen. In 2020, the European Medicines Agency (EMA) in turn granted a marketing authorization for alpelisib.

Therefore, the detection of PIK3CA mutations has a crucial role in identifying patients who will benefit from treatment with alpelisib. There is currently no consensus on the best analytical method (liquid biopsy or tissue) or the best type of biopsy (primary tumor or metastases).

The presence of this tumor heterogeneity makes its treatment challenging. Furthermore, there is a high frequency of discordance in PIK3CA mutations between primary, locally advanced, breast cancer tumors and metastatic stage carcinomas. Adequate samples for tissue analysis are not always available or accessible. Even when available, tissue obtained during primary surgical resection or biopsy may not reflect the current molecular characteristics of the tumor [13, 14, 15]. Liquid biopsy analyzes plasma-derived circulating tumor DNA (ctDNA) and offers less invasive real-time information on the genetic changes that have occurred [16].

CONCLUSIONS

Liquid biopsy is an alternative for the diagnosis of tumors in which it is difficult or impossible to perform re-invasive examinations, as well as for restaging and molecular analysis of metastases. According to the ESMO recommendations, cfDNA evaluation is considered a good alternative for metastatic tumor analysis and is an option to detect patients suitable for targeted therapy with alpelisib. The high sensitivity, efficiency and low cost of multiplex dPCR assays make them suitable for qualitative and quantitative clinical detection of PIK3CA mutations in plasma. Liquid biopsy could be a screening method for populations at increased risk of developing malignancy, thus reducing the side effects of therapies and healthcare costs.

Acknowledgments: *Project BG05M2OP001-1.002-0005 – Competence Center; „Personalized Innovative Medicine (PERIMED)“, financed by Operational Program „Science and Education for Smart Growth“, EU, ESIF.*

REFERENCES

1. World Health Organization. Global Health Observatory, 2020.
2. F. Bray, M. Colombet, L. Mery et al. Cancer Incidence in Five Continents, Vol. XI (electronic version). Lyon: International Agency for Research on Cancer. 2017, Available from: ci5.iarc.fr/Default.aspx.
3. L. Brinton, M. Gaudet, G. Gierach, in: Cancer Epidemiology and Prevention, 4th ed., Oxford University Press, Oxford, 2018, p. 861.
4. C. Duggan, A. Dvaladze, A. Rositch et al., *Cancer*, **126** (suppl. 10), 2339 (2020).
5. L. Tabar, P. Dean, T. Chen et al., *Cancer*, **125**, 515 (2019).
6. National Cancer Institute’s Surveillance, Epidemiology, and End Results Program. N/A.
7. F. Cardoso, E. Senkus, A. Costa et al., *Ann. Oncol*., **29**(8), 1634 (2018).
8. F. Mosele et al., *Ann. Oncol*., **31**, 377 (2020).
9. Y. Chae et al., *Mol. Cancer Ter*., **16**, 1412 (2017).
10. R. Kodahl et al., *Mol. Oncol*., **12**, 925 (2018).
11. F. Andre et al., *N. Engl. J. Med*., **380**, 1929 (2019).
12. 12. F. Andre et al., *Ann. Oncol*., **32**, 208 (2021).
13. 13. I. Dagogo-Jack, *Nat. Rev. Clin. Oncol*., **15**(2), 81 (2018).
14. 14. J. Jensen, A. Laenkholm, A. Knoop et al., *Clin. Cancer Res*., **17**(4), 667 (2011).
15. 15. M. Tellez-Gabriel, E. Knutsen, M. Perander, *Int. J. Mol. Sci*., **21**(24), 9457 (2020).
16. 16. G. Rossi, Z. Mu, A. Rademaker et al., *Clin. Cancer. Res*., **24**(3), 560 (2018).

Bulgarian Chemical Communications, Volume 55, Special Issue C (pp. 95–102) 2023 *DOI: 10.34049/bcc.55.C.0011*

Bioinformatics pipeline for variant detection in targeted sequencing panel

M. Topalov[1], V Stoyanova[1], H. Ivanov[1], G. Raycheva[2], V. Popov[1], A. Linev[1], N. Miteva-Marcheva[1], D. Dimitrov[1], Zh. Grudeva-Popova[2]

[1] *Department of Pediatrics and Medical Genetics, Medical University Plovdiv*
[2] *Department of Clinical Oncology, Medical University Plovdiv*

Received: November 2023; Revised: December 2023

Bioinformatics pipeline development is fundamental for extracting meaningful results from high-throughput sequencing data in robust manner. This study introduces a meticulously crafted bioinformatics pipeline customized for the analysis of Illumina TruSight Tumor 15 panel data, utilizing the QIAGEN CLC Genomics Workbench software. The panel serves as a comprehensive solution for detecting somatic mutations in genes associated with cancer, proving it applicable for cancer research.

Keywords: next-generation sequencing, bioinformatics, single nucleotide variants, oncology, molecular genetics.

INTRODUCTION

Targeted sequencing, alternatively referred to as "targeted resequencing" or "amplicon sequencing," is a precision-oriented method for DNA sequencing, allowing researchers to delve deep into specifically chosen regions of the genome. In the context of cancer research and diagnostics, targeted sequencing commonly involves the utilization of sequencing panels designed to cover sets of specific genes associated with cancer. By concentrating on these exact genomic areas, targeted sequencing facilitates a more efficient and cost-effective analysis on regions of particular interest for cancer detection and characterization.

The integration of bioinformatics tools into pipelines is crucial in deriving significant insights from high-throughput sequencing data efficiently. As the volume of sequencing data continues to surge, the automation of bioinformatics analysis emerges as an imperative solution. The development of a bioinformatics pipeline tailored for variant detection from targeted sequencing panel data plays a pivotal role in gaining in-depth insights into the genetic intricacies of cancer. This perspective proves invaluable for the customization of personalized treatment strategies, particularly within the realms of Oncology and Molecular Genetics, where precision is paramount. The insights derived from such an adept bioinformatics pipeline designed for variant detection in targeted sequencing panel data offer a valuable foundation for advancing the understanding and treatment of cancer.

MATERIALS AND METHODS

Illumina Trusight Tumor 15 is a panel for targeted NGS sequencing of fifteen genes for which mutations are known to be found in solid tumors. The panel accurately detects low frequency genetic variants from 20 ng of DNA and is optimized for Formalin-Fixed Paraffin-Embedded (FFPE) tissue samples. The list of genes covered by Illumina Trusight Tumor 15 is:

AKT1	AKT serine/threonine kinase 1
BRAF	B-Raf proto-oncogene, serine/threonine kinase
EGFR	epidermal growth factor receptor
ERBB2	erb-b2 receptor tyrosine kinase 2
FOXL2	forkhead box L2
GNA11	G protein subunit alpha 11
GNAQ	G protein subunit alpha q
KIT	KIT proto-oncogene, receptor tyrosine kinase
KRAS	KRAS proto-oncogene, GTPase
MET	MET proto-oncogene, receptor tyrosine kinase

* To whom all correspondence should be sent:
E-mail: momchil.topalov@phd.mu-plovdiv.bg

NRAS	NRAS proto-oncogene, GTPase
PDGFRA	platelet derived growth factor receptor alpha
PIK3CA	phosphatidylinositol-4,5-bisphosphate 3-kinase catalytic subunit alpha
RET	ret proto-oncogene
TP53	tumor protein p53

The panel consists of 1850 target regions, spreading over 370942bp to ensure optimal coverage over these fifteen genes.

Thirty-seven libraries from anonymized breast cancer patients were prepared with the Illumina Trusight Tumor 15 panel at the Department of Pediatrics and Medical Genetics, Medical University Plovdiv.

Illumina MiSeq is an advanced platform for next-generation DNA sequencing, applying sequencing-by-synthesis technology. Illumina MiSeq is suitable for sequencing data from targeted sequencing libraries with the pair-end protocol [1]. This technique carries information of the nucleotide sequence as well as the distance between the reads of the pair. This increases accuracy when assembling new genomes or detecting genetic mutations in known ones [1].

The sequencing of the libraries was conducted according to the protocol [2] on Illumina MiSeq sequencer at the Department of Pediatrics and Medical Genetics, Medical University Plovdiv [3–9].

Illumina BaseSpace is a cloud-based genomics platform offering NGS data management and analysis. The data generated by Illimina MiSeq is archived in BaseSpace. Using the BaseSpace Downloader client, the raw sequencing data is downloaded locally in FASTQ format.

QIAGEN CLC Genomics Workbench v23.0.4 is an easy-to-use graphical interface software for bioinformatic analysis of next-generation sequencing data. The tools in it can be run individually or linked together in workflows, enabling the development of complex bioinformatics pipelines.

Biomedical Genomics Analysis v.23.0.2 is a plugin for QIAGEN CLC Genomics Workbench designed mainly for biomedical and oncological sequencing data [10].

RESULTS AND DISCUSSION

The QIAGEN CLC Genomics Workbench and Biomedical Genomics Analysis were used to develop automated bioinformatics pipeline for the analysis of NGS sequencing data of fifteen breast cancer-associated genes by to extracting meaningful information from the targeted sequencing data. Key steps in the bioinformatics pipeline include:

QC for sequencing reads

Quality control (QC) for sequencing reads is a pivotal process in ensuring the integrity of high-throughput sequencing data. Analyzing various aspects of the data is crucial for reliable downstream analyses. The sequencing yield of the Illumina Trusight Tumor 15 libraries was with 94.9% of bases being ≥ Q30 quality per sample in a 2×150nt pair-end reads protocol.

Trimming the sequencing reads

The trimming step refines the sequence reads before mapping. The trimming consists of adapter trimming, quality trimming, and length trimming altogether (Table 1).

Read mapping

Mapping reads to a human reference genome is a fundamental step in most applications of high-throughput sequencing data. In the current bioinformatics pipeline, the reference genome is Hg38. The parameters are tuned towards adding an extra affine cost associated with opening a such that long contiguous gaps are favored over short gaps, reflecting the mutagenic potential of cancer cells.

Removing ligation artifacts

During the adapter ligation of the Illumina Trusight Tumor 15 library preparation, there can be the case that two different DNA sequences also get ligated together. Such ligation artifacts are prone to occur with higher probability between short DNA fragments, such as the ones generated from FFPE samples. This step of the pipeline removes reads from the read mapping which are likely the result of such an event (Table 2).

Calling for structural variants

A key step of the pipeline is calling structural variants such as deletions, insertions, tandem duplications and inversions by looking for unaligned read ends at each chromosome position. The estimated breakpoints which are instrumental for the downstream analysis as well. In the pool of thirty-

Table 1. Trimming report

Sample name	Reads after trim (%)	Avg. length after trim
LIN_S3_S8	99.9998717	131.3978193
NAK_S4_S9	99.99984623	130.9411136
CAA_S5_S10	99.99984689	130.3090855
NAD_S2_S7	99.9999303	128.9517914
VKI_S1_S6	99.99989479	123.1953821
EKD_S7_S8	99.99965306	129.3947973
LNN_S3_S4	99.99973685	134.1213624
NRG_S5_S6	99.99940513	122.8248149
RCG_S1_S2	99.9997592	134.2346325
RGG_S9_S10	99.99977549	137.2786
LIS_S7_S8	99.99973795	119.6411268
NGT_S3_S4	99.99983826	117.9993056
NPG_S1_S2	99.99984732	121.9701612
PRV_S5_S6	99.99958752	111.1261861
TTG_S9_S10	99.99975481	115.3774664
AAS_S5_S6	99.9998814	117.334696
DHG_S9_S10	99.99957716	95.45574896
EDK_S7_S8	99.99978278	115.2351194
IDD_S1_S2	99.99983687	119.6345178
PGA_S3_S4	99.99988502	117.129644
CDA_SVA_SVB_Sample1	99.9996475	136.5618026
CDA_VGA_VGN_Sample2	99.99969203	133.5521548
CDA_DVA_DVB_Sample3	99.9996645	137.5169503
CDA_AMA_AMB_Sample4	99.99947557	133.2611848
CDA_ZGA_ZGB_Sample5	99.99959254	133.6849961
CDA_MTA_MTB_Sample6	99.9995558	128.814802
CDA_DKA_DKB_Sample7	99.99959025	131.2575002
CDA_SBA_SBB_Sample8	99.99939711	129.5844282
FCD_SVA_SVB_Sample1	99.99981521	136.5594603
FCD_ZGA_ZGB_Sample2	99.99972504	133.8112269
FCD_DKA_DKB_Sample3	99.99976356	131.2795209
FCD_SBA_SBB_Sample4	99.99966349	129.6751804
MD_S2_S7	99.9995275	136.4810005
MS_S3_S8	99.99852922	107.8014028
SA_S4_S9	99.99926349	126.8381724
SG_S5_S10	99.99881518	126.1098424
SK_S1_S6	99.99954313	138.3859788
Minimum	99.99852922	95.45574896
Median	99.99972504	129.5844282
Maximum	99.9999303	138.3859788
Mean	99.99964081	126.6142966
Standard deviation	0.000284196	9.61145427

seven samples, only deletions and tandem duplications are called (Table 3).

Local Realignment

The goal of the local realignment tool is to improve the alignments of the reads in an existing read mapping. An opening for realignment may occur in areas around insertions and deletions in the reads relative to the reference. As a result, an alternative mapping, as good as or better than the original, can be generated.

QC for read mapping

Another QC metric step is included in the pipeline, measuring the performance of the read mapping after the improvements and modifications introduced by remove ligation artifacts and local realignment steps (Table 4).

Table 2. Remove ligation artifacts report

Sample name	Matches in input	Ligation artifacts found and removed	Artifacts trimmed	Artifacts trimmed from single or broken pair reads	Artifacts trimmed from paired read ends
LIN_S3_S8	6247055	22	197335	27988	169347
NAK_S4_S9	5873331	13	171633	27852	143781
CAA_S5_S10	6559845	35	204194	26183	178011
NAD_S2_S7	6476281	4	219959	27687	192272
VKI_S1_S6	6671510	11	221403	32774	188629
EKD_S7_S8	6095406	17	189669	40346	149323
LNN_S3_S4	6694825	44	131072	32817	98255
NRG_S5_S6	6427431	46	195126	44301	150825
RCG_S1_S2	6068593	21	163613	29899	133714
RGG_S9_S10	6278232	19	145073	30773	114300
LIS_S7_S8	6302898	13	137208	15846	121362
NGT_S3_S4	5875878	10	89043	23155	65888
NPG_S1_S2	5246639	5	145398	19301	126097
PRV_S5_S6	6414330	30	173912	21957	151955
TTG_S9_S10	6312553	17	136956	28507	108449
AAS_S5_S6	5508925	20	116398	25556	90842
DHG_S9_S10	6543034	46	167751	46203	121548
EDK_S7_S8	5321912	35	119833	29626	90207
IDD_S1_S2	5553372	33	125841	34886	90955
PGA_S3_S4	5691248	28	125760	33401	92359
CDA_SVA_SVB_Sample1	3979621	8	28224	4748	23476
CDA_VGA_VGN_Sample2	4067005	3	31179	5741	25438
CDA_DVA_DVB_Sample3	3734476	3	28321	5095	23226
CDA_AMA_AMB_Sample4	3821816	2	29450	5571	23879
CDA_ZGA_ZGB_Sample5	3812025	5	32506	6270	26236
CDA_MTA_MTB_Sample6	4847841	6	40336	8822	31514
CDA_DKA_DKB_Sample7	4646628	4	38920	7232	31688
CDA_SBA_SBB_Sample8	4154239	11	34148	6557	27591
FCD_SVA_SVB_Sample1	7867491	13	63113	11537	51576
FCD_ZGA_ZGB_Sample2	7475663	7	77211	14483	62728
FCD_DKA_DKB_Sample3	9330096	12	85711	16722	68989
FCD_SBA_SBB_Sample4	8342277	6	82185	15867	66318
MD_S2_S7	3920462	12	17166	2030	15136
MS_S3_S8	3908374	12	25353	3257	22096
SA_S4_S9	4144416	17	21205	2707	18498
SG_S5_S10	3166411	3	17614	2240	15374
SK_S1_S6	3508904	13	13807	2207	11600
Minimum	3166411	2	13807	2030	11600
Median	5873331	13	116398	19301	90207
Maximum	9330096	46	221403	46203	192272
Mean	5591650	16.3783784	103881.8	19463.3514	84418.4324
Standard deviation	1448724	12.6564682	68025.84	13187.7593	56832.79

Target region coverage

Measuring the read coverage over target regions is instrumental for evaluating the overall quality of the sample and determining if the variant calling results are reliable. In the pool of thirty-seven samples, above 98.7 of all targets were covered by 160 reads or more, securing high sensitivity for the variant calling of single nucleotide polymorphisms (SNPs) (Table 5).

Low Frequency Variant Detection

Variant calling is the primary step in deciphering the genetic code, involving the identification of variations such as single SNPs, small insertions, and deletions. A step for calling variants with low frequency is a necessary attribute in the pipeline for targeted sequencing analysis of samples of mixed tissue types such as cancer samples. In such samples, low frequent variants are likely to be present,

Table 3. Structural variant caller report

Sample name	Left breakpoints	Right breakpoints	Deletions	Tandem Duplications
LIN_S3_S8	45	47	1	1
NAK_S4_S9	47	47	2	1
CAA_S5_S10	53	49	1	1
NAD_S2_S7	49	35	1	1
VKI_S1_S6	50	58	1	2
EKD_S7_S8	34	57	2	0
LNN_S3_S4	43	54	2	0
NRG_S5_S6	55	70	2	0
RCG_S1_S2	46	48	1	1
RGG_S9_S10	31	45	2	0
LIS_S7_S8	48	53	2	0
NGT_S3_S4	73	97	1	1
NPG_S1_S2	50	69	0	0
PRV_S5_S6	60	62	1	0
TTG_S9_S10	39	59	0	1
AAS_S5_S6	32	52	1	0
DHG_S9_S10	55	67	1	0
EDK_S7_S8	48	49	0	0
IDD_S1_S2	37	40	2	0
PGA_S3_S4	59	54	1	1
CDA_SVA_SVB_Sample1	21	39	1	0
CDA_VGA_VGN_Sample2	17	42	1	0
CDA_DVA_DVB_Sample3	22	35	0	0
CDA_AMA_AMB_Sample4	26	43	1	0
CDA_ZGA_ZGB_Sample5	21	39	1	1
CDA_MTA_MTB_Sample6	25	38	1	0
CDA_DKA_DKB_Sample7	27	38	1	0
CDA_SBA_SBB_Sample8	20	45	1	1
FCD_SVA_SVB_Sample1	31	52	1	1
FCD_ZGA_ZGB_Sample2	28	53	2	0
FCD_DKA_DKB_Sample3	30	54	1	0
FCD_SBA_SBB_Sample4	28	66	1	0
MD_S2_S7	22	64	0	2
MS_S3_S8	24	47	1	0
SA_S4_S9	31	57	3	0
SG_S5_S10	24	51	0	0
SK_S1_S6	20	61	1	1
Minimum	17	35	0	0
Median	32	52	1	0
Maximum	73	97	3	2
Mean	37.0540541	52.324324	1.108108	0.43243243
Standard deviation	14.1596962	12.213504	0.698561	0.60279629

as well as for samples for which the ploidy is unknown or not well defined. The step allows for calling variants with minimum frequency starting from 0.4%, calculated as 'count of reads supporting the variant'/'the overall coverage in that region'.

This low minimum frequency of 0.4% is less than the industry standard of 0.5% as it aims to detect significantly low frequency variants that have cancer origin but are not represented definitively in the sample.

Variant filtering cascade

The increased the risk of introducing false positive variants, requires for the pipeline to provide a stricter variant filtering cascade of steps that filters out marginal variants, variants in regions of insufficient read depth, sequencing errors, alignment artifacts and random noise in the data. The filtering cascade applies criteria that balances between sensitivity and specificity, keeping only the true variants.

Table 4. QC for read mapping report

Sample name	Reads (#)	Mapped reads (#)	Mapped reads (%)	Not mapped reads (#)	Not mapped reads (%)
LIN_S3_S8	12470686	12281843	98.4857	188843	1.514295
NAK_S4_S9	11706112	11500925	98.24718	205187	1.752819
CAA_S5_S10	13062798	12790260	97.91363	272538	2.086368
NAD_S2_S7	12911622	12692645	98.30403	218977	1.695968
VKI_S1_S6	13307256	13041130	98.00014	266126	1.999856
EKD_S7_S8	12105606	11926284	98.51869	179322	1.481314
LNN_S3_S4	13300456	13119071	98.63625	181385	1.36375
NRG_S5_S6	12775740	12514999	97.95909	260741	2.040907
RCG_S1_S2	12043094	11849744	98.39452	193350	1.605484
RGG_S9_S10	12471656	12294052	98.57594	177604	1.424061
LIS_S7_S8	12592868	12381540	98.32184	211328	1.678156
NGT_S3_S4	11747372	11562761	98.42849	184611	1.571509
NPG_S1_S2	10479330	10299609	98.285	179721	1.715005
PRV_S5_S6	12849046	12566297	97.79946	282749	2.200545
TTG_S9_S10	12642988	12379329	97.91458	263659	2.085417
AAS_S5_S6	10961534	10725781	97.84927	235753	2.15073
DHG_S9_S10	13007040	12590283	96.79591	416757	3.204088
EDK_S7_S8	10588342	10348217	97.73218	240125	2.267824
IDD_S1_S2	11034058	10817898	98.04097	216160	1.959025
PGA_S3_S4	11306646	11055941	97.78268	250705	2.217324
CDA_SVA_SVB_Sample1	7943146	7916378	99.66301	26768	0.336995
CDA_VGA_VGN_Sample2	8117528	8081209	99.55259	36319	0.447415
CDA_DVA_DVB_Sample3	7451546	7420524	99.58368	31022	0.416316
CDA_AMA_AMB_Sample4	7627260	7594159	99.56602	33101	0.433983
CDA_ZGA_ZGB_Sample5	7608106	7571658	99.52093	36448	0.479068
CDA_MTA_MTB_Sample6	9680330	9636050	99.54258	44280	0.457422
CDA_DKA_DKB_Sample7	9273790	9224873	99.47252	48917	0.527476
CDA_SBA_SBB_Sample8	8293230	8247843	99.45272	45387	0.547278
FCD_SVA_SVB_Sample1	15693192	15630866	99.60285	62326	0.397153
FCD_ZGA_ZGB_Sample2	14911090	14824909	99.42203	86181	0.577966
FCD_DKA_DKB_Sample3	18609030	18499235	99.40999	109795	0.590009
FCD_SBA_SBB_Sample4	16641354	16533409	99.35134	107945	0.648655
MD_S2_S7	7830650	7812792	99.77195	17858	0.228053
MS_S3_S8	7818742	7789944	99.63168	28798	0.36832
SA_S4_S9	8282230	8256896	99.69412	25334	0.305884
SG_S5_S10	6329902	6311764	99.71346	18138	0.286545
SK_S1_S6	7004062	6985695	99.73777	18367	0.262234
Minimum	6329902	6311764	96.79591	17858	0.228053
Median	11706112	11500925	98.57594	179322	1.424061
Maximum	18609030	18499235	99.77195	416757	3.204088
Mean	11148093	11002076	98.77499	146016.9	1.225006
Standard deviation	2883528.5	2828923	0.807734	104113.8	0.807734

Functional Annotation

The filtered variants are annotated with ClinVar and dbSNP[11]. The variants are categorized based on their location within coding regions, splice sites, or regulatory elements. Predictive algorithms were employed to assess the deleteriousness of the variants, prioritizing those with potential clinical relevance which are further scrutinized for their potential implications in cancer development.

Since the target regions are covering both strands of DNA, the result of annotated variants is split into two groups.

The first group contains only variants overlapping with the genes from Illumina Trusight Tumor 15 list. These variants are the primary focus on the pipeline. In all thirty-seven samples, an average of 43 mutations associated with cancer were detected, 97.98% of which were single nucleotide polymorphisms (SNV) and 2.02% were deletions [12–16].

Table 5. Target region coverage report

Sample name	Max coverage	Avg. coverage	Target regions with low coverage (%)	Length of target region positions with low coverage (%)
LIN_S3_S8	86027	333.717	98.7027027	98.87260003
NAK_S4_S9	74626	291.8734	98.7027027	98.87206086
CAA_S5_S10	85181	337.4652	98.7027027	98.87233045
NAD_S2_S7	163235	409.5384	98.7027027	98.87233045
VKI_S1_S6	105854	385.5133	98.7027027	98.87206086
EKD_S7_S8	80433	331.3737	98.7027027	98.87260003
LNN_S3_S4	92358	357.5401	98.7027027	98.87260003
NRG_S5_S6	81814	310.9182	98.7027027	98.87260003
RCG_S1_S2	90000	324.8757	98.7027027	98.87260003
RGG_S9_S10	155637	318.3564	98.7027027	98.87206086
LIS_S7_S8	83242	294.9421	98.7027027	98.87260003
NGT_S3_S4	107295	338.3943	98.7027027	98.87233045
NPG_S1_S2	89869	291.8255	98.7027027	98.87233045
PRV_S5_S6	101883	271.4018	98.7027027	98.87260003
TTG_S9_S10	71662	273.177	98.7027027	98.87260003
AAS_S5_S6	70122	257.7923	98.7027027	98.87260003
DHG_S9_S10	144870	220.1225	98.7027027	98.87260003
EDK_S7_S8	66832	246.0914	98.7027027	98.87260003
IDD_S1_S2	69096	258.6306	98.7027027	98.87260003
PGA_S3_S4	75957	246.8681	98.7027027	98.87260003
CDA_SVA_SVB_Sample1	62177	219.9835	98.7027027	98.87260003
CDA_VGA_VGN_Sample2	51875	216.3667	98.7027027	98.87260003
CDA_DVA_DVB_Sample3	52585	212.0567	98.7027027	98.87260003
CDA_AMA_AMB_Sample4	52292	216.2776	98.7027027	98.87260003
CDA_ZGA_ZGB_Sample5	52648	216.4168	98.7027027	98.87260003
CDA_MTA_MTB_Sample6	72336	238.4238	98.7027027	98.87260003
CDA_DKA_DKB_Sample7	71213	249.8491	98.7027027	98.87260003
CDA_SBA_SBB_Sample8	67409	226.2924	98.7027027	98.87260003
FCD_SVA_SVB_Sample1	123303	435.3392	98.7027027	98.87260003
FCD_ZGA_ZGB_Sample2	104546	427.1888	98.7027027	98.87260003
FCD_DKA_DKB_Sample3	139052	501.2281	98.7027027	98.87233045
FCD_SBA_SBB_Sample4	135785	452.3595	98.7027027	98.87260003
MD_S2_S7	57901	219.9873	98.7027027	98.87260003
MS_S3_S8	73860	174.4307	98.75675676	98.88742714
SA_S4_S9	52779	208.149	98.7027027	98.87260003
SG_S5_S10	40647	161.1073	98.7027027	98.87260003
SK_S1_S6	54232	209.2885	98.7027027	98.87260003
Minimum	40647	161.1073	98.7027027	98.87206086
Median	75957	271.4018	98.7027027	98.87260003
Maximum	163235	501.2281	98.75675676	98.88742714
Mean	85422.51	288.7882	98.70416362	98.87292062
Standard deviation	31100.4	82.41751	0.008886432	0.002456715

The second group contains variants that passed all filtering criteria and belong to the opposite strand of DNA for the respective gene. Such variants may overlap with another genes, pseudogenes, or long non-coding RNA. This is an extra piece of information available from the targeted sequencing panel that is usually is overlooked by the standard pipelines. The current pipeline records such variants as they have the potential of additional insights and may have application in populational genetics [17] if the pipeline is run for a larger cohort of patients.

Analysis of the thirty-seven samples using this pipeline reveals a comprehensive landscape of somatic SNVs and indel mutations within cancer-related genes [18]. The pipeline effectively identifies putative mutations, thus providing valuable insights into their significance within cancer research, contributing to the development of personalized treatment strategies [19].

The pipeline finishes with an export step that is preparing the lists with variants in format suitable for further interpretation by medical genetics and oncology experts.

CONCLUSION

In conclusion, this bioinformatics pipeline demonstrates its effectiveness in systematically analyzing Illumina TruSight Tumor 15 panel data across thirty-seven samples. It presents an in-depth overview of the performance of the sample during the library preparation and sequencing by generating detailed reports with high precision metrics. It serves as a promising resource for advancing cancer research and clinical care. The pipeline provides a descriptive grouping of the variants. Further validation and seamless integration with clinical data and functional annotation with more external resources are imperative next steps in realizing the full potential of this pipeline in oncology research. The application of this bioinformatics pipeline for variant detection in targeted sequencing panel expands our knowledge of these specific genes but also paves the way for further research into personalized medicine and targeted therapies.

Acknowledgments: *Project BG05M2OP001-1.002 -0005 – Competence Center "Personalized Innovative medicine (PERIMED)", financed by Operational Program "Science and Education for Smart Growth", EU, ESIF.*

REFERENCES

1. J. J. Kozich, S. L. Westcott, N. T. Baxter, S. K. Highlander, P. D. Schloss, *Appl. Environ. Microbiol.*, **79**, 5112 (2013).
2. Illumina, MiSeq System Guide (15027617), www.illumina.com (2021).
3. Liu, L. et al., *J. Biomed. Biotechnol.*, **2012**, 251364 (2012).
4. J. Podnar, H. Deiderick, G. Huerta, S. Hunicke-Smith, *Curr. Protoc. Mol. Biol.*, **106**, 4.21.1 (2014).
5. R. H. Deurenberg et al., *J. Biotechnol.*, **243**, 16 (2017).
6. J. Plitnick et al., *J. Clin. Microbiol.*, **59**(12), e0064921 (2021).
7. D. A. Read, G. Pietersen, *Methods Mol. Biol*., **2015**, 179 (2019).
8. T. Unno, *J. Microbiol. Biotechnol.*, **25**(6), 765 (2015).
9. V. Valentini et al., *Front. Oncol.*, **12**, 1092201 (2022).
10. R. K. Ravi, K. Walton, M. Khosroheidari, *Methods Mol. Biol.*, **1706**, 223 (2018).
11. S. T. Sherry et al., *Nucleic Acids Res*., **29**, 308 (2001).
12. A. Z. Dayem Ullah, N.R. Lemoine, C. Chelala, *Brief Bioinform*., **14**, 437 (2013).
13. J. Oscanoa et al., *Nucleic Acids Res.*, **48**, W185 (2020).
14. A. Z. Dayem Ullah et al., *Nucleic Acids Res.*, **46**, W109 (2018).
15. A. Z. Dayem Ullah, N. R. Lemoine, C. Chelala, *Nucleic Acids Res.*, **40**, W65 (2012).
16. C. Chelala, A. Khan, N. R. Lemoine, *Bioinformatics*, **25**, 655 (2009).
17. G. Ribas et al., *Hum. Genet.*, **118**, 669 (2006).
18. I. Adzhubei, D. M. Jordan, S. R. Sunyaev, *Curr. Protoc. Hum. Genet*., **7**, 7.20.1 (2013).
19. P. C. Ng, S. Henikoff, *Nucleic Acids Res.*, **31**, 3812 (2003).

Bulgarian Chemical Communications, Volume 55, Special Issue C (pp. 103–108) 2023 *DOI: 10.34049/bcc.55.C.0012*

Synthesis and single crystal structure of N-Dansyl-o-n-pentoxy aniline

R. Russew[1*], J. Karadjov[2], B. Shivachev[1]

[1] *Institute of Mineralogy and Crystallography, Bulgarian Academy of Sciences, acad. G. Bonchev bl. 107, 1113 Sofia, Bulgaria*
[2] *Space Research and Technology Institute, Bulgarian Academy of Sciences, acad. G. Bonchev bl. 1, 1113 Sofia, Bulgaria*

Received: November 2023; Revised: December 2023

Here we present a three step synthesis of 5-(dimethylamino)-N-(2-(pentyloxy)phenyl)naphthalene-1-sulfonamide. The first step, is producing of o-n-pentoxynitrobenzene using a classical alkylation of o-nitrophenols. The second step provides o-n-pentoxyaniline using a catalytic transfer hydrogenation. In the last step the title compound is obtained by reacting dansyl(5-(dimethylamino)naphthalene-1-sulfonyl) chloride and o-n-pentoxyaniline in a two phase system. Single crystals of N-dansyl-o-n-pentoxy aniline were obtained from isopropyl/water solution (1:1 *v/v*). The crystal structure was solved in the monoclinic $P2_1/c$ space group with unit cell parameters a = 11.926(2), b = 17.328(5), c = 10.9760(14), β = 99.4457(18)°, and Z = 4. The molecular structure is stabilized by an intramolecular C–H…O interaction, while the crystal structure is stabilized by N–H…O hydrogen bonds.

Keywords: Dansyl chloride, (pentyloxy)aniline, single crystal, DTA-TGA

INTRODUCTION

Dansyl chloride, chemically known as 5-(dimethylamino)naphthalene-1-sulfonyl chloride, is a versatile and widely used fluorescent probe in chemistry and biochemistry[1–3]. Its popularity stems from its high fluorescence intensity and the ability to react with primary and secondary amines, forming stable dansyl derivatives[4, 5]. These derivatives are fluorescent and can be easily detected and quantified by fluorescence spectroscopy, making dansyl chloride an essential tool in qualitative and quantitative analysis of amines in complex mixtures[6, 7]. The high fluorescence efficiency of dansyl derivatives allows for the detection of very low concentrations of target molecules[8, 9]. A high sensitivity and specificity can be obtained if dansyl chloride derivatives are obtained and specifically labeled for a range of biomolecules [8]. The compound (pentyloxy)aniline, is a notable organic molecule that integrates both an aniline (phenylamine) and a pentyloxy group[10, 11]. This combination of aromatic and aliphatic moieties provides to (pentyloxy)aniline quite distinct chemical properties and potential applications, particularly in the fields of organic chemistry and materials science[12]. The specific electronic properties of aniline combined with the flexibility and solubility conveyed by the pentyloxy group could be advantageous in designing materials for pharmaceutical applications. Combining the insights from Dansyl chloride and (pentyloxy)aniline into a comprehensive compound e.g. 5-(dimethylamino)-N-(2-(pentyloxy) phenyl)naphthalene-1-sulfonamide establishes an intriguing synergy of properties and discloses a large field for potential applications stemming from properties of both parent compounds. Having in mind the bioactive nature of aniline derivatives in pharmaceutical contexts, the title compound could serve as a novel probe or therapeutic scaffold. The (pentyloxy)aniline portion might increase the solubility and thus biological distribution, membrane permeability, etc. The Dansyl group hints at applications as a fluorescent marker in biological systems or in the field of organic electronics e.g. as organic semiconductors, photodetectors, or light-emitting diodes (LEDs).

Herein we report the synthesis of 5-(dimethylamino)-N-(2-(pentyloxy)phenyl)naphthalene-1-sulfonamide using well established protocols (Scheme 1) and its crystal structure.

* To whom all correspondence should be sent:
E-mail: r.rusev93@gmail.com

MATERIALS AND METHODS

Synthesis of N-dansyl-o-n-pentoxy aniline

All reagents were purchased from Alfa Aesar or Sigma Aldrich and were used without further purification. The title compound N-dansyl-o-n-pentoxy aniline was prepared by a three step synthetic protocol (Scheme 1). First, o-n-pentoxynitrobenzene (**2**, Scheme 1) was obtained according to a standard procedure [13] by refluxing o-nitrophenol (0.1 mol), n-bromopentane (0.11 mol) and anhydrous K_2CO_3 (0.1 mol) as a base in dry acetone for 48 h. The isolation and purification procedures involved distillation of the acetone, extraction of the residue with water/benzene mixture, washing with 10% NaOH, distillation of the benzene at ambient pressure and finally vacuum distillation of the residual oil. The o-n-pentoxynitrobenzene (b.p. 160-165 at 5 mm Hg) was obtained in 85% yield. In the second step, o-n-pentoxynitrobenzene was then reduced by catalytic transfer hydrogenation [14] with hydrazine hydrate ($NH_2NH_2 \times H_2O$) and nickel boride (Ni_2B) as a catalyst to obtain o-n-pentoxyaniline (**3**, b.p. 148–156 °C at 5 mm Hg, yield 95%). Finally, o-n-pentoxyaniline (**3**) was reacted with dansyl (5-(dimethylamino)naphthalene-1-sulfonyl) chloride in a two phase system, dichloromethane and 10% sodium hydroxide water solution. After washing the reaction mixture with 3% hydrochloric acid and water, the product, N-dansyl-o-n-pentoxy aniline, was crystallized from isopropyl alcohol/water to obtain green crystals, m.p. 68–70, yield 90%.

Single crystal X-ray diffraction

Suitable single crystals of the title compound were mounted on glass capillaries. The intensity and diffraction data were collected on Agilent SupernovaDual diffractometer equipped with an Atlas CCD detector using micro-focus Cu*K*α radiation (λ = 1.54184 Å, respectively). The structures were solved by direct methods and refined by the full-matrix least-squares method on F^2 with ShelxS and ShelxL programs[15,16]. All non-hydrogen atoms, were located successfully from Fourier map and were refined anisotropically. Hydrogen atoms were placed at calculated positions using a riding scheme (*Ueq* = 1.2 for $C\text{-}H_{aromatic}$ = 0.93 Å and $C\text{-}H_{methylene}$ = 0.97 Å) while the N hydrogen was located from Fourier map. The ORTEP [17] views of the molecule present in the asymmetric unit and the most important crystallographic parameters from the data collection and refinement are shown in Fig. 1 and Table 1 respectively. Selected bonds lengths, angles and torsion angles are given in Table 2. The figures concerning crystal structure description and comparison were prepared using Mercury software (version 4.0) [18]. Complete crystallographic data for the reported structure were deposited in the CIF format with the Cambridge Crystallographic Data Centre as 2344357. These data can be obtained free of charge via http://www.ccdc.cam.ac.uk/conts/retrieving.html, or from the CCDC, 12 Union Road, Cambridge CB2 1EZ, UK; Fax: +441223336033; E-mail: depos-it@ccdc.cam.ac.uk.

RESULTS AND DISCUSSION

The original intention for creating a novel organic compound by leveraging the structural and functional traits of Dansyl chloride and (pentyloxy) aniline was successfully achieved by integrating a three-step synthetic protocol, described above. Emulating the methodology for integrating organic molecules with specific functionalities the goal was

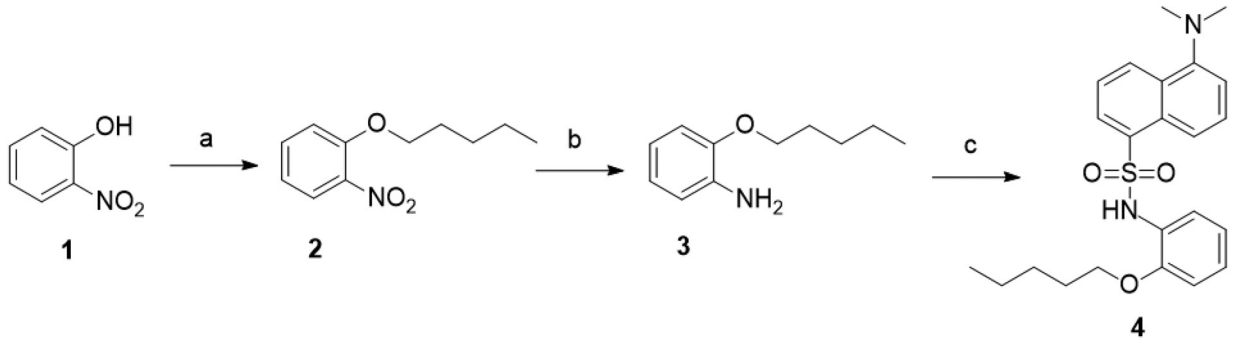

Scheme 1. General synthetic procedure for the preparation of N-dansyl-o-n-pentoxy aniline – (a) bromopentane, anxydrous K_2CO_3, dry acetone, reflux, 48h, (b) NH_2NH_2 x H_2O, cat. Ni_2B and (c) dansyl chloride, 10% aq. NaOH/DCM.

Table 1. Most important crystallographic parameters for structures **4**

Compound	4
Empirical formula	$C_{23}H_{28}N_2O_3S$
Formula weight	412.53
Temperature/K	290
Crystal system	Monoclinic
Space group	$P2_1/c$
a/Å	11.926(2)
b/Å	17.328(5)
c/Å	10.9760(14)
α/°	90.0
β/°	99.457(18)
γ/°	90.0
Volume/Å^3	2237.4(7)
Z	4
ρ_{calc} (g/cm^3)	1.225
μ/mm^{-1}	1.486
F(000)	880.0
Crystal size/mm^3	0.32 × 0.25 × 0.2
Radiation, λ [Å]	Cu Kα (λ = 1.54184)
2Θ range for data collection/°	7.516 to 154.966
Index ranges	$-14 \le h \le 14$, $-21 \le k \le 17$, $-8 \le l \le 13$
Reflections collected/ independent	8322/4322
R_{int}/ R_{sigma}	R_{int} = 0.0359, R_{sigma} = 0.0334
Data/restraints/parameters	4322/1/270
Goodness-of-fit on F^2	1.136
Final R indexes [I>=2σ (I)]	$R1$ = 0.0884, $wR2$ = 0.2694
Final R indexes [all data]	$R1$ = 0.1141, $wR2$ = 0.3088
Largest diff. peak/hole / e Å^{-3}	0.82/-0.34
CCDC number	2344357

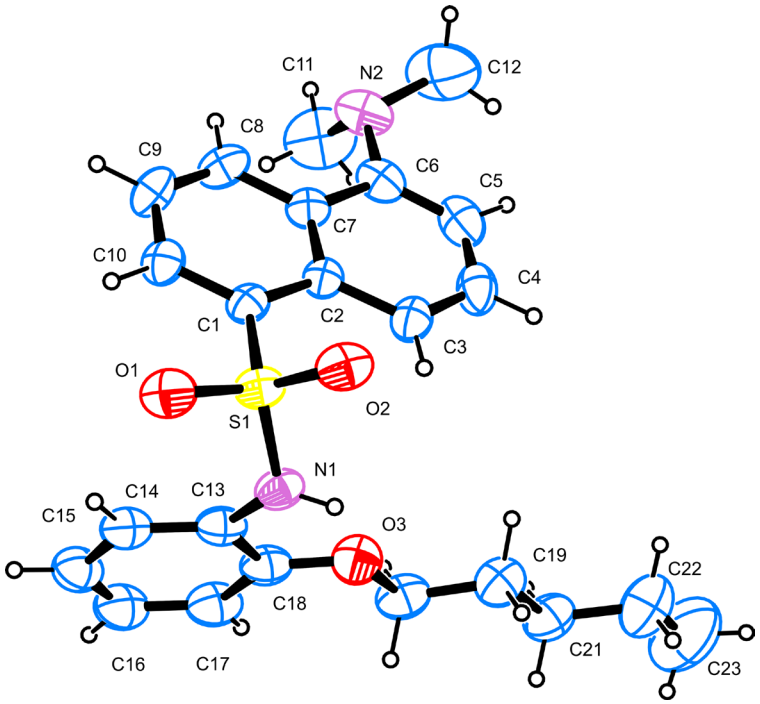

Fig. 1. *ORTEP* view of molecule present in the asymmetric unit of **4** along with employed numbering scheme; displacement ellipsoids are at 50% probability and hydrogen atoms are shown as spheres with arbitrary radii.

Table 2. Selected bond lengths s and angles for **4**

Bond lengths						Bond angles							
Atom	Atom	distance	Atom	Atom	distance	Atom	Atom	Atom	Angle	Atom	Atom	Atom	Angle
S1	O2	1.422(3)	C9	C10	1.413(6)	O2	S1	O1	118.8(2)	C6	N2	C12	113.8(6)
S1	O1	1.426(3)	C9	C8	1.337(6)	O2	S1	N1	105.87(19)	C11	N2	C6	116.1(5)
S1	N1	1.628(3)	N2	C6	1.418(6)	O2	S1	C1	109.35(19)	C11	N2	C12	103.0(7)
S1	C1	1.774(4)	N2	C11	1.405(9)	O1	S1	N1	108.0(2)	C6	C5	C4	121.1(4)
O3	C18	1.347(6)	N2	C12	1.474(9)	O1	S1	C1	107.08(19)	N2	C6	C7	118.2(4)
O3	C19	1.441(5)	C5	C6	1.368(8)	N1	S1	C1	107.26(17)	C5	C6	C7	118.5(4)
N1	C13	1.421(5)	C5	C4	1.376(7)	C18	O3	C19	118.6(4)	C5	C6	N2	123.3(4)
C3	C2	1.423(6)	C17	C16	1.400(8)	C13	N1	S1	123.8(3)	C3	C4	C5	122.5(4)
C3	C4	1.356(6)	C14	C13	1.372(7)	C4	C3	C2	120.0(5)	C1	C10	C9	119.3(4)
C18	C17	1.394(7)	C14	C15	1.391(7)	O3	C18	C17	125.6(5)	C18	C17	C16	119.2(5)
C18	C13	1.406(6)	C20	C19	1.489(8)	O3	C18	C13	115.9(4)	C13	C14	C15	119.8(5)
C2	C7	1.417(5)	C20	C21	1.549(7)	C17	C18	C13	118.6(5)	C19	C20	C21	110.2(4)
C2	C1	1.429(5)	C21	C22	1.503(10)	C3	C2	C1	123.6(4)	C18	C13	N1	116.3(4)
C7	C6	1.459(5)	C16	C15	1.334(8)	C7	C2	C3	118.5(3)	C14	C13	N1	123.0(4)
C7	C8	1.402(6)	C22	C23	1.542(14)	C7	C2	C1	117.9(3)	C14	C13	C18	120.5(4)
C1	C10	1.364(6)				C2	C7	C6	119.4(4)	O3	C19	C20	107.8(4)

Table 3. Hydrogen Bonding and weak interaction for **4**

D	H	A	d(D-H)/Å	d(H-A)/Å	d(D-A)/Å	D-H-A/°
C14	H14	O1	0.93	2.45	3.072(6)	124.5
N1	H1	O2[1]	0.824(18)	2.42(2)	3.190(5)	157(3)
N1	H1	O3	0.824(18)	2.22(3)	2.625(5)	110(3)

symmetry operation: [1] *2-x,1-y,1-z*

to create an organic molecule with distinct photophysical properties and potential applications in areas such as bioimaging, material science, pharmaceuticals and possibly optoelectronics.

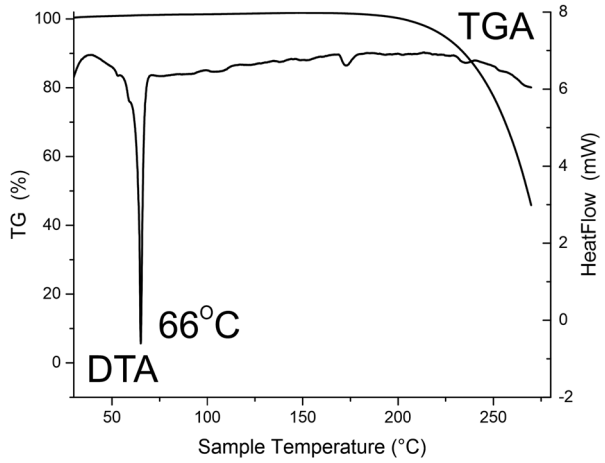

Fig. 2. DTA-TGA thermogram of compound **4**.

The thermal stability of the reported compound was studied with differential thermal analysis (DTA) and thermo-gravimetric analysis (TGA). The DTA thermogram (Fig. 2) reveals a sharp *endothermic* effect spanning from ~48 °C to 72 °C. This effect is attributed to the melting of the compound e.g. the destruction off the crystal structure. Having in mind the presence of a pentoxy moiety in the molecule, the relatively low melting temperature for such a compound is expected. There are two very shallow effect at ~160 and 230 °C probably related the decomposition of the compound. The TGA curve shows that compound **4** conserved its molecular structure up to ~160 °C. With the increase of the temperature above 160 °C significant weight losses are registered thus e.g. thermal decomposition of compound **4** is observed.

The crystal structure of compound **4** discloses that the bond lengths and angles are comparable to similar compounds bearing a chain on the aniline moiety [19–22] or possessing a Dansyl moiety [23–26] (Table 2). The molecular geometry is stabi-

lized by a weak C–H…O intramolecular interaction (Table 3). It is quite probable that one of the shallows endothermic effects visible on the DTA thermogram is related to the disruption of the intramolecular interaction, followed by the decomposition of compound **4**. Adjacent molecules of **4** interact through two N–H…O hydrogen bonding interactions that produce a dimmer with an $R^2_2(8)$ graph set motif [27] (Fig. 3).

The crystal packing of the molecules of **4** does not reveal additional hydrogen bonding or weak interactions. The flexible pentyl chains are locked in between two Dansyl moieties (Fig. 4) thus the steric hindrance is minimized.

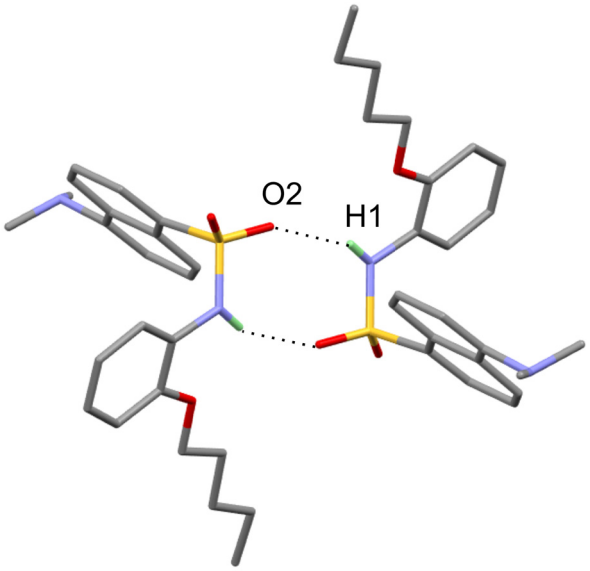

Fig. 3. Hydrogen bonding interactions (for details see Table 3) stabilizing the three-dimensional arrangement in compound **4**.

CONCLUSIONS

The title compound N-Dansyl-o-n-pentoxy aniline was obtained in good yield by a classical three-step reactions starting using o-nitrophenol, n-bromopentane and dansyl (5-(dimethylamino)naphthalene-1-sulfonyl) chloride as starting reagents. The product was purified and characterized using powder and single-crystal XRD, DTA-TGA analyses. The single-crystal XRD analysis revealed that the compound crystallizes in the monoclinic $P2_1/c$ space group, the molecular structure being stabilized by an intramolecular interactions, while the crystal packing is governed by N-H…O hydrogen bonding and the flexibility of the pentoxy chains.

Acknowledgments: *This article is published with the support of the Project № BG05M2OP001-1.002-0005-C 03, Center for Competence "Personalized*

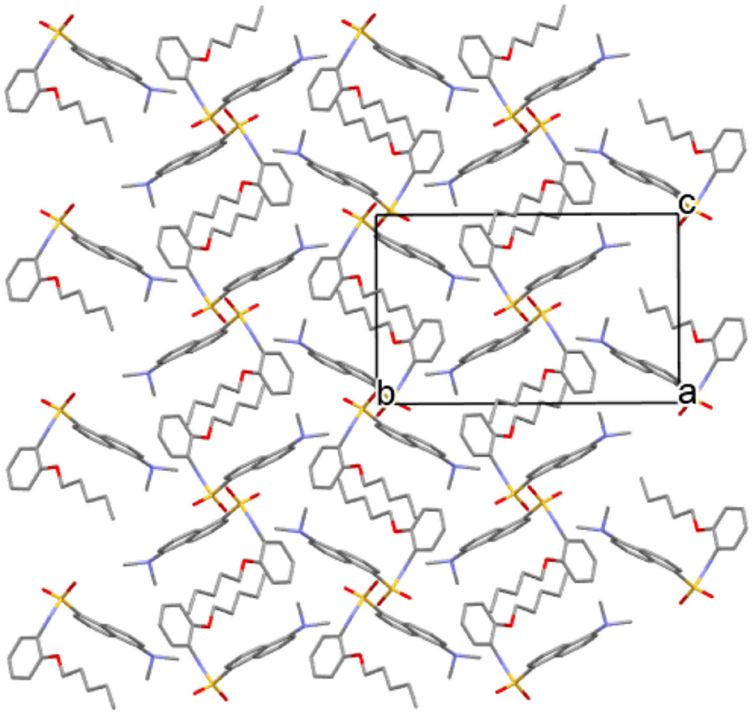

Fig. 4. Crystal packing arrangement in **4** disclosing the pseudo parallel positing of the pentoxy chains.

Innovative Medicine (PERIMED)", work package – 9; funded by the Operational Program "Science and Education for Intelligent Growth" 2014–2020, co-financed by the European Union through the European Regional Development Fund.

REFERENCES

1. Z. Si-qi, Z. Pan-pan, D. Cong-wen, L. Ming, Z. Yuling,Y. Chun-gang, *Applied Chemical Industry* **53** (2024).
2. M. Schenk, N. König, E. Hey-Hawkins,A. G. Beck-Sickinger, *ChemBioChem*, e202300857 (2024).
3. P. Bal, G. Sinam, C. Yahavi, S. P. Singh, S. Jena, A. B. Pant,S. K. Barik, *Toxicon* **238**, 107566 (2024).
4. D. Barik M. Porel, *ACS Macro Letters* **13**, 65 (2024).
5. A. Jastrzębska, A. Kmieciak, Z. Gralak, K. Brzuzy, M. Krzemiński, D. Gorczyca,E. Szłyk, *Food Chemistry* **436**, 137686 (2024).
6. K. Kayano, T. Tsutsumi, Y. Murata, C. Ogasa, T. Watanabe, R. Sato, S. Karanjit,K. Namba, *Angewandte Chemie*, e202401411 (2024).
7. H.-Y. Lin, C.-H. Liu, Y.-T. Kang, S.-W. Lin, H.-Y. Liu, C.-T. Lee, Y.-C. Liu, M.-C. Hsu, Y.-Y. Chien,S.-M. Hong, *Biomolecules* **14**, 372 (2024).
8. J. Lin, L. Chen, Y. Wang, M. Zhao, M. Zhao, J. Shen, C. Zhang, B. Chen, T. Chen,D. Chen, *Journal of Luminescence* **268**, 120410 (2024).
9. Y. Oku, N. Nakajima, M. Hamada,Y. Koyama, *Chemistry – A European Journal*, e202400092 (2024).
10. C. Schilling, A. Zens,S. Laschat, *Liquid Crystals*, 1 (2024).
11. C. Pathak U. D. Kabra, *Bioorganic Chemistry*, 107152 (2024).
12. 1A. Thakor, V. Sharma, S. Rathod, P. Shrivastav,R. Shah, *Current Chemistry Letters* **12**, 641 (2023).
13. C. Allen J. Gates Jr, *Organic Syntheses* **25**, 9 (2003).
14. S. Nishimura, *Handbook of heterogeneous catalytic hydrogenation for organic synthesis* (Wiley New York, 2001).
15. G. M. Sheldrick, *Acta Crystallographica Section A: Foundations and Advances* **71**, 3 (2015).
16. G. M. Sheldrick, *Acta Crystallographica Section C: Structural Chemistry* **71**, 3 (2015).
17. L. J. Farrugia, *Journal of Applied Crystallography* **45**, 849 (2012).
18. C. F. Macrae, I. Sovago, S. J. Cottrell, P. T. Galek, P. McCabe, E. Pidcock, M. Platings, G. P. Shields, J. S. Stevens,M. Towler, *Journal of applied crystallography* **53**, 226 (2020).
19. M. Kazem-Rostami A. Moghanian, *Organic Chemistry Frontiers* **4**, 224 (2017).
20. F. Pavelčík, M. Remko, J. Čižmárik,J. Majer, *Collection of Czechoslovak chemical communications* **51**, 264 (1986).
21. F. Rakotondradany, M. Whitehead, A. M. Lebuis,H. F. Sleiman, *Chemistry–A European Journal* **9**, 4771 (2003).
22. Z. Wang, L. Mei, C. Guo, S. Huang, W. Q. Shi, X. Li, W. Feng, X. Li, C. Yang,L. Yuan, *Angewandte Chemie* **135**, e202216690 (2023).
23. W. Chen, C. Zhang, X. Han, S. H. Liu, Y. Tan,J. Yin, *The Journal of Organic Chemistry* **84**, 14498 (2019).
24. E. Conterosito, I. Benesperi, V. Toson, D. Saccone, N. Barbero, L. Palin, C. Barolo, V. Gianotti,M. Milanesio, *ChemSusChem* **9**, 1279 (2016).
25. K. Kavallieratos, J. M. Rosenberg, W.-Z. Chen,T. Ren, *Journal of the American Chemical Society* **127**, 6514 (2005).
26. R. C. Knighton, M. R. Sambrook, J. C. Vincent, S. A. Smith, C. J. Serpell, J. Cookson, M. S. Vickers,P. D. Beer, *Chemical communications* **49**, 2293 (2013).
27. M. C. Etter, J. C. MacDonald,J. Bernstein, *Acta Crystallographica Section B: Structural Science* **46**, 256 (1990).

Instructions about Preparation of Manuscripts

General remarks: Manuscripts are submitted in English by e-mail. The text must be prepared in A4 format sheets using Times New Roman font size 11, normal character spacing. The manuscript should not exceed 15 pages (about 3500 words), including photographs, tables, drawings, formulae, etc. Authors are requested to use margins of 2 cm on all sides.

Manuscripts should be subdivided into labelled sections, e.g. INTRODUCTION, EXPERIMENTAL, RESULTS AND DISCUSSION, etc. **The title page** comprises headline, author(s)' names and affiliations, abstract and key words. Attention is drawn to the following:

a) **The title** of the manuscript should reflect concisely the purpose and findings of the work. Abbreviations, symbols, chemical formulae, references and footnotes should be avoided. If indispensable, abbreviations and formulae should be given in parentheses immediately after the respective full form.

b) **The author(s)'** first and middle name initials and family name in full should be given, followed by the address (or addresses) of the contributing laboratory (laboratories). **The affiliation** of the author(s) should be listed in detail (no abbreviations!). The author to whom correspondence and/or inquiries should be sent should be indicated by an asterisk (*) with e-mail address.

The abstract should be self-explanatory and intelligible without any references to the text and containing up to 250 words. It should be followed by keywords (up to six).

References should be numbered sequentially in the order, in which they are cited in the text. The numbers in the text should be enclosed in brackets [2], [5, 6], [9−12], etc., set on the text line. References are to be listed in numerical order on a separate sheet. All references are to be given in Latin letters. The names of the authors are given without inversion. Titles of journals must be abbreviated according to Chemical Abstracts and given in italics, the volume is typed in bold, the initial page is given and the year in parentheses. Attention is drawn to the following conventions: a) The names of all authors of a certain publications should be given. The use of "et al." in the list of references is not acceptable; b) Only the initials of the first and middle names should be given. In the manuscripts, the reference to author(s) of cited works should be made without giving initials, e.g. "Bush and Smith [7] pioneered...". If the reference carries the names of three or more authors it should be quoted as "Bush et al. [7]", if Bush is the first author, or as "Bush and co-workers [7]", if Bush is the senior author.

Footnotes should be reduced to a minimum. Each footnote should be typed double-spaced at the bottom of the page, on which its subject is first mentioned. **Tables** are numbered with Arabic numerals on the left-hand top. Each table should be referred to in the text. Column headings should be as short as possible but they must define units unambiguously. The units are to be separated from the preceding symbols by a comma or brackets. Note: The following format should be used when figures, equations, etc. are referred to the text (followed by the respective numbers): Fig., Eqns., Table, Scheme.

Schemes and figures. Each manuscript should contain or be accompanied by the respective illustrative material, as well as by the respective figure captions in a separate file. As far as presentation of units is concerned, SI units are to be used. However, some non-SI units are also acceptable, such as °C, ml, l, etc. Avoid using more than 6 (12 for review articles) figures in the manuscript. Since most of the illustrative materials are to be presented as 8-cm wide pictures, attention should be paid that all axis titles, numerals, legend(s) and texts are legible.

The authors are required to submit the text with a list of three individuals and their e-mail addresses that can be considered by the Editors as potential reviewers. Please note that the reviewers should be outside the authors' own institution or organization. The Editorial Board of the journal is not obliged to accept these proposals.

The authors are asked to submit **the** final text (after the manuscript has been accepted for publication) in electronic form by e-mail. The main text, list of references, tables and figure captions should be saved in separate files (as *.rtf or *.doc) with clearly identifiable file names. It is essential that the name and version of the word-processing program and the format of the text files is clearly indicated. It is recommended that the pictures are presented in *.tif, *.jpg, *.cdr or *.bmp format. The equations are written using "Equation Editor" and chemical reaction schemes are written using ISIS Draw or ChemDraw programme.

EXAMPLES FOR PRESENTATION OF REFERENCES

REFERENCES

1. D. S. Newsome, Catal. Rev.–Sci. Eng., 21, 275 (1980).
2. C.-H. Lin, C.-Y. Hsu, J. Chem. Soc. Chem. Commun., 1479 (1992).
3. R. G. Parr, W. Yang, Density Functional Theory of Atoms and Molecules, Oxford Univ. Press, New York, 1989.
4. V. Ponec, G. C. Bond, Catalysis by Metals and Alloys (Stud. Surf. Sci. Catal., vol. 95), Elsevier, Amsterdam, 1995.
5. G. Kadinov, S. Todorova, A. Palazov, in: New Frontiers in Catalysis (Proc. 10th Int. Congr. Catal., Budapest (1992), L. Guczi, F. Solymosi, P. Tetenyi (eds.), Akademiai Kiado, Budapest, 1993, Part C, p. 2817.
6. G. L. C. Maire, F. Garin, in: Catalysis. Science and Technology, J. R. Anderson, M. Boudart (eds.), vol. 6, Springer Verlag, Berlin, 1984, p. 161.
7. D. Pocknell, GB Patent 2 207 355 (1949).
8. G. Angelov, PhD Thesis, UCTM, Sofia, 2001, pp. 121-126.
9. JCPDS International Center for Diffraction Data, Power Diffraction File, Swarthmore, PA, 1991.
10. CA 127, 184 762q (1998).
11. P. Hou, H. Wise, J. Catal., in press.
12. M. Sinev, private communication.
13. http://www.chemweb.com/alchem/articles/1051611477211.html.

Texts with references which do not match these requirements will not be considered for publication!!!

CONTENTS